FUNCTIONALIZED ZEOLITES WITH HIERARCHICAL AND CORE-SHELL ARCHITECTURES

A thesis submitted in fulfilment of the requirements for the Degree of

Doctor of Philosophy in Chemical and Process Engineering

at the

University of Canterbury

By

XICHENG JIA

UC
UNIVERSITY OF
CANTERBURY
Te Whare Wānanga o Waitaha
CHRISTCHURCH NEW ZEALAND

2018

Acknowledgements

Finally, all of these wouldn't have been possible without my family - mom, dad, grandma and grandpa. The biggest thanks to my mom for all those years of love, encouragement and support, and motivating me to purse the path that I want to.

Abstract

Zeolites are well known for their ordered microporous networks, good hydrothermal stability, large surface area, high acidity and selectivity. These excellent properties make zeolites extremely useful for petrochemical processes and refining. However, the sole presence of microporous channels also restricts the diffusion of reactants and products into and out of the microporous networks, especially limiting zeolite applications involving bulky molecules. The importance of developing hierarchical zeolites has attracted great attention in recent years due to the prospect of increased accessibility for bulky molecules. Introducing additional mesoporosity, and even macroporosity, into conventional zeolites produces a combination of three different size scales of porosity. It expands the original zeolite hierarchical structure and greatly enhances the mass transport of molecules while maintaining the intrinsic size, shape and transition state selectivity of zeolite. The promising applications of this new zeolite architecture have prompted a multitude of efforts to develop a variety of different synthesis strategies. Apart from hierarchical modification, core-shell structure also gives zeolites great advantages from both core and shell zeolites, such as ion exchange property for deposition of metal particles on inner zeolite, meanwhile a hydrophobic zeolite shell can protect the core complex from inhibition by water. The thesis herein focused on the development of zeolites with hierarchical and core-shell structures.

We designed a zeolite stacking structure by using hydraulic pressing and programmed temperature calcination synthesis procedures. ZSM-5 type zeolites with particle sizes of approximately 100 nm, 1 µm and 2 µm were used to synthesize stacking ZSM-5 with a size ranging from 45 to 63 µm. The prepared ZSM-5 zeolite stacking structure was used as a support to deposit palladium. The performance of the palladium/stacking ZSM-5 was investigated on Sonogashira coupling reactions. Stacking samples with micro-sized units (1 µm and 2 µm)

showed a 200-300% higher turnover number (TON) than their unit counterparts. However, stacking samples with nano-sized units (100 nm) showed decreased TON conversion compared with that of their unit counterparts, probably due to partial destruction of the nano-sized ZSM-5 structure during the stacking synthesis process at high temperature. The palladium/stacking ZSM-5 (micro-sized units) also showed better conversion on different bromides and alkynes than that of traditional homogenous catalysts. Moreover, the stacking composites showed good durability by recycling 4 runs without losing significant catalytic activity. The design of the stacking MFI structure exhibited improved catalytic activity, sustainability and hierarchical-resemblance properties.

We also investigated the structure-performance relationships in different zeolite-solvent systems that are suitable for microwave-assisted dehydration of fructose to 5-hydroxymethylfurfural (HMF). Different types of zeolites (MFI, BEA, and Y) were examined as acid catalysts. The results showed that the HMF yield is independent of particle size for MFI zeolite in water. The secondary porosities improved the HMF yield, while byproducts formation (via rehydration or polymerization) was also increased due to the enlarged channels in zeolites. All tested zeolites showed higher fructose conversion, HMF yield, and HMF selectivity in organic-water solvent systems than in water. The synergistic effect of the substrates, catalysts, and solvent-product interactions in the hydrophobic Y zeolite/DMSO system yielded the highest fructose conversion (72.4%) and HMF yield (49.2%). This study supports the understanding of the requirement for microwave-assisted biomass conversion in biorefinery.

Next, we developed a core-shell zeolite structure comprised of palladium-deposited ZSM-5 core and silicalite-1 (S-1) shell which favors selectivity towards light olefin in hydrogenation via increased diffusion length. A well designed S-1/Pd/ZSM-5 core-shell structure was

prepared via secondary crystallization of S-1 layer on the Pd/ZSM-5 core. The catalytic and selectivity performance of the S-1/Pd/ZSM-5 composite was evaluated in catalytic hydrogenation of alkenes in liquid phase. The synthesized S-1/Pd/ZSM-5 gives a much higher selectivity towards 1-hexene (87%) over cyclohexene (13%) even though both reactants are able to enter the 10-membered ring channels of the core-shell structure. The zeolitic core-shell composite also showed an increased selectivity towards 1-hexene over 1-heptene as the S-1 layers built up, even though both are linear alkenes with similar kinetic diameters that are accessible to the MFI framework. In this work, we demonstrated a strong correlation between the thickness of the S-1 shell layer and the selectivity towards light olefins due to faster mass transfer rate. The design of the core-shell MFI structure is a new example of how selectivity in a zeolite-catalyzed reaction can be changed and enhanced without relying on typical molecular size exclusion process.

Lastly, we synthesized a core-shell zeolite structure comprised of palladium-deposited nano-sized ZSM-5 core and silicalite-1 (S-1) shell, which favors ethylene adsorption and shows improved humidity tolerance. A well designed S-1/Pd/ZSM-5 core-shell structure was prepared via secondary crystallization of S-1 layer on the nano-sized Pd/ZSM-5 core. The ethylene removing ability of the S-1/Pd/ZSM-5 in both dry and humid conditions was evaluated by pressure drop method. The synthesized S-1/Pd/ZSM-5 gives a much higher ethylene uptake up to 290% than plain ZSM-5. The S-1 coated samples also shows strong humidity tolerance by only losing 7.6% of the ethylene uptake under 5 h of humidity pre-treatment, while the Pd/ZSM-5 lost 20% of ethylene uptake under the same condition. The design of the core-shell structure may offer the advantages of long-term economic benefit and sustainability for the fresh products market.

Table of contents

Lists of Figures

Lists of Tables

Publications

Journal Articles

[1] **Jia X.,** Jeong Y., Baik H., Choi J. and Yip ACK. (2018) *"Increasing Resolution of Selectivity in Alkene Hydrogenation via Diffusion Length in Core-shell MFI zeolite."* Catalysis Today 314: 94-100.

[2] **Jia X.,** Jiang D., Tsang DCW., Choi J. and Yip ACK. (2018) *"Stacking MFI Zeolite Structures for Improved Sonogashira Coupling Reactions."* Microporous and Mesoporous Materials 276: 147-153.

Conference contributions

[3] **Jia X.,** Yu IKM., Tsang DCW. and Yip ACK. (2018) *"Tailored Hierarchical ZSM-5 for Fructose Conversion to Hydroxymethylfurfural."* Yokohama, Japan: International Symposium on Zeolites and Microporous Crystals 2018 (ZMPC 2018), 5-9 Aug 2018.

[4] **Jia X.,** Choi J. and Yip ACK. (2017) *"Design of core-shell MFI zeolite: An alternative way of achieving zeolite selectivity."* Hong Kong S. A. R.: The 17th Asia Pacific Confederation of Chemical Engineers Congress (APCChE 2017), 23-27 Aug 2017.

[5] **Jia X.,** Choi J. and Yip ACK. (2017) *"Selective hydrogenation of olefins via diffusion length in core-shell MFI zeolite."* Bali, Indonesia: The 3rd Euro-Asia Zeolite Conference (3rd EAZC), 22-25 Jan 2017.

UC

UNIVERSITY OF CANTERBURY
Te Whare Wānanga o Waitaha
CHRISTCHURCH NEW ZEALAND

Co-Authorship Form

This form is to accompany the submission of any thesis that contains research reported in co-authored work that has been published, accepted for publication, or submitted for publication. A copy of this form should be included for each co-authored work that is included in the thesis. Completed forms should be included at the front (after the thesis abstract) of each copy of the thesis submitted for examination and library deposit.

Please indicate the chapter/section/pages of this thesis that are extracted from co-authored work and provide details of the publication or submission from the extract comes:

Part of Chapter 2 of this thesis has been submitted to the journal of "Advanced Powder Technology" for publication.
Jia X., Khan W., Wu Z., Choi J. and Yip ACK. "Modern synthesis strategies for hierarchical zeolites: Bottom-up versus Top-down strategies." Advanced Powder Technology, under review, 10/12/2018.

Chapter 3 has been published in the journal of "Microporous and Mesoporous Materials".
Jia X., Jiang D., Tsang DCW., Choi J. and Yip ACK. (2018) "Stacking MFI Zeolite Structures for Improved Sonogashira Coupling Reactions." Microporous and Mesoporous Materials 276: 147-153.

Chapter 5 has been published in the journal of "Catalysis Today".
Jia X., Jeong Y., Baik H., Choi J. and Yip ACK. (2018) "Increasing Resolution of Selectivity in Alkene Hydrogenation via Diffusion Length in Core-shell MFI zeolite." Catalysis Today 314: 94-100.

Please detail the nature and extent (%) of contribution by the candidate:
The experimental work and writing up was primarily completed by the candidate. The candidate contributed 70-80% of the co-authored works.

Certification by Co-authors:
If there is more than one co-author then a single co-author can sign on behalf of all

The undersigned certifies that:

▪ The above statement correctly reflects the nature and extent of the PhD candidate's contribution to this co-authored work
▪ In cases where the candidate was the lead author of the co-authored work he or she wrote the text

Name: *Alex Yip*

Signature: Date: *10/12/2018*

Glossary

Å	Angstroms
CTA	Cetyltrimethylammonium
EDS	Energy-dispersive X-ray spectroscopy
FID	Flame ionization detector
HPLC	High-performance liquid chromatography
GC	Gas chromatography
MOF	Metal-organic framework
MTG	Methanol-to-gasoline
MTH	Methanol-to-hydrocarbons
MTP	Methanol-to-propene
NMR	Nuclear magnetic resonance
SDA	Structure-directing agent
SEM	Scanning electron microscopy
TGA	Thermo-gravimetric analysis
TEM	Transmission electron microscopy
TCD	Thermal conductivity detector
TON	Turnover number
TPD	Temperature programmed desorption
XRD	X-ray diffraction
$\emptyset$	Thiele modulus
P_i	Initial pressure
P_f	Final pressure
R	The ideal gas constant

Chapter 1

Introduction

1.1 Background of Research

Zeolites are crystalline aluminosilicates with periodic arrangements of pores or channels within the microporous (typically < 2 nm) range. Their unique structures, thermal/mechanical stability, superior catalytic activity and shape-selectivity have led to broad applications in chemical and petrochemical industries [1]. For example, ion-exchange, adsorption, heterogeneous catalysis, molecular sieves and gas membrane separation [2-10].

The catalytically active sites in zeolite micropores can be acid sites or redox-active sites. Acid sites resulted from the charge balancing of the zeolite framework with protons, which is necessary when, for example, Al^{3+} substitutes Si^{4+} in the framework. Redox-active sites resulted from the charge compensation that is done by ion-exchange with redox active ions such as Fe(III), Cu(II), Co(II), or Ag(I) rather than with protons. Additionally, redox-active sites can be obtained by incorporating redox-active metal ions, e.g., Ti, V, Mn, Fe, Co, Ga, Sn, etc., directly into the zeolite framework by isomorphous substitution of other Si or Al atoms [11]. Therefore, zeolite catalysts attract significant attention in many areas of heterogeneous catalysis, because they can be tailored to allow careful and systematic studies of various structure–activity relationships. Zeolites are of interest in numerous industrial applications, where they can be active, selective, durable, and relatively inexpensive catalysts.

However, the sole presence of micropores imposes significant limitations on the range of reactions that can be efficiently catalyzed by zeolite catalysts. Some reactions require reactants or products that are too large to access or escape the zeolite micropores. If the zeolite catalyst transforms the reactants into the target products at a rate higher than the rate of diffusion of reactants, intermediates, and products, then the overall reaction rate is limited by the rate of diffusion. Even though several strategies have been pursued to increase the accessibility of the

active sites in zeolite catalysts [12-20], novel synthesis technologies for hierarchical zeolites with improved catalytic activity, sustainability and economic efficiency are still needed.

On the other hand, zeolites and zeolitic materials with core-shell structure, which consists of an inner guest zeolite particle inside of another different functional zeolite (same/different type), have drawn great attention in recent decades [21-25]. Due to the existence of the shell layer, core-shell particles can have distinctive property combinations from different materials. For example, zeolites and zeolitic materials have been used as support for many metals due to their high surface area, ion-exchange ability, and inhibiting agglomeration of the doped metal particles. Metal-doped zeolites or zeolitic materials with protective shell of a particular pore size can prevent poisoning of the metal particles attached to the core by size exclusion [26]. Similarly, the development of functionalized core-shell zeolites with properties such as hydrophobicity are also of interest.

1.2 Thesis scope and structure

Since the hierarchical modification and core-shell functionalization on zeolites have shown improved performance than conventional zeolites, the focus of this thesis was on the development of core-shell zeolites with different shell thickness and distinctive core size, and the new strategies of hierarchical zeolites synthesis. The hierarchical and core-shell zeolites were probed on Sonogashira reaction, glucose/fructose conversion, selective hydrogenation, and ethylene adsorption. This thesis has been written in seven chapters. The brief description of each chapters are listed below:

Chapter 1: An introduction of this study, including general backgrounds, motivations, and overview of the whole thesis were explained in this chapter.

Chapter 2: A literature review is presented in this chapter, which provides the readers with the foundations and rationale of the proposed research project. The major findings from literature thus far were summarized and some key issues in the research work were discussed.

Chapter 3: This chapter describes the novel synthesis strategy of zeolite stacking structure by using hydraulic pressing and programmed temperature calcination synthesis procedures. ZSM-5 type zeolites with particle sizes of approximately 0.1 µm, 1 µm and 2 µm were used to synthesize stacking ZSM-5 with a size ranging from 45 to 63 µm. The prepared ZSM-5 zeolite stacking structure was used as a support to deposit palladium. The performance of the palladium/stacking ZSM-5 was investigated on Sonogashira coupling reactions. The design of the stacking MFI structure exhibited improved catalytic activity, sustainability and hierarchical-resemblance properties. This work was published as *"Stacking MFI Zeolite Structures for Improved Sonogashira Coupling Reactions"* in Microporous and Microporous Materials.

Chapter 4: This study elucidates the role of zeolite-solvent combinations in microwave-assisted, catalytic dehydration of biomass-derived fructose to 5-hydroxymethylfurfural (HMF). Different types of zeolites (MFI, BEA, and Y) were examined as acid catalysts. Water was first tested as the greenest solvent (baseline), followed by dimethyl sulfoxide (DMSO), acetone, γ-valerolactone (GVL), and propylene carbonate (PC)/water (1:1 v/v) binary solvent systems. This study differentiated the effects of structure, acidity and water affinity of the zeolite-solvent media on the simultaneous pathways of biomass-derived conversion in biorefinery. This work was presented at ZMPC2018 as *"Tailored Hierarchical ZSM-5 for Fructose Conversion to Hydroxymethylfurfural"* and the manuscript is ready to submit.

Chapter 5: We designed a core-shell zeolite structure comprises of palladium-deposited ZSM-5 core and silicalite-1 (S-1) shell which favors selectivity towards light olefin in hydrogenation

via increased diffusion length. A well designed S-1/Pd/ZSM-5 core-shell structure was prepared via secondary crystallization of S-1 layer on the Pd/ZSM-5 core. The catalytic and selectivity performance of the S-1/Pd/ZSM-5 composite was evaluated in catalytic hydrogenation of alkenes in liquid phase. In this work, we demonstrate a strong correlation between the thickness of the S-1 shell layer and the selectivity towards light olefins due to faster mass transfer rate. The design of the core-shell MFI structure is a new example of how selectivity in a zeolite-catalyzed reaction can be changed and enhanced without relying on typical molecular size exclusion process. This work was published as *"Increasing Resolution of Selectivity in Alkene Hydrogenation via Diffusion Length in Core-shell MFI zeolite"* in Catalysis Today.

Chapter 6: The core-shell MFI zeolite with a nano-sized ZSM-5 core was synthesized in this work. Pd was impregnated over a ZSM-5 core by the ion-exchange method. The silicalite-1 shell with different thickness was synthesized by secondary crystallization method. The as-prepared core-shell zeolites were characterized via XRD, SEM, TEM, ICP and TGA. The performance of the core-shell zeolites as ethylene scavenger was tested by pressure drop method. The design of the core-shell zeolites with nano-sized core showed a new way to improve ethylene adsorption in a humid environment, due to the combined functions of nano-sized core, hydrophobic shell and Pd that well dispersed over ZSM-5 core. The manuscript is completed and ready to submit.

Chapter 7: The key findings of current study are concluded and recommendations for future work is proposed.

1.3 References

[1] J. Huang, Y. Jiang, V.R. Marthala, M. Hunger, Insight into the mechanisms of the ethylbenzene disproportionation: Transition state shape selectivity on zeolites, J. Am. Chem. Soc., 130 (2008) 12642-12644.

[2] S. Kesraoui-Ouki, C.R. Cheeseman, R. Perry, Natural zeolite utilisation in pollution control: A review of applications to metals' effluents, Journal of Chemical Technology & Biotechnology: International Research in Process, Environmental AND Clean Technology, 59 (1994) 121-126.

[3] S.E. Bailey, T.J. Olin, R.M. Bricka, D.D. Adrian, A review of potentially low-cost sorbents for heavy metals, Water Res., 33 (1999) 2469-2479.

[4] E. Van Steen, L.H. Callanan, M. Claeys, Recent advances in the science and technology of zeolites and related materials: proceedings of the 14th International Zeolite Conference, Cape Town, South Africa, 25-30th April 2004, Elsevier2004.

[5] J. Čejka, H. van Bekkum, Zeolites and ordered mesoporous materials: progress and prospects: the 1st FEZA School on Zeolites, Prague, Czech Republic, August 20-21, 2005, Gulf Professional Publishing2005.

[6] M.E. Davis, Ordered porous materials for emerging applications, Nature, 417 (2002) 813.

[7] M. Tsapatsis, Molecular sieves in the nanotechnology era, AlChE J., 48 (2002) 654-660.

[8] A. Stein, Advances in microporous and mesoporous solids—highlights of recent progress, Adv. Mater., 15 (2003) 763-775.

[9] X. Zhang, W. Li, H. Xu, Application of zeolites in photocatalysis, (2004).

[10] X. Xu, J. Wang, Y. Long, Zeolite-based materials for gas sensors, Sensors, 6 (2006) 1751-1764.

[11] K. Egeblad, C.H. Christensen, M. Kustova, C.H. Christensen, Templating mesoporous zeolites, Chem. Mater., 20 (2007) 946-960.

[12] S. Van Donk, A.H. Janssen, J.H. Bitter, K.P. de Jong, Generation, characterization, and impact of mesopores in zeolite catalysts, Catalysis Reviews, 45 (2003) 297-319.

[13] M. Hartmann, Hierarchical zeolites: A proven strategy to combine shape selectivity with efficient mass transport, Angew. Chem. Int. Ed., 43 (2004) 5880-5882.

[14] T.O. Drews, M. Tsapatsis, Progress in manipulating zeolite morphology and related applications, Current Opinion in Colloid & Interface Science, 10 (2005) 233-238.

[15] F. Schüth, Engineered porous catalytic materials, Annu. Rev. Mater. Res., 35 (2005) 209-238.

[16] J.C. Groen, J.A. Moulijn, J. Pérez-Ramírez, Desilication: on the controlled generation of mesoporosity in MFI zeolites, J. Mater. Chem., 16 (2006) 2121-2131.

[17] Y. Tao, H. Kanoh, L. Abrams, K. Kaneko, Mesopore-modified zeolites: preparation, characterization, and applications, Chem. Rev., 106 (2006) 896-910.

[18] J. Čejka, S. Mintova, Perspectives of micro/mesoporous composites in catalysis, Catalysis Reviews, 49 (2007) 457-509.

[19] V. Meynen, P. Cool, E. Vansant, Synthesis of siliceous materials with micro-and mesoporosity, Microporous Mesoporous Mater., 104 (2007) 26-38.

[20] S.N. Azizi, S. Rostami, N. Asemi, Preparing hierarchical nanoporous ZSM-5 zeolite via post-synthetic modification of zeolite synthesized from bagasse and its application for removal of Pb^{2+}, Quarterly Iranian Chemical Communication, 6 (2018) 75-86.

[21] A. Ghorbanpour, A. Gumidyala, L.C. Grabow, S.P. Crossley, J.D. Rimer, Epitaxial growth of ZSM-5@ Silicalite-1: A core–shell zeolite designed with passivated surface acidity, ACS nano, 9 (2015) 4006-4016.

[22] J. Yang, F. Zhang, H. Lu, X. Hong, H. Jiang, Y. Wu, Y. Li, Hollow Zn/Co ZIF Particles Derived from Core–Shell ZIF-67@ ZIF-8 as Selective Catalyst for the Semi-Hydrogenation of Acetylene, Angew. Chem., 127 (2015) 11039-11043.

[23] J. Zheng, G. Wang, M. Pan, D. Guo, Q. Zhao, B. Li, R. Li, Hierarchical core–shell zeolite composite ZSM-5@ SAPO-34 fabricated by using ZSM-5 as the nutrients for the growth of SAPO-34, Microporous Mesoporous Mater., 206 (2015) 114-120.

[24] K. Miyake, Y. Hirota, K. Ono, Y. Uchida, S. Tanaka, N. Nishiyama, Direct and selective conversion of methanol to para-xylene over Zn ion doped ZSM-5/silicalite-1 core-shell zeolite catalyst, J. Catal., 342 (2016) 63-66.

[25] X. Wang, G. Yang, J. Zhang, S. Chen, Y. Wu, Q. Zhang, J. Wang, Y. Han, Y. Tan, Synthesis of isoalkanes over a core (Fe–Zn–Zr)–shell (zeolite) catalyst by CO_2 hydrogenation, Chem. Commun., 52 (2016) 7352-7355.

[26] H. Yin, J. Choi, A.C. Yip, Anti-poisoning core–shell metal/ZIF-8 catalyst for selective alkene hydrogenation, Catal. Today, 265 (2016) 203-209.

Chapter 2

Literature Review

2.1 Zeolites

Zeolites have been applied as catalysts since the 1960s. They are defined as hydrated aluminosilicates that consist of three-dimensional networks of SiO_4 and AlO_4 tetrahedra linked together by shared oxygen atoms [1]. The ordered framework gives zeolites high thermal and mechanical stability. In addition, the crystalline features cause zeolites to consist of a uniform microporous framework (diameter < 2 nm), which provides them with shape selectivity by imposing a size-exclusion limit on molecules entering and exiting the zeolite channels [2-5]. Because of this unique shape selectivity, zeolites are extensively used throughout numerous industries as shape-selective adsorbents and catalysts [6-8].

The structural formula of a zeolite crystallographic unit cell is shown in Equation 1.

$$M_{x/n} = [(AlO_2)_x(SiO_2)_y] \cdot wH_2O \tag{1}$$

where M is the cation of valence n, w is the number of water molecules, and the ratio y/x varies from 1 to ∞ depending on the structure. Moreover, the sum of y and x is the total number of tetrahedra in the unit cell, and the portion within the bracket represents the framework composition [9]. This structure results in a microporous crystalline network that can accommodate water molecules and facilitate reversible dehydration. The presence of aluminium in the zeolite framework can generate negative charges, which can be balanced by the small cations of hydroxyl protons, providing weak Lewis or strong Brønsted acid sites, respectively, which makes zeolites excellent catalysts and ion exchangers [10]. Moreover, the ratio of Lewis and Brønsted acid sites can be tuned by adjusting the Si/Al ratio during the synthesis process. Different types of zeolites also contain distinctive weak/strong acids. This ion-exchange property and adjustable acidity make them useful in a great range of applications in the detergent production, water treatment, oil refining and petrochemical industries [11-15].

High surface area is another excellent property of zeolites. Due to their countless microporous cavities, zeolites have much higher surface area than similarly sized non-porous particles such as Al_2O_3 or TiO_2. This property along with ion-exchange characteristics makes zeolites very useful as supports for accommodating metal particles. Many studies have been performed on the synthesis methods of doping different metals into the zeolite framework, which are widely used for applications such as xylene isomerization, the combustion of toluene and the depolymerization of lignin [16-21].

In summary, four properties make zeolites especially interesting for heterogeneous catalysis: (1) they have a pore size usually below 2 nm, causing them to have good shape selectivity for particular molecules; (2) they have ion-exchange properties that allow them to accommodate many different cations with various catalytic properties; (3) when the cationic sites are exchanged to H^+, they can have a high number of weak/strong acid sites; and (4) they contain pores with different sizes and directions: for example, ZSM-5 has both sinusoidal and linear channels. The first and last properties account for their molecular sieving properties.

The pore size of molecular sieves is determined mainly by the number of tetrahedra in a ring. Table 2.1 shows some common examples of zeolites with their ring sizes. The existence of cations also influences the actual pore size. Molecules such as hydrogen, oxygen, ammonia and argon can generally pass through every type of zeolite. In a typical type A zeolite, which has a cubic structure, the pore diameter is large enough (approximately 0.4 nm) to let linear paraffins pass through. Monovalent cations such as sodium and potassium occupy the active sites and block part of the pores, so essentially no organic molecules can pass through a NaA zeolite except for methane. However, divalent cations will occupy only every other cationic position, leaving enough space for linear paraffins to diffuse through. Some molecules with a nominal dimension slightly larger than the pore mouth can still diffuse into active sites inside the cavities because molecular vibration allows them to wiggle through [22].

Table 2.1 Examples of different ring sizes in zeolites.

No. of T-atoms in ring	Maximum free diameter, Å	Examples (IZA code)
8	3.9	CHA, KFI
10	5.7	FER, MTT, TON, MFI
12	7.4	VET, BEA, FAU
18	15	Not Yet Observed

The microporous framework of zeolite makes them highly selective regarding which molecules can react at the active sites inside the cavities. In other words, only molecules whose dimensions are smaller than the pore mouth can penetrate into the zeolite network and react there. Similarly, only molecules that are smaller than the critical size are possible final products.

There are three common types of shape selectivity in zeolites, as illustrated in Fig. 2.1: (a) reactant shape selectivity, in which reactants that are too large to diffuse into the active sites inside the network generate no products; (b) transition state selectivity, in which the transition state molecules are restricted by the spatial constraints inside the zeolite channels; while reactants can diffuse into the active sites without severe obstacles, the space around the reactive sites may be too small to accommodate the transitional molecules; and (c) product shape selectivity, in which product molecules are too large to diffuse out from the zeolite framework; these bulky molecules that remain inside the zeolite channels can be converted to smaller molecules, which may block the pores or even generate coke, deactivating the zeolites [23]. Examples of reactant/product shape selectivity include the selective hydrogenation of n-olefins over CaA [24] and the Pt-catalysed hydrogenation of olefins over ZSM-5 [25]. In addition, examples of transition state shape selectivity include the acid-catalysed transalkylation of dialkylbenzenes [26] and isobutane isomerization over HZSM-5 [27, 28]. More than 200

zeolites with different configurations have thus far discovered in nature and in man-made forms [29].
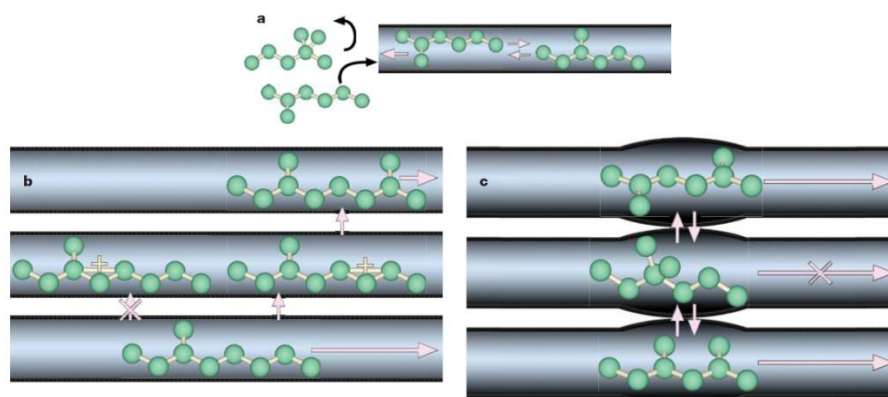
Fig. 2.1 Three different types of shape selectivity in zeolites. (a) Reactant shape selectivity: molecules that are too large to enter the zeolite pores cannot reach acid sites for reaction and are therefore not converted into products. (b) Transition state shape selectivity: molecules (and transition states) that are too large to fit inside a pore do not form. (c) Product shape selectivity: new molecules are formed in the adsorbed phase but are too large to desorb as products. (Adapted from Ref. [23]. Copyright 2008 Springer Nature)

Even though their ordered microporous structure makes zeolites highly useful in shape-selective catalysis, the presence of micropores alone in zeolites has drawbacks for their further application. The molecular dimensions cause them to suffer from significant diffusion limitation. In addition, the microporous structure limits the selectivity range of the desired products. Moreover, the microporous network makes zeolites very susceptible to coking, leading to rapid deactivation and resulting in low accessibility for reactants/products and production of undesired by-products by side reactions [30-32]. Therefore, the modification of zeolite structure with more efficient mass transfer characteristics, in order to allow molecules

to diffuse more easily into the active sites inside channels and out to the surface of the zeolites, have been attracting increasing research attention in recent years [33-36].

2.2 Hierarchical zeolites

We call zeolites that have at least two levels of pore diameters, i.e., < 2 nm (micropores) and > 2 nm (meso-/macropores) "hierarchical structure zeolites". In other words, hierarchical zeolites not only have inherent microporosity, but also have mesoporosity or even macroporosity. For most cases, however, the secondary porosity lies in the mesoporous range. Hierarchical zeolites can generally be obtained by (i) generating intracrystalline mesopores inside the microporous zeolite structure or (ii) introducing intercrystalline mesopores into spaces that are intergrown by nano-sized zeolite crystals. The synthesis methods play a very important role in different levels of hierarchical porosity [37].

Hierarchical zeolites show improved catalytic performance compared to conventional microporous zeolites. This improvement is largely ascribed to the participation of large compounds, as the secondary porosity allows them to diffuse into active sites inside channels unimpeded. Some general advantages associated with hierarchical zeolites are as follows:

In general, if the diffusivity of one kind of molecule is at least one or two orders of magnitude higher than that of its competing molecules, a preferential and selective reaction involving the former molecules will occur in shape-selective catalysts [38-41]. Molecules that are much larger than the pore size of the zeolites will be absolutely unable to diffuse into the active sites inside conventional zeolites. Molecules with a dimension smaller than the zeolite pore diameter will have a faster diffusion rate in larger channels compared to large molecules. It is well-established that intracrystalline transport is the rate-controlling step for many catalytic process using zeolites as catalysts. The diffusion limitation can be greatly decreased by using

hierarchical zeolites, as the secondary porosity significantly shortens the length of the diffusional pathway, which can be explained by Knudsen diffusion [42, 43]. The overall diffusion rate in hierarchical zeolites can be measured by the nuclear magnetic resonance (NMR) technique reported by Mehlhorn et al. [44].

The hierarchical modification of zeolite is considered to result in less steric hindrance due to the introduction of secondary porosities (mesopores and macropores). Thus, the dimensions of molecules can be increased to a much larger range as needed for a reaction, which extends the application of zeolites to wider areas. Two types of active sites may exist in secondary porosity networks based on their different locations. (i) Active sites accessible from the external surface via secondary channels to the mouth of the microporous network will have almost no steric hinderance; (ii) however, active sites located at the entrance of the microporous network, will potentially have a few steric limitations and affect the accessibility for bulky molecules [37].

We have discussed in the above sections that the shape selectivity of zeolites arises from their ordered microporous network. It is assumed that the introduction of secondary porosity will have a negative effect on the shape selectivity of zeolite, which does indeed occur for certain reactions such as xylene isomerization: p-xylene selectivity has been observed to decrease over hierarchical zeolites compared to conventional microporous zeolites [35, 45]. However, the use of hierarchical zeolites increased the selectivity towards xylenes during toluene disproportionation and branched hydrocarbons during hydrocracking, probably due to the shortened reaction time and fast molecular diffusion inside microporous channels, which suppressed the production of undesired secondary products such as light hydrocarbon species in hydrocracking [46, 47]. Kim et al. [48] have reported that the selectivity effects of hierarchical structure can be either beneficial or detrimental to hydroisomerization selectivity depending on the spatial location of the acid sites. The internal mesopores of SAPO-11 can facilitate the hydrocarbon diffusion, resulting in the enhanced hydroisomerization selectivity

of the catalysts. In the case of Methanol to hydrocarbons (MTH) reaction, hierarchical MFI zeolites produce less aromatics than light olefin compared with conventional MFI zeolites, due to the fast diffusion of aromatic intermediate out of the zeolite micropores that suppress the aromatic-based catalytic cycle over olefin-based cycle [49].

Catalytic deactivation due to coke deposition is a common phenonmena occuring in heterogeneous catalysis which mainly results from the formation of bulky organic compounds which are not able to desorb under reaction conditions [50, 51]. There are three mechanisms that usually cause zeolite deactivation by coke formation, whose effects are increased in the order of active site coverage, micropore blockage and deposition over the external surface of the zeolite [52]. It is well known that zeolites with nano-sized dimensions are usually less affected by coke formation than those with micro-sized dimensions, which can be assigned to the size and shape of zeolite pores. Coke can be advantageous, especially, controlled coke deposition at external surface may enhance the shape selectivity of zeolites, also known as selectivation. Toluene disproportionation is one of the examples in which pre-coked ZSM-5 exhibits higher yield of para-xylene [51]. Moreover, coke molecules can also take part in reaction as being active sites, e.g., the reaction mechanism involving hydrocarbon production from methanol and ethanol over zeolites (H-ZSM-5 or SAPO-34). Hierarchical zeolites are expected to exhibit similar behaviour. Nevertheless, it is worth noting that the net coke content will increase compared to that of conventional zeolites because the secondary porosity potentially accommodate more external coke deposits, although hierarchical zeolites may suffer lower deactivating effects [53, 54].

Compared to conventional zeolites that mainly contain internal acid sites, hierarchical zeolites have shown weaker acid strength due to the large presence of external acid sites, yet they show much stronger acidity than the amorphous mesoporous aluminosilicates such as Al-MCM-41. It has been reported that hierarchical zeolites synthesized using gemini-surfactants could

catalyze reactions that require very strong acidity such as alkane cracking and MTG reaction. Additionally, hierarchical zeolites can show remarkably higher hydrothermal stability than conventional zeolites because mild acid sites (mainly external) are less prone to be dealuminated [55]. Moreover, an earlier study by Suzuki et al. [56] reported that mesoporous HZSM-5 prepared using amphiphilic organosilane template molecules showed less Brønsted acid sites concentration than that of conventional HZSM-5. Density functional calculations revealed that the change of acid sites strength over mesoporous HZSM-5 could be ascribed to the attachment of Al-OH and Si-OH defect sites to Brønsted acid sites.

2.3 Modern strategies for the synthesis of hierarchical zeolites

Many efforts have been made to develop novel strategies for synthesizing hierarchical zeolites in order to widen their applications. Many excellent reviews have been published in recent years covering various aspects of hierarchical zeolite synthesis methods as well as their applications [29, 37, 57-66]. In this section, we aim to give a summary of the emerging synthesis strategies for hierarchical zeolites with successful examples. A great number of strategies have been developed for tailoring zeolites with secondary porosity in the past two decades. For example, various approaches have been utilized to modify ZSM-5 to enhance its efficiency for the catalytic pyrolysis of biomass; two of these approaches commonly used in petrochemistry are outer surface passivation and diffusion enhancement [67-72].The methods involved in generating hierarchical zeolites are classified as top-down and bottom-up techniques [73]. Hydrothermal modifications from hard-templating and soft-templating methods are categorized as bottom-up approaches, while post-synthesis treatments involving dealumination and desilication are categorized as top-down strategies. These strategies are schematically presented in Fig. 2.2.
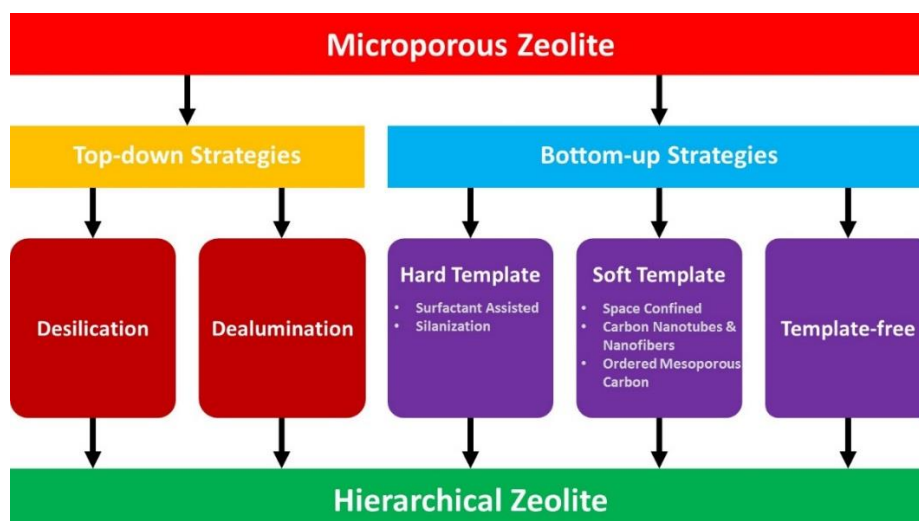
Fig. 2.2 The schematic representation of various hierarchical zeolite formation strategies.

2.3.1 Hard templates

Hard template methods are performed by introducing solid materials, usually with a relatively rigid structure, into the zeolite mother gel to act as mesoporous/macroporous templates during the zeolite crystallization process. The general procedures for using hard template methods are as follows: first, introducing zeolite precursor gel into the matrix of the templates; second, ageing the zeolite mother liquor with the templates for a certain time period at either room temperature or low temperature (usually below 100 °C), followed by a crystallization process performed by hydrothermal treatment in a controlled atmosphere; and finally, removal of the templates by combustion or dissolution treatment. The use of hard template methods have been extensively studied in recent years, and carbonaceous materials are one of the most investigated type of hard templates. Carbonaceous templates include carbon nanoparticles, nanotubes, nanofibres, mesoporous carbons, aerogels, etc. All these materials have been used for hierarchical zeolite tailoring, and various hierarchical zeolites have thereby been obtained. The most valuable properties of carbonaceous templates are their structural diversity, chemical inertness and simple removal. However, their drawbacks, such as hydrophobicity, also limit

their applications. Examples of advantages and disadvantages will be given in the subsections below.

The application of carbon black for hierarchical zeolite synthesis was first reported by Madsen and Jacobsen [74]. They used commercial carbon blacks (Black Pearls 700 and Black Pearls 2000) as a matrix for the confined-space synthesis of nan-osized ZSM-5. The commercial carbon black templates were impregnated with ZSM-5 precursor gel by the incipient wetness technique. After ageing for 3 h, the mixtures were hydrothermally treated at 180 °C for 48 h. Then, the products were washed with DI water and ethanol, followed by a calcination step at 550 °C. The as-prepared zeolites had a particle size between 8 and 30 nm, and the BET surface area increased from 185 to 412 m^2/g. The hierarchical framework was successfully made, and the source of mesoporosity/macroporosity was ascribed to the interconnection between nano-ZSM-5 particles. The confined-space method was further employed by the same authors for nano-sized zeolite beta, zeolite X and zeolite A [75]. The mechanism behind the 'confined-space' method is that hard templates restrict the growth of zeolite crystals during the crystallization process inside the cavities, resulting in the generation of nano-sized particles. The compact zeolite nanoparticles then led to the formation of hierarchical structure. The hierarchical zeolites were produced after the combustion of the carbon black. However, it was observed that the nano-sized zeolite particles made by the above method had only little connection with each other, which would potentially cause instability and durability problems after long-term catalysis. A modification was made by adding excess zeolite synthesis gel into a carbon black matrix during the impregnation step instead of using an equal or lower amount of zeolite synthesis gel compared to the carbon pore volume. This strategy successfully improved the encapsulation of zeolite particles during the growth procedures, and a broad mesopore distribution (5 – 50 nm) was achieved for both hierarchical ZSM-5 and TS-1 zeolites [76, 77]. Fig. 2.3 shows a schematic diagram of hierarchical zeolite templated by carbon black

with excess zeolite precursor gel added. The excess of zeolite gel grew around the carbon particles from inside to outside of the carbon matrix and over the whole system. Zeolite crystals were nucleated inside the pore system of carbon templates, and further connected during the crystallization step. After combustion treatment, the carbon templates were completely removed to leave the hierarchical zeolites, as the crystal size of ZSM-5 particles is ~300 – 1200 nm, and the mesopore volume is 1.01 cm^3/g. Extensive research on the confined-space method has been adapted for different type of zeolites and zeolitic materials, such as MFI (ZSM-5 and silicalite-1) [43, 78-81], MEL (ZSM-11, silicalite-2 and TS2) [79, 82], MWT (ZSM-12), BEA (beta), AFI (AlPO-5) and CHA (AlPO-34). These modified hierarchical zeolites or zeolitic materials showed significant improvements in diffusion and catalytic performance compared to conventional microporous zeolites due to the introduction of secondary porosity. However, the drawbacks of the zeolites made from this method are that they usually have a very broad porosity dispersion, and some of the secondary porosity can only be accessed by first passing through micropores, in which cases the secondary porosity basically does not contribute to mass transfer.
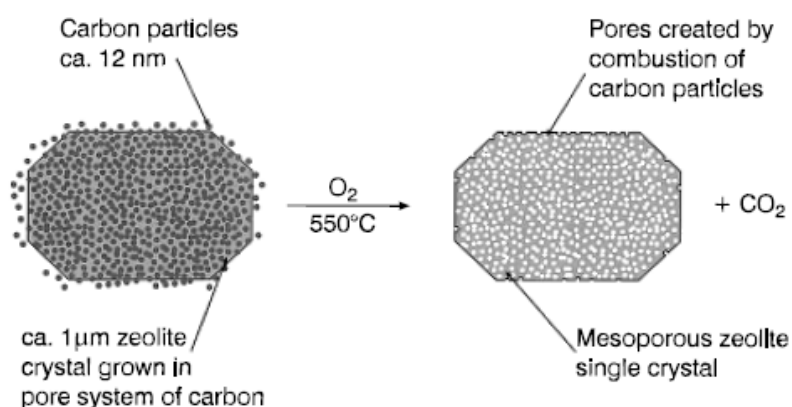
Fig. 2.3 Growth of zeolite crystals around carbon particles. A hierachical network was generated after the combustion of the carbon particles. (Adapted from Ref. [77]. Copyright 2000 American Chemical Society)

Carbon nanotubes and nanofibres have also been used as hard templates for the synthesis of hierarchical zeolite [78, 83-85]. Carbon nanotubes were first used as a template for mesoporous zeolite synthesis by Schmidt et al. [83], who used commercial multiwall carbon nanotubes (MWNTs) pretreated with hydrochloric acid for 24 h. The procedure was repeated until no colored impurities were observed. Then, the as-prepared MWNTs were impregnated with silicalite-1 precursor gel, and the mixture was hydrothermally treated at 175 °C for 24 h. The products were then collected after washing, drying, and calcination. Fig. 2.4(left) shows the schematic illustration of the zeolite synthesis by introducing carbon nanotubes. It shows that carbon nanotubes penetrated the zeolite crystal and that uniform mesopores were generated after the removal of the templates. TEM images (Fig. 2.4(right)) showed that straight mesopore channels were successfully synthesized, and the disordered orientation of these channels clearly showed that the zeolites crystallized around the MWNTs. It was worth noting that the impregnation of carbon nanotubes is a critical procedure, as there would be no mesopores formed if the nanotubes were just simply dip-coated with zeolite precursor gel [86, 87]. The ratio of carbon nanotubes to zeolite gel was considered to determine the amount of mesopores in zeolite crystals. Janssen et al. [78] reported a comparison of mesoporous silicalite-1 (S-1) crystals templated by carbon nanofibres and carbon black, respectively. The results showed that nanofibres-templated S-1 has a lower tortuosity of mesopores than the ones templated by carbon black. In addition, the amount of ink-bottle type mesopores began to increase as zeolite crystal size grew larger due to the high likelihood of agglomeration of the carbon black particles. Schmidt et al. [85] reported that SAPO-34 zeolites could be templated by both carbon nanotubes and carbon nanoparticles and described their application in the methanol-to-olefins (MTO) reaction. The results showed that carbon nanotube-templated SAPO-34 exhibited significant improvement in the kinetic uptake of n-butane and in the conversion of methanol compared to SAPO-34 synthesized by carbon nanoparticles, as the mesopores generated by the

carbon nanoparticles were mostly located inside the zeolite network instead of penetrating through it. Carbon nanotube-templated SAPO-34 generated more accessible mesopores from the surface of zeolite particles.
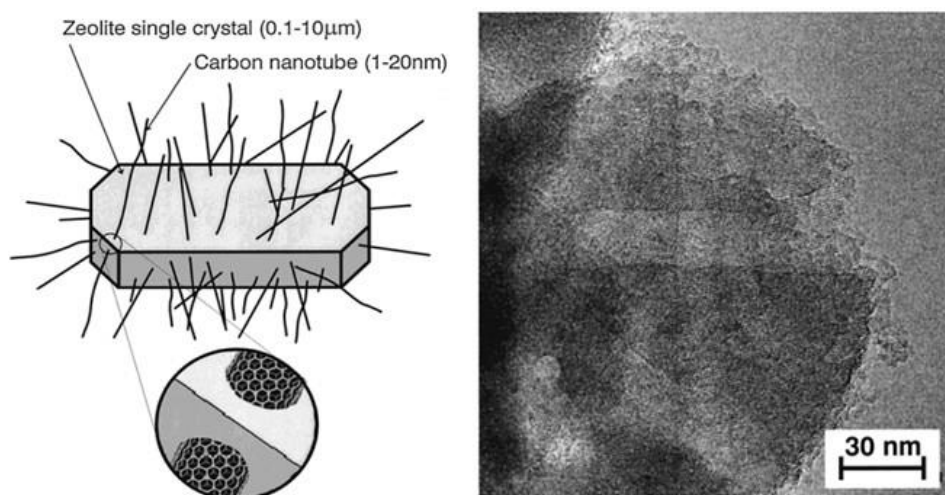
Fig. 2.4 Schematic illustration of the synthesis principle for mesoporous zeolite using carbon nanotubes (left) and TEM image of silicalite-1 single-crystal encapsulated around carbon nanotubes (right). (Adapted from Ref. [83]. Copyright 2001 American Chemical Society)

Ordered mesoporous carbon and colloidal silica particles have also been used as hard templates for the synthesis of hierarchical zeolites [88-95]. Not only do ordered mesoporous carbons have highly ordered networks, but also the hierarchical zeolites made from them generally have a smaller mesoporous dimension and narrower pore size dispersion than those made from commercial carbon black. In addition, the hierarchical zeolite structure can be tailored by changing the synthesis conditions of mesoporous carbon. For example, the formation of ZSM-5 with unique supermicropores templated by mesoporous carbon was reported by Yang et al. [90]. The resulting mesoporous ZSM-5 can be tailored to have a bi-modal or tri-modal pore distribution, and large mesopores can be tuned by changing the nature of the mesoporous

carbon templates. Fang et al. [91] reported a synthesis method for mesoporous zeolite with a completely crystalline wall structure, denoted by OMZ-1, which was synthesized by the recrystallization of SBA-15 using in situ-formed CMK-5 as the carbon template. In this case, CMK-5 has double roles, serving as a hard template and kinetically controlling the crystallization process. A slight structural difference was observed between SBA-15/CMK-3 and SBA-15/CMK-5 (Fig. 2.5), which led to the differing ratios between the nucleation and growth rates of zeolite crystals, thereby affecting the crystal dimensions. Fan et al. [93] reported the hierarchical nanofabrication of zeolite crystals grown confined within three-dimensionally ordered mesopores (3DOm). By this method, silicalite-1 nanoparticles with tunable size and uniform shape were synthesized. This study provided new insight into the constricted crystal growth mechanism underlying confined synthesis. Chen et al. [94] reported another study on 3DOm carbon templated zeolites. BEA, LTA, FAU, and LTL zeolites were synthesized in the confined space of 3DOm carbon by conventional hydrothermal treatment and then compared. Fig. 2.6 clearly shows that the different types of zeolites were well formed, and the insets show the single-crystal pattern. However, the drawbacks of the confined-space method using 3DOm carbon include high time consumption and high cost, and thus, this methodology is not proposed for commercial implementation at this time. A less expensive and easier way to prepare mesoporous carbon templates was reported by Zhu et al. [96]. The mesoporous carbon was prepared by mixing sucrose and ammonia. After a certain period of hydrothermal treatment, brown solids were produced, and after crushing and heating treatment at 850 °C under a N_2 environment, porous black carbonaceous solids were successfully produced. The as-prepared carbon black had a BET surface area of 416 m^2/g and a broad pore size distribution range within 10-100 nm. Another approach using similar low-cost feedstock materials was reported by Wang et al. [97] for synthesizing hierarchical TS-1.
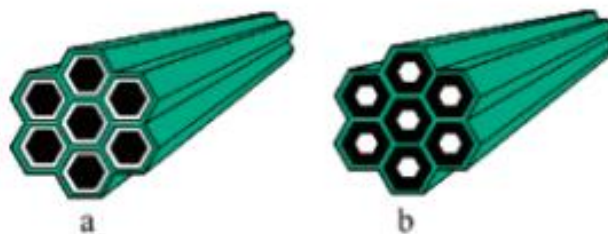
Fig. 2.5 Structural difference between (a) SBA-15/CMK-3 and (b) SBA-15/CMK-5 nanocomposites. (Adapted from Ref. [91]. Copyright 2006 American Chemical Society)
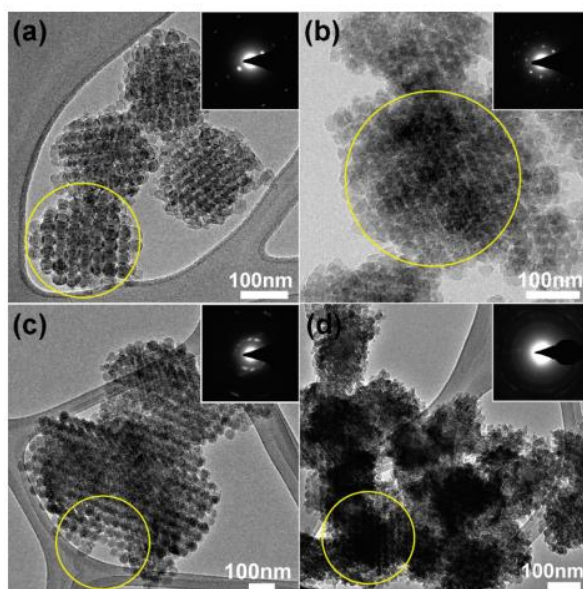
Fig. 2.6 TEM images of 3DOm-i (a) LTA, (b) FAU, (c) BEA, and (d) LTL, grown within a 40 nm 3DOm carbon template. Insets: electron diffraction patterns from the circled areas in the corresponding TEM images. (Adapted from Ref. [94]. Copyright 2011 American Chemical Society)

Hierarchical zeolites have also been developed using other hard templates, such as aerogel monoliths [98-101], polystyrene beads [102, 103], resin beads [104, 105], urea-formaldehyde resin [106, 107] and $CaCO_3$ [108], among others. Some biological materials were also tested

as templates, such as bacteria [109], wood [110, 111], sugarcane bagasse [112], leaves [113, 114] and carbonized rice husks [115]. In most of the hierarchical zeolites synthesized by these hard templates, the secondary porosity contained a broad range of pore size. In addition, the lack of thermal and mechanical stability data make these alternative templates difficult to compare to conventional carbon templates.

2.3.2 Soft templates

In addition to hard templates, soft templates have been extensively used for synthesizing hierarchical zeolites or zeolitic materials. Soft templates offer advantages such as flexibility and diversity. Surfactants and polymers are the two most common and important soft templates. Novel soft templates such as silanized zeolitic seeds, organosilanes, silylane cationic polymers, and amphiphilic organosilanes have also been developed in recent years and recognized as useful and effective methods to introduce secondary porosity into zeolite networks.

The first attempt to synthesize ordered mesoporous molecular sieves using a surfactant was reported by Kresge et al. [116]. They proposed that the silicate material forms inorganic walls among ordered surfactant micelles, leading to the formation of mesopores after calcination. However, the solids made by this method showed low-angle diffraction peaks, and their pore walls were amorphous; thus, they were not considered truly zeolitic materials. The underlying mechanism of using surfactants to create mesoporous materials is that the surfactant molecules tend to form micelles in aqueous solution. The micelles act as mesopore templates during crystallization and are removed afterwards via calcination, and the space they occupied then becomes the mesopores in the solids. Many researchers have been inspired by this idea and proposed new strategies to introduce secondary porosity into zeolites or zeolitic materials by combining the use of structure-directing agents (SDAs) and various surfactants in the zeolite precursor gel at the very first stage, which is known as the dual templating method. In this

method, the surfactants are responsible for templating the mesostructure, while the SDAs build up the whole zeolite along the pore walls of the mesostrucutre.

The dual templating method was first used to introduce secondary porosity into a zeolite crystal network soon after [117-119]. However, the hierarchical structure was not successfully created due to the phase-segregation of the zeolite crystals and zeolitic materials with amorphous pore walls. More modifications have been attempted, including the kinetic control of zeolite seeds, usage of cationic polymers and optimization of reaction conditions to obtain a hierarchical zeolite structure [120-128]. However, those methods were found to have drawbacks such as creating a negligible amount of micropores, producing a structure rich in defects, consuming excessive time or depending heavily on synthesis conditions. Choi et al. [34] for the first time reported the utilization of a dual-porogenic surfactant ($C_{22}H_{45}$-$N^+(CH_3)_2$-$C_6H_{12}N^+(CH_3)_2$-C_6H_{13}) to directly synthesize MFI zeolite nanosheets on the mesoporous and microporous length scales. Later on the same group [129] reported a strategy to synthesize a hierarchical zeolite with similar dual-porogenic surfactant, which has a molecular formula of $C_{18}H_{37}$–$N^+(CH_3)_2$–C_6H_{12}–$N^+(CH_3)_2$–C_6H_{12}–$N^+(CH_3)_2$–$C_{18}H_{37}(Br^-)_3$ (abbreviated as 18–N_3–18). This surfactant has a head group of three quaternary ammoniums and two hydrophobic tails, which allow it to function as both SDA and mesostructure agent. The as-prepared zeolites had enhanced mesoporosity and matchable MFI XRD patterns. Moreover, the mesopore size was tunable in the range of 3.8-21 nm by varying the hydrophobic alkyl chain and swelling agents. Fig. 2.7 shows the structure of the 18–N_3–18 surfactant, along with the successful introduction of secondary porosity into the ZSM-5 network.
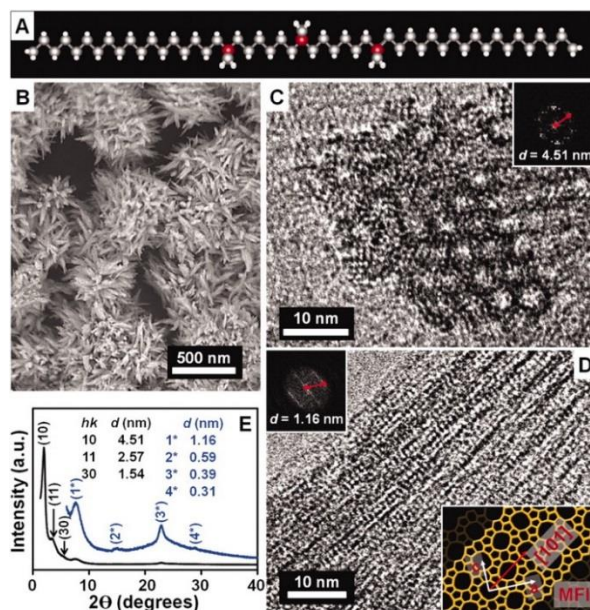
Fig. 2.7 (a) 18–N$_3$–18 surfactant (white spheres, hydrogen; gray spheres, carbon; red spheres, nitrogen). (b) SEM, (c and d) TEM, [(c) and (d), insets] Fourier diffractogram, and (e) XRD pattern of hexagonally ordered crystalline MMS after surfactant removal. (Adapted from Ref. [129]. Copyright 2011 American Association for the Advancement of Science)

Hierarchical zeolites synthesized by the crystallization of silanized zeolite seeds were first reported by Serrano et al. [130]. This strategy was inspired by the occurrence of small proto-zeolitic units (approximately 2-5 nm) in the early stages of zeolite crystallization observed in previous studies [131-134]. The addition of organosilanes during the initial stages of zeolite crystallizaiton can lead to anchoring on the external surface of the zeolitic seeds, preventing the growth of large zeolite crystals. Fig. 2.8 illustrates a schematic diagram of the silanization of ZSM-5 nanocrystals to form mesoporous channels. The hierarchical zeolites made by this method showed enhanced surface area, porosity and catalytic activity. Generally, there are four steps involved in this method: (i) the pre-crystallization of zeolite gel to form zeolitic seeds; (ii) the functionalization of the external surface of the zeolitic seeds with an organosilane such as phenylaminopropyl-trimethoxysilane; (iii) the hydrothermal treatment of the functionalized

zeolitic seeds to complete the crystallization process; and (iv) the calcination of the products to remove SDAs and organosilane. The synthesized hierarchical ZSM-5 samples have particle sizes of approximately 300-400 nm, aggregated by ultrasmall nanounits below 10 nm with a high degree of intergrowth, giving rise to larger sponge-like hierarchical crystals [130]. The as-prepared hierarchical ZSM-5 samples showed significant improvement on textural properties; the BET surface area and mesopore volume were increased from 435 to 670 m^2/g and from 0.25 to 0.51 cm^3/g, respectively. It was also found that the organosilane was grafted only onto the external surface of the zeolitic seeds at the early stage and not inside the nanounit pores, which was confirmed by the 2D spectrum. Moreover, the sizes of both the nanounits and the mesopores could be tuned by changing the synthesis conditions, such as the temperature, the concentration or the organic moiety nature of the silanization agent [135, 136]. The same group also reported that the addition of alcohols such as 2-propanol or methanol during the silanization stage could enhance the textural properties due to the strong interaction between organosilane and linear alcohols. This leads to the generation of a stable and hydrophobic protective layer on the external surface of the zeolitic seed [137]. In addition, it was reported that the aluminium dispersion in hierarchical ZSM-5 made by this method was less uniform than in conventional ZSM-5 due to the decreased Si/Al connectivity over the secondary surface, and the aluminium present in hierarchical ZSM-5 is very susceptible to calcination conditions [127, 138].
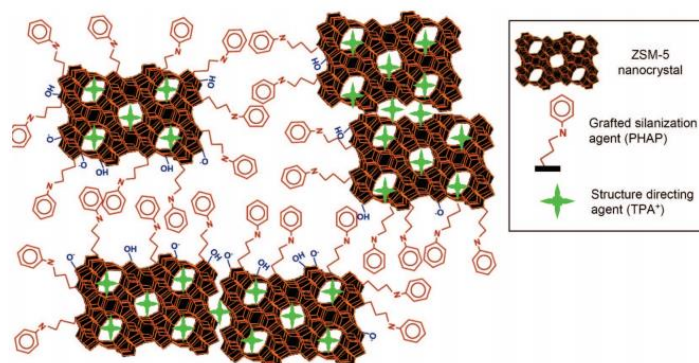
Fig. 2.8 Schematic diagram showing the distributions of the TPA$^+$ zeolite-structure-directing and PHAPTMS surface-silanization species with respect to the interior nanopores and exterior surfaces of ZSM-5 zeolite nanocrystals. (Adapted from Ref. [136]. Copyright 2009 American Chemical Society)

Silane-functionalized polymer was also reported as a soft template for synthesizing hierarchical ZSM-5 with intracrystal mesopores [139]. A silylated polymer made from (3-glycidoxypropyl) trimethoxysilane and polyethyleneimine was added to the zeolite precursor gel. After hydrothermal treatment of the mixture and subsequent calcination, a hierarchical ZSM-5 network with a mesopore size of ~2 nm and a very narrow pore size distribution was successfully synthesized. The underlying mechanism is illustrated in Fig. 2.9. The presence of –SiO$_3$ units in the polymer could be grafted onto the proton-zeolite surface via covalent Si-O-Si linkages during the nucleation of the zeolite phase. The incorporated polymer became phase-segregated from the zeolite matrix as the crystallization of zeolite progressed, forming an intracrystal polymer network that was covalently linked inside the zeolite crystals. The space that was occupied by the polymer porogen became intracrystal mesopores after the calcination procedure. It was found that the size of the mesopore could be tuned by changing the degree of silylation of the polymer. The silylated polymer-templated MFI zeolites were then used for selective petroleum refining [140]. The as-prepared mesoporous zeolites exhibited enhanced

29

reactivity and product selectivity compared to conventional ZSM-5 due to the introduction of uniform small intracrystal mesopores created by the silylated polymer.
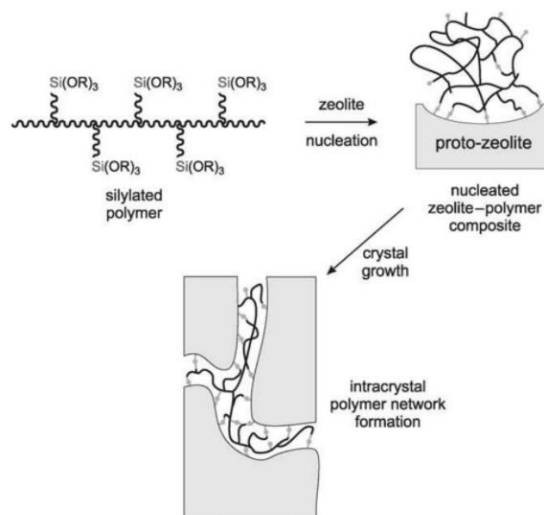
Fig. 2.9 Conceptual approach to the synthesis of a zeolite with intracrystal mesopores using a silylated polymer as the mesoporogen. (Adapted from Ref. [139]. Copyright 2006 Wiley-VCH)

In addition to the dual templating method and the silylated polymer templating method, the amphiphilic organosilane method was first reported by Choi et al. [141] for the direct synthesis of mesoporous zeolites with tunable mesostructures. The dual templating systems worked in a competitive manner instead of the expected cooperative one, which led to the formation of amorphous mesoporous material, bulk zeolite or physical mixtures thereof. The amphiphilic surfactant molecules have the benefits of both SDA and common surfactants. They contain a hydrolysable methoxysilyl moiety, an SDA group such as quaternary ammonium and a hydrophobic alkyl chain moiety. The methoxysilyl moiety can link the amphiphilic molecules with zeolite domains by the formation of covalent bonds with SiO_2 and Al_2O_3 sources. The authors synthesized ($[(CH_3O)_3SiC_3H_6N(CH_3)_2C_{16}H_{33}]Cl$, TPHAC) and structural analogues for the templating of mesoporous MFI and LTA zeolites. These molecules contained a surfactant-like long-chain alkylammonium moiety linked to a hydrolysable methoxysilyl group by a Si-C

bond, which is reported to be chemically stable during the zeolite synthesis process. These amphiphilic organosilanes were added to the initial stage of the zeolite precursor gel, followed by conventional zeolite hydrothermal treatment. Fig. 2.10 shows the LTA mesoporous particle made by the above method. These images clearly show the successful production of the mesostructure with a uniform particle size distribution. The later test reactions showed that mesoporous ZSM-5 zeolites made by this preparation method have better acidity and selectivity than bulky zeolites, MCM-41 and ZSM-5 dual templated materials. In addition, it was found that the mesopore size could be tuned within the range of 2-20 µm by changing the chain length of the organosilanes and the hydrothermal synthesis temperature. This strategy was applied for the synthesis of sodalite, BEA and FAU [142-144]. However, the drawback of this method is the high cost of the SDAs, which are made in multiple alkylation steps, making them economically unviable for industrial application. Recently, Meng et al. [145] reported a hierarchical ZSM-5 synthesis strategy using cetyltrimethylammonium (CTA) – a similar amphiphilic template with a single quaternary ammonium head group, mixed with KOH instead of the traditional alkaline solution NaOH as a mesoporogen and structure-directing agent. Fig. 2.11 illustrates how CTAOH worked better with KOH than NaOH. The as-prepared ZSM-5 zeolite showed excellent catalytic performance in methanol-to-hydrocarbons reactions due to the successful introduction of secondary porosity.
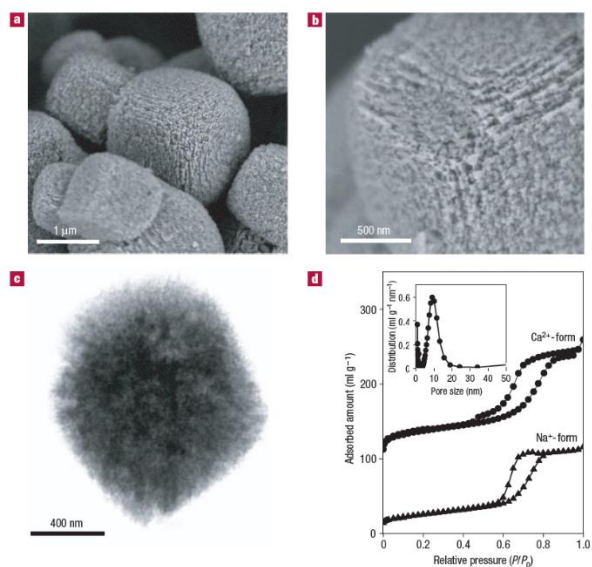
Fig. 2.10 Mesoporous LTA zeolite synthesized using [(CH$_3$O)$_3$SiC$_3$H$_6$N(CH$_3$)$_2$C$_{16}$H$_{33}$]Cl. (a), (b) SEM images, (c) TEM image, and (d) pore size distribution from N$_2$ adsorption isotherm. Inset: Mesopore diameter distribution of Na$^+$ form. (Adapted from Ref. [141]. Copyright 2006 Springer Nature)
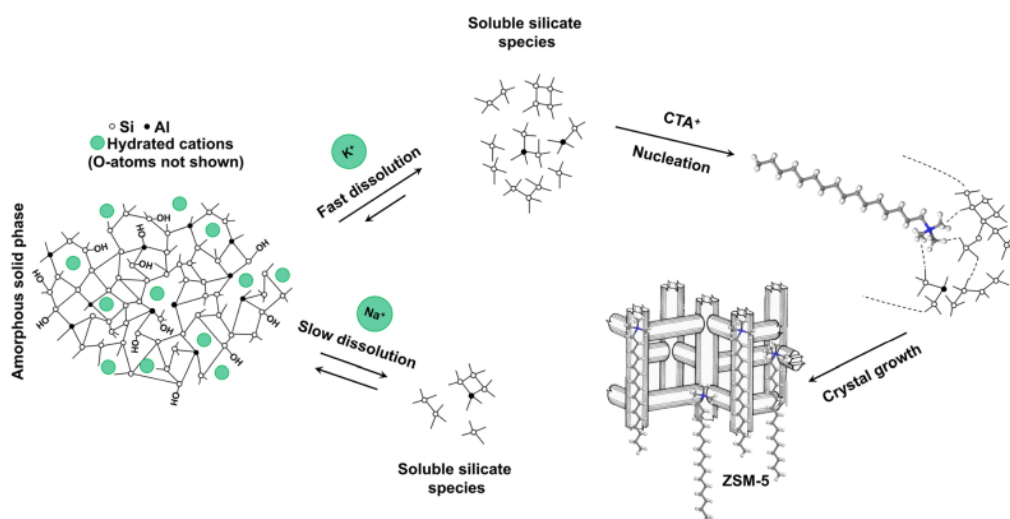
Fig. 2.11 Mechanism of hierarchical ZSM-5 zeolite formation in the presence of CTAOH and KOH and of amorphous silica formation in the presence of NaOH. (Adapted from Ref. [145]. Copyright 2017 American Chemical Society)

2.3.3 Template-free methods

Hierarchical zeolites can also be directly synthesized without using any templates for mesopores generation. Template-free methods are mainly based on three strategies: (1) intercrystalline mesoprosity that generated from nanocrystals aggregation [146-148]; (2) intracrystalline mesoporosity embedded via controlling crystallization of amorphous gels [149]; (3) mesoporosity formed among self-pillared zeolite nanosheets which were made from rotational intergrowths of certain type of zeolites [150, 151].

Even though the aggregation or self-assembly of nanocrystals is a widely used method to form zeolites with intercrystalline mesoprosity that avoids the utilization of meso- or macroporogens, the drawback of this method is also obvious. The unstable intercrystalline meso-/macropores can be easily lost due to the very tight agglomeration among the nanocrystals [152]. However, such drawbacks can be overcomed via the synthesis of intracrystalline mesopores, which were preserved during the dry synthesis gel process [149]. Synthesis of ultrasmall EMT zeolites (6 to 15 nm) without using expensive organic templates has been reported by Ng et al. [153], which demonstrated the importance of controlling the very early stages of zeolite crystallization in colloidal systems to access the nanoscale zeolite phase. The zeolite materials obtained from this way might exhibit intercrystalline mesoporosity, if the ultrasmall nanocrystals are assembled in the form of aggregation.

The preparation of self-pillared zeolite nanosheets is another excellent way to generate mesopores without using any templates. Tsapatsis et al. [150] have reported the utilization of rotational intergrowths of zeolites to fabricate self-pillared zeolite MFI nanosheets, the mesopores were formed among these nanosheets as shown in Fig. 2.12. The formation of such a unique morphology is attributed the generation of MEL-type zeolite domains within the MFI structure, due to MFI and MEL are isotructural (structure twins). This rotational intergrowth

strategy has been extended to fabricate hierarchical FAU/EMT zeolites later on by the same group [154]. This template-free method is facile and effective, however there are disadvantages such as: these zeolites are usually difficult to prepare, post-treatment for organic molecules removal is required, and only very few zeolite types are suitable for synthesis via this method.
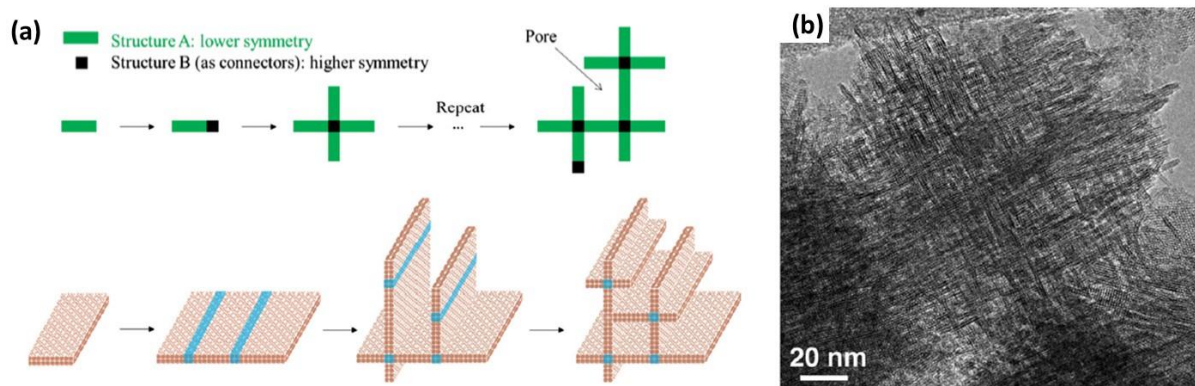
Fig. 2.12 (a) Schematic illustration of the formation of template-free self-pillared hierarchical zeolites by rotational intergrowth. (Adapted from Ref. [151]. Copyright 2014 Wiley-VCH) (b) TEM image of self-pillared zeolite MFI. (Adapted from Ref. [150]. Copyright 2012 American Association for the Advancement of Science)

Synthesizing layered zeolite crystals from growth modifying agents (molecular modifiers) is another promising way to obtain hierarchical structure zeolites. Molecular modifiers can selectively be absorbed on certain crystal faces and further change their growth rate [155]. When the layered crystals obtained from this method assembled as stacking shape, the meso-/macro porosity may exist between the layers.

2.3.4 Dealumination

Demetallation consists of dealumination and desilication, which are two relatively traditional approaches of hierarchical zeolites synthesis. Dealumination has been considered as one of the most useful methods for incorporating hierarchy into conventional zeolites. It has been extensively applied for synthesizing zeolites with a high Si/Al ratio, good stability and enhanced mesoporosity [156-158]. Steaming, calcination and acid leaching are three ways to hydrolyse Al-O-Si bonds in the zeolite structure to achieve dealumination. Dealumination was originally used to increase the Si/Al ratio in zeolite to obtain a more stable structure, but it was later found that some random mesopores were unexpectedly created [57]. The steaming process is usually carried out above 500 °C, at such high temperature that the Al-O-Si bonds are broken, resulting in the loss of aluminium, which then lead to the generation of defects in the zeolite structure. The movement of less stable silicon to the sites that used to be occupied by aluminium results in the formation of silanol-rich domains. The described process can heal part of the amorphous structure, and many mesopores are generated during it [159]. The formation of mesopores is schematically presented in Fig. 2.13. The formation of new mesopores upon steam treatment has been reported by Sheng et al. [160]. The increasing in steaming temperature results in the coexistance of micro and mesopores. The loss of acid sites and the ratio of Brønsted to Lewis acid sites was also evident post-steaming treatment. The zeolites (HZSM-5) after steaming exhibited excellent catalytic performance during ethylene production from dehydration of ethanol. The formation of new mesopores accommodated the coke that generated during the reaction, and thus coke deposition was suppressed over micropores in steam treated HZSM-5 as compared to parent HZSM-5.
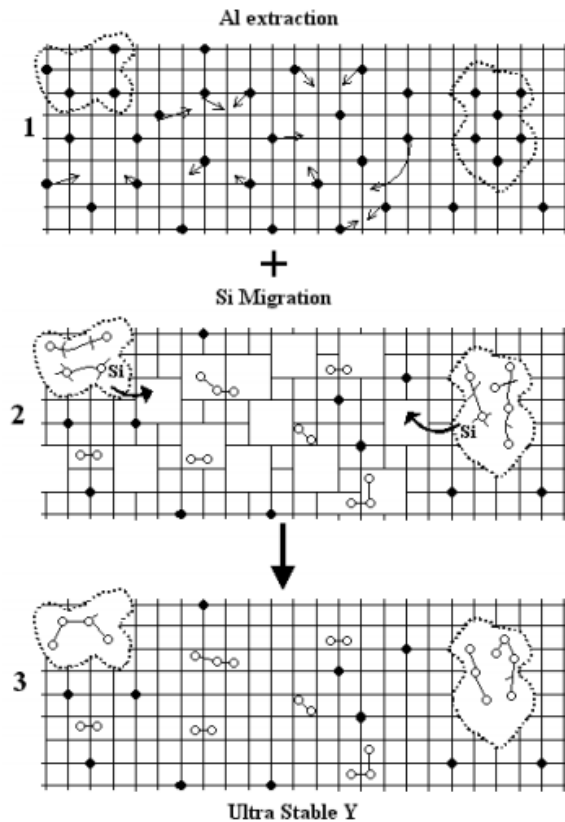
Fig. 2.13 Schematic illustration of the formation of mesopores. The grid denotes the zeolite framework, the black dots are framework aluminium atoms, the open circles are aluminium atoms extracted from the framework, and the dotted lines indicate the mesopores. (Adapted from Ref. [159]. Copyright 2003 Taylor & Francis Online)

The steaming method is usually combined with acid treatment due to the debris generated during the process, which could potentially deposit on the surface of the zeolite particles or inside the channels, leading to blockage. Nitric acid, hydrochloric acid or organic acids such as oxalate, acetic and tartaric acid are commonly used for the debris removal [156]. Since the main purpose of dealumination is to extract aluminium, in most cases, the feedstock zeolites have a low Si/Al ratio.

Dealumination can also be achieved by a calcination process. Müller et al. [161] reported a comparison of the dealumination of the zeolites beta, mordenite, ZSM-5 and ferrierite by a

calcination method. As in the steaming treatment, some mild acid also needs to be applied after the calcination process for debris removal [162]; for example, in this case, they used oxalic acid. The NMR results showed that the extent of dealumination increased with the number of Brønsted acid sites interacting with the zeolite framework, and meanwhile, defects were generated. The zeolite framework became more flexible under different conditions, enabling Brønsted acid sites and oxygen atoms to interact more inside the zeolite network. Zhang et al. [163] also reported that mesoporous ZSM-5 synthesized by thermal treatment could retain its crystallinity up to 1000 °C. The effects of both steaming and calcination treatments were investigated for beta zeolite and it was found that Lewis acid sites increased at the expense of Brønsted acid sites as a result of both steaming and calcination treatments [164]. The post-treated beta zeolite was further subjected to direct transformation of glucose to 5-hydroxymethylfurfural (HMF), and the activity results revealed 55% and 51% selectivity to HMF for beta zeolite calcined at 750 °C and steam treated at 500 °C, respectively.

Acid leaching is another alternative way to remove aluminium from a zeolite framework. As mentioned above, mild acids are usually used for debris removal after steaming or heat treatment. However, it is reported that the presence of concentrated aqueous acids alone can also promote the hydrolysis of Si-O-Al bonds, leading to the extraction of aluminium species from the zeolite network and resulting the generation of mesopores [54, 161, 165-168]. The type of zeolites, nature of acid and pH can all influence the dealumination performance [169, 170]. The dealumination of various commercial zeolites such as beta, mordenite and ZSM-5 using microwave irradiation under acidic environment was studied, and the extent of dealumination was ascribed to the structure of corresponding zeolite and heating methods used [171]. The use of microwave irradiation led to faster dealumination in comparison with conventional heat treatment. Among the three zeolites investigated, beta zeolite was easiest to dealuminate while ZSM-5 showed very low dealumination. The impact of microwave

irradiation on the textural and acidic properties of the post-treated zeolites was evident by the increase in mesoporosity, surface area and Brønsted acid sites for mordenite zeolite treated with HCl under microwave irradiation. Beta zeolite showed lower surface area and insignificant variation in mesoporosity and acidic sites.

Although hierarchical porosity in zeolites can be achieved by dealumination, there are drawbacks to this method. Because of the extraction of aluminium, the acidity of the zeolite materials decreases accordingly. Moreover, the mesopores created by this method generally have a very broad pore size distribution range. Some pores are created inside the zeolite structure and are not connected with external surface, thus they do not contribute to improving the mass transfer.

2.3.5 Desilication

Similar to dealumination, desilication is another well-known way to tailor zeolites with a hierarchical framework by selectively extracting silicon atoms. The potential of desilication as post-synthesis method for the development of secondary mesoporosity has not been recognised for a long time, but in recent decades this approach has been investigated significantly by scientists. The treatment of ZSM-5 crystals in hot alkaline sodium carbonate solution resulted in excessive dissolution of zeolites, due to the presence of aluminium gradient in these crystals as reported by Dessau et al. [172] in the early 1990s. Later on Cizmek et al. [173] investigated the alkaline treatment using concentrated NaOH of silicate-1 and ZSM-5, and discussed the distinguished negative role of aluminium in suppressing silicon dissolution kinetics. These studies to explore the modification in the structure, textural properties and morphology of treated zeolites were reported at the start of 21st century. Ogura et al. [174] first reported that alkaline treatment of zeolites could result in mesoporosity. However, the created mesopores were at the expense of dramatically diminished micropores (~40%). A later study by the same

group found that both silica and aluminium were extracted out from the zeolite framework, but much less aluminium than silica was extracted in an alkaline environment [175]. Most silica atoms were found to have dissolved from the external surface, and thus, the crystallinity of the zeolite was retained. Fig. 2.14 shows the morphological change in ZSM-5 crystals caused by alkaline-treatment under varied conditions such as different times and concentrations. Fig. 2.14 (c) clearly shows that cracks and defects were generated on the outer surface of the zeolite particle. This work also concluded that the increased mesoporosity had little influence on the original microporosity inside the ZSM-5 framework. An enhancement in catalytic performance was found in a later test reaction for cumene cracking, which could be explained by an improvement in diffusivity caused by the introduction of mesopores.
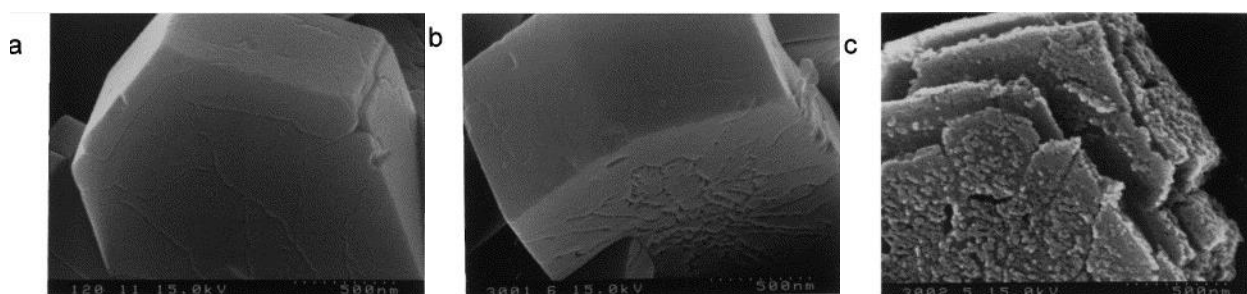
Fig. 2.14 SEM images of alkaline-treated ZSM-5. Treatment was carried out in a 0.1 M NaOH solution at 338 K for (a) 120 min, (b) 300 min and (c) in a 0.2 M solution at 353 K for 300 min. (Adapted from Ref. [175]. Copyright 2001 Elsevier)

A detailed study to explicate the role of various parameters including stirring speed, temperature, time, crystal size, different framework types and framework Si/Al ratio revealed aluminium in the framework to be the key factor in generating mesoporosity during desilication upon alkaline treatment [176, 177]. The selection of appropriate Si/Al ratio is another important factor in directing the framework Si–O–Si bonds towards mesoporosity development. The

extraction of silicon is suppressed by the presence of neighbouring aluminium species in the framework. Groen et al. [178] tested a series of commercial ZSM-5 zeolites with Si/Al ratios ranging from 15 to 1000. They found that the percentage of aluminium inside the zeolite framework played a key role in mesopore formation in MFI zeolite undergoing alkaline treatment. As Fig. 2.15 illustrates, when the Si/Al ratio is below 15, the high concentration of Al atoms in the zeolite framework prevent Si atoms from being extracted, resulting in very limited mesopores generation; however, when the Si/Al ratio is above 200, the excess Si atoms are unselectively extracted, leading to the generation of large pores. A Si/Al ratio of 50 was finally found to be optimal for forming mesoporous structure while preserving the crystallinity of the zeolite.
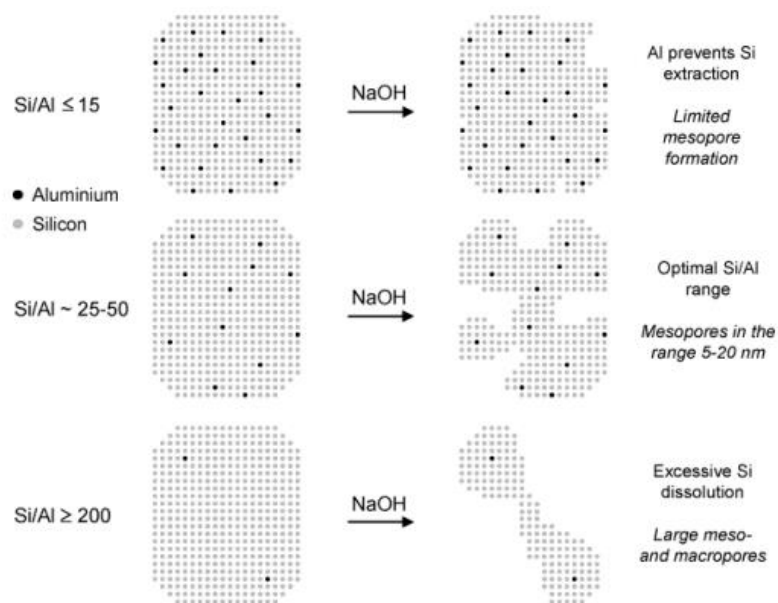
Fig. 2.15 Simplified schematic representation of the influence of the Al content on the desilication treatment of MFI zeolites in NaOH solution and the associated mechanism of pore formation. (Adapted from Ref. [178]. Copyright 2004 American Chemical Society)

The desilication process has been extensively applied to many types of zeolites, including MFI, MTW, MOR, BEA, AST, FER, MWW, IFR, STF, CHA, FAU, TON and TUN [179-192]. The most common procedure for desilication is to treat zeolite samples with 0.2 M NaOH solution for 30 min at 65 °C, with a ratio of zeolite to solution of ~33 g/L. However, different types of zeolites showed different characteristics under the standard desilication treatment conditions. Groen et al. [181] have reported that beta zeolite showed high silicon extraction and generated many mesopores due to the lower stability of aluminium in its framework than in that of ZSM-5 or mordenite, but it also caused high losses of microporosity and crystallinity. Another example is ZSM-22, reported by Verboekend et al. [191]. The generation of mesopore surface area by NaOH treatment is lower than in MFI; after mild acid treatment, the mesopore area increased from 95 to 114 m^2/g, and 90% of the original microporosity was restored, while only 37% of the original Brønsted acidity remained after the treatment. The desilication efficiency is relatively low compared to that in ZSM-5, likely due to morphology of ZSM-22.

Many developments have been achieved in desilication procedures. Hierarchical zeolites with both microporosity and mesoporosity were prepared by the desilication of ZSM-5 in aqueous solutions of organic hydroxides (TPAOH, TBAOH) [193]. The organic base makes the desilication process highly controllable compared to the fast silicon-leaching kinetics in NaOH due to the lower reactivity of organic bases than inorganic ones towards silicon. In addition, the use of organic hydroxides directly introduces the proton into the mesoporous framework without NH_4NO_3 ion-exchange treatment which is a necessary step when using NaOH instead. Moreover, it was observed mesoporous zeolites with higher Si/Al ratios were synthesized due to the lower selectivity of organic hydroxide for silicon extraction. A modified desilication procedure to produce hierarchical zeolite without severe losses of micropore volume was later reported by the same group [194]. Organic cations (TPA^+ or TBA^+) were added along with NaOH as a pore-growth moderator. The hierarchical zeolites synthesized by this novel method

showed improved transport and superior catalytic performance. Verboekend et al. [195] reported that the same method can also be applied to zeolites with a high Si/Al ratio or even pure silica zeolitic materials. The as-prepared silicalite-1 showed enhanced mesoporosity without severe loss of microporosity. However, the drawback of using organic hydroxides as desilication agents is the high cost compared to that of NaOH, even without using NH_4NO_3 for the ion-exchange procedure.

The heating up system also has influence on the synthesis of hierarchical zeolites. Compare to traditional hydrothermal method, microwave-assisted synthesis of zeolites has the advantages of uniform and fast heating of the mother gel, leading to the reduction of crystallization time. In addition, microwave-assisted synthesis tends to give a narrow particle size distribution in the final products. The using of ultrasound bath during the nucleation period also can help the uniform growth of the zeolite crystalline.

The discussion of various synthesis routes to generate secondary porosity in order to attain hierarchical zeolites needs the comparison and critical overview of the strengths and limitations of all studied methods. On the other hand, the analysis of top-down and bottom-up strategies is also important before choosing a particular synthesis strategy. Therefore Table 2.2 presents the advantages and weaknesses associated with all studied synthesis routes.

Table 2.2 Comparison between various synthesis routes of hierarchical zeolites.

Strategy	Synthesis route	Strengths	Weaknesses
Bottom-up	Hard Template	- Structural diversity - Chemical inertness - Simple template removal - Broad mesopores distribution - Tailored structure - Possible variation of Si/Al ratio	- Hydrophobicity - Insignificant contribution of secondary mesoporosity - Low thermal stability - Poor mechanical strength - Less tunable secondary porosity - More expensive
	Soft Template	- Diversity - Enhanced surface area and porosity - Tunable pore size - Tunable mesoporosity	- Structural defects - Time consuming - High cost of production - Unavailability of commercial template
	Template-free	- Low cost - Environmentally-friendly	- Less tunable secondary porosity - Limited to a few zeolites
Top-down	Dealumination	- High Si/Al ratio - Good stability - Enhanced mesoporosity - Low cost - Possibility of Scaling up	- Broad pore size distribution - Poor pore-to-surface interconnectivity - Limited to Al-rich zeolites
	Desilication	- Applicable to wide range of zeolites - Better pore-to-surface interconnectivity - Possibility of Scale up	- Expensive in case of organic templates - Less tunable secondary porosity

2.4 Core-shell zeolites

Hierarchical zeolites can also be synthesized by core-shell modification, i.e., altering the layer properties of core zeolite nanoparticle, sequentially absorbing macromolecules with opposite charges can on the inner-shell with the help of spherical latex beads. These nano-structured composite shells can be further tuned to have controlled thickness. The prefabricated core-shell building blocks were then assembled to close packed structures in the range of macroscopic dimensions. After the removal of organic templates and latex, hierarchical zeolites with tunable shell thickness and pore diameters are produced [196].

In addition, when employing shell zeolites with particular pore size, the composite core-shell structure can be utilized as molecular sieve for selective reaction with molecules that have a distinctive molecular size. For example, Miyake et al. [197] has reported that Zn ion-doped ZSM-5/silicalite-1 core-shell zeolite catalyst (as shown in Fig. 2.16) improved p-xylene and para-selectivity (para-xylene selectivity in xylene isomers) over the methanol to para-xylene (MTpX) reaction. Despite the presence of the shell, silicalite-1 selectively screened out the molecules with larger diameter or a structure with more branches. The coated silicalite-1 shell also covered the acid sites that only exist over the inner core ZSM-5, decreasing the side reactions. Such zeolite core-shell modifications have been studied where designed layers have passivated surface acidity [198-200].
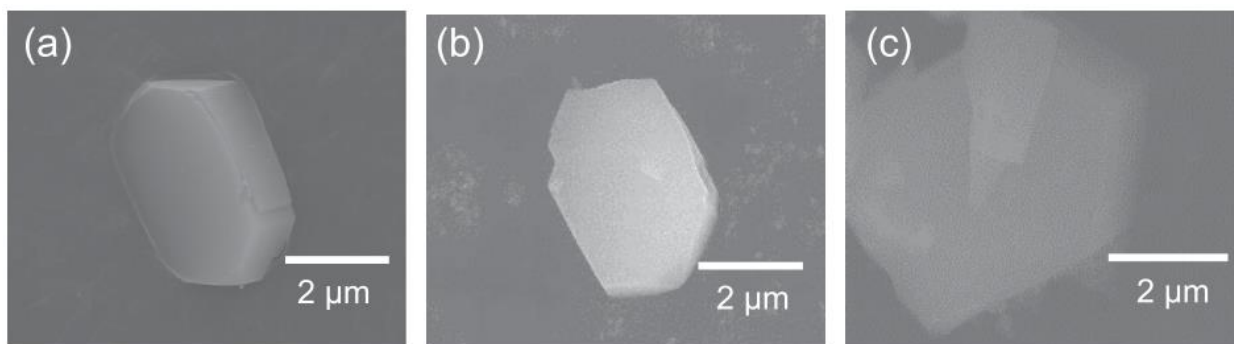
Fig. 2.16 FE-SEM images of (a) ZSM-5, (b) Zn/ZSM-5 and (c) Zn/ZSM-5/silicalite-1. (Adapted from Ref. [197]. Copyright 2016 Elsevier)

Given the advantages that core-shell structure has, this idea has also been introduced to modify metal-organic framework (MOF) materials [201]. It has been reported that core-shell metal/ZIF-8 catalyst has anti-poisoning characteristics and can selectivity catalyze alkene hydrogenation [202]. The core-shell ZIF-8/Pd/ZIF-8 exhibited higher selectivity towards to 1-hexene over cis-cyclooctene during hydrogenation, due to the smaller size of 1-hexene compared to cis-cyclooctene. Meanwhile, the existence of outer ZIF-8 layer showed successful resistance to thiophene and further prevented the Pd that was located over the inner ZIF-8 core from poisoning. Zeolite and MOF hybrids has also been successfully synthesized and showed size selectivity for alkene hydrogenation [203]. The structure composite was synthesized by a combination of seed-induction synthesis strategy and self-assembly methods. The zeolites and zeolitic core-shell materials show the promising application in the field of heterogeneous catalysis.

2.5 References

[1] E.M. Flanigen, J. Jansen, H. van Bekkum, Introduction to zeolite science and practice, Elsevier1991.

[2] S.M. Csicsery, Shape-selective catalysis in zeolites, Zeolites, 4 (1984) 202-213.

[3] C.B. Khouw, M.E. Davis, Shape-Selective Catalysis with Zeolites and Molecular Sieves, ACS Publications1993.

[4] M. Uguina, D. Serrano, R. Van Grieken, S. Venes, Adsorption, acid and catalytic changes induced in ZSM-5 by coking with different hydrocarbons, Appl Catal a-Gen, 99 (1993) 97-113.

[5] A. Kareem, S. Chand, I. Mishra, Disproportionation of Toluene to Produce Benzene and p-Xylene–A Review, (2001).

[6] A. Corma, Inorganic solid acids and their use in acid-catalyzed hydrocarbon reactions, Chem Rev, 95 (1995) 559-614.

[7] C.R. Marcilly, Where and how shape selectivity of molecular sieves operates in refining and petrochemistry catalytic processes, Top Catal, 13 (2000) 357-366.

[8] J. Weitkamp, Zeolites and catalysis, Solid State Ionics, 131 (2000) 175-188.

[9] P. Parthasarathi, Asymptotic and particle methods in nonlinear transport phenomena: membrane separations and drop dynamics, 2008.

[10] D.W. Breck, Zeolite molecular sieves: structure, chemistry and use, Krieger1984.

[11] H. Upadek, B. Kottwitz, B. Schreck, Zeolites and novel silicates as raw materials for detergents, Tenside Surfactants Detergents, 33 (1996) 385-392.

[12] G. Bellussi, M. Rigutto, Metal ions associated to molecular sieve frameworks as catalytic sites for selective oxidation reactions, Stud. Surf. Sci. Catal., 137 (2001) 911-955.

[13] C. Fruijtier-Pölloth, The safety of synthetic zeolites used in detergents, Arch. Toxicol., 83 (2009) 23-35.

[14] T. Humplik, J. Lee, S. O'hern, B. Fellman, M. Baig, S. Hassan, M. Atieh, F. Rahman, T. Laoui, R. Karnik, Nanostructured materials for water desalination, Nanotechnology, 22 (2011) 292001.

[15] N. Rahimi, R. Karimzadeh, Catalytic cracking of hydrocarbons over modified ZSM-5 zeolites to produce light olefins: A review, Appl Catal a-Gen, 398 (2011) 1-17.

[16] B. Chi, H. Qu, X. Xing, Q. Zhong, Assembly of hollow CeO_2@ Fe-ZSM-5 and SCR performance, J. Alloys Compd., 726 (2017) 906-912.

[17] I.H.A. El Maksod, A. Al-Shehri, S. Bawaked, M. Mokhtar, K. Narasimharao, Structural and photocatalytic properties of precious metals modified TiO_2-BEA zeolite composites, Molecular Catalysis, 441 (2017) 140-149.

[18] S. Jeong, S. Yang, D.H. Kim, Depolymerization of Protobind lignin to produce monoaromatic compounds over Cu/ZSM-5 catalyst in supercritical ethanol, Molecular Catalysis, 442 (2017) 140-146.

[19] M. Rasouli, H. Atashi, D. Mohebbi-Kalhori, N. Yaghobi, Bifunctional Pt/Fe-ZSM-5 catalyst for xylene isomerization, Journal of the Taiwan Institute of Chemical Engineers, (2017).

[20] A. Rokicińska, M. Drozdek, B. Dudek, B. Gil, P. Michorczyk, D. Brouri, S. Dzwigaj, P. Kuśtrowski, Cobalt-containing BEA zeolite for catalytic combustion of toluene, Appl. Catal. B Environ., 212 (2017) 59-67.

[21] T.K.R. de Oliveira, M. Rosset, O.W. Perez-Lopez, Ethanol dehydration to diethyl ether over Cu-Fe/ZSM-5 catalysts, Catal. Commun., 104 (2018) 32-36.

[22] S.M. Csicsery, Shape-selective catalysis in zeolites, Prepr. Pap.-Am. Chem. Soc., Div. Fuel Chem.;(United States), 28 (1983).

[23] B. Smit, T.L. Maesen, Towards a molecular understanding of shape selectivity, Nature, 451 (2008) 671-678.

[24] P. Weisz, V. Frilette, Intracrystalline and molecular-shape-selective catalysis by zeolite salts, The Journal of Physical Chemistry, 64 (1960) 382-382.

[25] R.M. Dessau, Shape-selective reactions of zeolites. Selective metal-catalyzed hydrogenation and oxidation using ZSM-5, J. Catal., 77 (1982) 304-306.

[26] S.M. Csicsery, Acid catalyzed isomerization of dialkylbenzenes, The Journal of Organic Chemistry, 34 (1969) 3338-3342.

[27] J. Valyon, J. Mihalyfi, H. Beyer, PA Jacobs Proceedings, Workshop on Adsorption, Berlin, 1979, pp. 134.

[28] P. Hilaireau, C. Bearez, F. Chevalier, G. Perot, M. Guisnet, Transition-state selectivity on HZSM-5 zeolite evidenced by isobutane conversion, Zeolites, 2 (1982) 69.

[29] Y. Wei, T.E. Parmentier, K.P. de Jong, J. Zecevic, Tailoring and visualizing the pore architecture of hierarchical zeolites, Chem. Soc. Rev., 44 (2015) 7234-7261.

[30] A. Zampieri, P. Colombo, G.T. Mabande, T. Selvam, W. Schwieger, F. Scheffler, Zeolite coatings on microcellular ceramic foams: a novel route to microreactor and microseparator devices, Adv. Mater., 16 (2004) 819-823.

[31] A. Corma, S. Iborra, A. Velty, Chemical routes for the transformation of biomass into chemicals, Chem. Rev., 107 (2007) 2411-2502.

[32] J. Perez-Ramirez, C.H. Christensen, K. Egeblad, C.H. Christensen, J.C. Groen, Hierarchical zeolites: enhanced utilisation of microporous crystals in catalysis by advances in materials design, Chem. Soc. Rev., 37 (2008) 2530-2542.

[33] V.N. Shetti, J. Kim, R. Srivastava, M. Choi, R. Ryoo, Assessment of the mesopore wall catalytic activities of MFI zeolite with mesoporous/microporous hierarchical structures, J. Catal., 254 (2008) 296-303.

[34] M. Choi, K. Na, J. Kim, Y. Sakamoto, O. Terasaki, R. Ryoo, Stable single-unit-cell nanosheets of zeolite MFI as active and long-lived catalysts, Nature, 461 (2009) 246-249.

[35] C. Fernandez, I. Stan, J.P. Gilson, K. Thomas, A. Vicente, A. Bonilla, J. Pérez-Ramírez, Hierarchical ZSM-5 Zeolites in Shape-Selective Xylene Isomerization: Role of Mesoporosity and Acid Site Speciation, Chemistry-A European Journal, 16 (2010) 6224-6233.

[36] H. Tao, H. Yang, X. Liu, J. Ren, Y. Wang, G. Lu, Highly stable hierarchical ZSM-5 zeolite with intra-and inter-crystalline porous structures, Chem. Eng. J., 225 (2013) 686-694.

[37] D.P. Serrano, J.M. Escola, P. Pizarro, Synthesis strategies in the search for hierarchical zeolites, Chem. Soc. Rev., 42 (2013) 4004-4035.

[38] N. Chen, W. Kaeding, F. Dwyer, Para-directed aromatic reactions over shape-selective molecular sieve zeolite catalysts, J. Am. Chem. Soc., 101 (1979) 6783-6784.

[39] W. Kaeding, C. Chu, L. Young, S. Butter, Shape-selective reactions with zeolite catalysts: II. Selective disproportionation of toluene to produce benzene and p-xylene, J. Catal., 69 (1981) 392-398.

[40] W. Kaeding, C. Chu, L. Young, B. Weinstein, S. Butter, Selective alkylation of toluene with methanol to produce para-xylene, J. Catal., 67 (1981) 159-174.

[41] J.C. Védrine, A. Auroux, P. Dejaifve, V. Ducarme, H. Hoser, S. Zhou, Catalytic and physical properties of phosphorus-modified ZSM-5 zeolite, J. Catal., 73 (1982) 147-160.

[42] C.H. Christensen, K. Johannsen, I. Schmidt, C.H. Christensen, Catalytic benzene alkylation over mesoporous zeolite single crystals: improving activity and selectivity with a new family of porous materials, J. Am. Chem. Soc., 125 (2003) 13370-13371.

[43] C.H. Christensen, K. Johannsen, E. Törnqvist, I. Schmidt, H. Topsøe, C.H. Christensen, Mesoporous zeolite single crystal catalysts: Diffusion and catalysis in hierarchical zeolites, Catal Today, 128 (2007) 117-122.

[44] D. Mehlhorn, R. Valiullin, J. Kärger, K. Cho, R. Ryoo, Exploring the hierarchy of transport phenomena in hierarchical pore systems by NMR diffusion measurement, Microporous Mesoporous Mater., 164 (2012) 273-279.

[45] Z. Musilová, N. Žilková, S.-E. Park, J. Čejka, Aromatic transformations over mesoporous ZSM-5: advantages and disadvantages, Top. Catal., 53 (2010) 1457-1469.

[46] K.P. de Jong, J. Zecevic, H. Friedrich, P.E. de Jongh, M. Bulut, S. van Donk, R. Kenmogne, A. Finiels, V. Hulea, F. Fajula, Zeolite Y crystals with trimodal porosity as ideal hydrocracking catalysts, Angew. Chem. Int. Ed. Engl., 49 (2010) 10074-10078.

[47] M.Y. Kim, J.-K. Kim, M.-E. Lee, S. Lee, M. Choi, Maximizing Biojet Fuel Production from Triglyceride: Importance of the Hydrocracking Catalyst and Separate Deoxygenation/Hydrocracking Steps, ACS Catalysis, 7 (2017) 6256-6267.

[48] M.Y. Kim, K. Lee, M. Choi, Cooperative effects of secondary mesoporosity and acid site location in Pt/SAPO-11 on n -dodecane hydroisomerization selectivity, J. Catal., 319 (2014) 232-238.

[49] R. Khare, D. Millar, A. Bhan, A mechanistic basis for the effects of crystallite size on light olefin selectivity in methanol-to-hydrocarbons conversion on MFI, J. Catal., 321 (2015) 23-31.

[50] C.H. Bartholomew, Mechanisms of catalyst deactivation, Appl Catal a-Gen, 212 (2001) 17-60.

[51] L. Lakiss, F. Ngoye, C. Canaff, S. Laforge, Y. Pouilloux, Z. Qin, M. Tarighi, K. Thomas, V. Valtchev, A. Vicente, On the remarkable resistance to coke formation of nanometer-sized and hierarchical MFI zeolites during ethanol to hydrocarbons transformation, J. Catal., 328 (2015) 165-172.

[52] H. Karge, Coke formation on zeolites, Stud. Surf. Sci. Catal., 137 (2001) 707-746.

[53] R. Srivastava, M. Choi, R. Ryoo, Mesoporous materials with zeolite framework: remarkable effect of the hierarchical structure for retardation of catalyst deactivation, Chem. Commun., (2006) 4489-4491.

[54] J. Kim, M. Choi, R. Ryoo, Effect of mesoporosity against the deactivation of MFI zeolite catalyst during the methanol-to-hydrocarbon conversion process, J Catal, 269 (2010) 219-228.

[55] K. Kim, R. Ryoo, H.-D. Jang, M. Choi, Spatial distribution, strength, and dealumination behavior of acid sites in nanocrystalline MFI zeolites and their catalytic consequences, J. Catal., 288 (2012) 115-123.

[56] K. Suzuki, Y. Aoyagi, N. Katada, M. Choi, R. Ryoo, M. Niwa, Acidity and catalytic activity of mesoporous ZSM-5 in comparison with zeolite ZSM-5, Al-MCM-41 and silica–alumina, Catal. Today, 132 (2008) 38-45.

[57] R. Chal, C. Gerardin, M. Bulut, S. Van Donk, Overview and industrial assessment of synthesis strategies towards zeolites with mesopores, ChemCatChem, 3 (2011) 67-81.

[58] Z. Le Hua, J. Zhou, J.L. Shi, Recent advances in hierarchically structured zeolites: synthesis and material performances, Chem. Commun., 47 (2011) 10536-10547.

[59] S. Lopez-Orozco, A. Inayat, A. Schwab, T. Selvam, W. Schwieger, Zeolitic materials with hierarchical porous structures, Adv. Mater., 23 (2011) 2602-2615.

[60] D. Verboekend, J. Pérez-Ramírez, Design of hierarchical zeolite catalysts by desilication, Catalysis Science & Technology, 1 (2011) 879-890.

[61] L.-H. Chen, X.-Y. Li, J.C. Rooke, Y.-H. Zhang, X.-Y. Yang, Y. Tang, F.-S. Xiao, B.-L. Su, Hierarchically structured zeolites: synthesis, mass transport properties and applications, J. Mater. Chem., 22 (2012) 17381-17403.

[62] I.I. Ivanova, E.E. Knyazeva, Micro–mesoporous materials obtained by zeolite recrystallization: synthesis, characterization and catalytic applications, Chem. Soc. Rev., 42 (2013) 3671-3688.

[63] K. Möller, T. Bein, Mesoporosity–a new dimension for zeolites, Chem. Soc. Rev., 42 (2013) 3689-3707.

[64] K. Na, M. Choi, R. Ryoo, Recent advances in the synthesis of hierarchically nanoporous zeolites, Micropor Mesopor Mat, 166 (2013) 3-19.

[65] K. Li, J. Valla, J. Garcia-Martinez, Realizing the commercial potential of hierarchical zeolites: new opportunities in catalytic cracking, ChemCatChem, 6 (2014) 46-66.

[66] K. Na, G.A. Somorjai, Hierarchically nanoporous zeolites and their heterogeneous catalysis: current status and future perspectives, Catal. Lett., 145 (2015) 193-213.

[67] J. Jae, G.A. Tompsett, A.J. Foster, K.D. Hammond, S.M. Auerbach, R.F. Lobo, G.W. Huber, Investigation into the shape selectivity of zeolite catalysts for biomass conversion, J. Catal., 279 (2011) 257-268.

[68] A.J. Foster, J. Jae, Y.T. Cheng, G.W. Huber, R.F. Lobo, Optimizing the aromatic yield and distribution from catalytic fast pyrolysis of biomass over ZSM-5, Appl Catal a-Gen, 423 (2012) 154-161.

[69] D.J. Mihalcik, C.A. Mullen, A.A. Boateng, Screening acidic zeolites for catalytic fast pyrolysis of biomass and its components, J. Anal. Appl. Pyrolysis, 92 (2011) 224-232.

[70] A.Q. Zheng, Z.L. Zhao, S. Chang, Z. Huang, H.X. Wu, X.B. Wang, F. He, H.B. Li, Effect of crystal size of ZSM-5 on the aromatic yield and selectivity from catalytic fast pyrolysis of biomass, J Mol Catal a-Chem, 383 (2014) 23-30.

[71] S. Kelkar, C.M. Saffron, Z.L. Li, S.S. Kim, T.J. Pinnavaia, D.J. Miller, R. Kriegel, Aromatics from biomass pyrolysis vapour using a bifunctional mesoporous catalyst, Green Chem., 16 (2014) 803-812.

[72] J. Li, X.Y. Li, G.Q. Zhou, W. Wang, C.W. Wang, S. Komarneni, Y.J. Wang, Catalytic fast pyrolysis of biomass with mesoporous ZSM-5 zeolites prepared by desilication with NaOH solutions, Appl Catal a-Gen, 470 (2014) 115-122.

[73] D.P. Gamliel, H.J. Cho, W. Fan, J.A. Valla, On the effectiveness of tailored mesoporous MFI zeolites for biomass catalytic fast pyrolysis, Appl Catal a-Gen, 522 (2016) 109-119.

[74] C.H. Jacobsen, Nanosized zeolite crystals—convenient control of crystal size distribution by confined space synthesis, Chem. Commun., (1999) 673-674.

[75] I. Schmidt, C. Madsen, C.J. Jacobsen, Confined space synthesis. A novel route to nanosized zeolites, Inorg. Chem., 39 (2000) 2279-2283.

[76] I. Schmidt, A. Krogh, K. Wienberg, A. Carlsson, M. Brorson, C.J. Jacobsen, Catalytic epoxidation of alkenes with hydrogen peroxide over first mesoporous titanium-containing zeolite, Chem. Commun., (2000) 2157-2158.

[77] C.J. Jacobsen, C. Madsen, J. Houzvicka, I. Schmidt, A. Carlsson, Mesoporous zeolite single crystals, J Am Chem Soc, 122 (2000) 7116-7117.

[78] A. Janssen, I. Schmidt, C. Jacobsen, A. Koster, K. De Jong, Exploratory study of mesopore templating with carbon during zeolite synthesis, Micropor Mesopor Mat, 65 (2003) 59-75.

[79] M.Y. Kustova, S.B. Rasmussen, A. Kustov, C.H. Christensen, Direct NO decomposition over conventional and mesoporous Cu-ZSM-5 and Cu-ZSM-11 catalysts: Improved performance with hierarchical zeolites, Applied Catalysis B: Environmental, 67 (2006) 60-67.

[80] J.-B. Koo, N. Jiang, S. Saravanamurugan, M. Bejblová, Z. Musilová, J. Čejka, S.-E. Park, Direct synthesis of carbon-templating mesoporous ZSM-5 using microwave heating, J. Catal., 276 (2010) 327-334.

[81] A. Martínez, M. Arribas, M. Derewinski, A. Burkat-Dulak, Enhanced sulfur resistance of bifunctional Pd/HZSM-5 catalyst comprising hierarchical carbon-templated zeolite, Appl Catal a-Gen, 379 (2010) 188-197.

[82] M.Y. Kustova, P. Hasselriis, C.H. Christensen, Mesoporous MEL–type zeolite single crystal catalysts, Catal. Lett., 96 (2004) 205-211.

[83] I. Schmidt, A. Boisen, E. Gustavsson, K. Ståhl, S. Pehrson, S. Dahl, A. Carlsson, C.J. Jacobsen, Carbon nanotube templated growth of mesoporous zeolite single crystals, Chem. Mater., 13 (2001) 4416-4418.

[84] A. Boisen, I. Schmidt, A. Carlsson, S. Dahl, M. Brorson, C.J. Jacobsen, TEM stereo-imaging of mesoporous zeolite single crystals, Chem. Commun., (2003) 958-959.

[85] F. Schmidt, S. Paasch, E. Brunner, S. Kaskel, Carbon templated SAPO-34 with improved adsorption kinetics and catalytic performance in the MTO-reaction, Microporous Mesoporous Mater., 164 (2012) 214-221.

[86] M. Landau, N. Zaharur, M. Herskowitz, Silica-supported small crystals of ZSM-5 zeolite, Appl Catal a-Gen, 115 (1994) L7-L14.

[87] H. Beyer, J. Nagy, H. Karge, I. Kiricsi, Catalysis by microporous materials, Elsevier1995.

[88] S.-S. Kim, J. Shah, T.J. Pinnavaia, Colloid-imprinted carbons as templates for the nanocasting synthesis of mesoporous ZSM-5 zeolite, Chem. Mater., 15 (2003) 1664-1668.

[89] A. Sakthivel, S.-J. Huang, W.-H. Chen, Z.-H. Lan, K.-H. Chen, T.-W. Kim, R. Ryoo, A.S. Chiang, S.-B. Liu, Replication of mesoporous aluminosilicate molecular sieves (RMMs) with zeolite framework from mesoporous carbons (CMKs), Chem. Mater., 16 (2004) 3168-3175.

[90] Z. Yang, Y. Xia, R. Mokaya, Zeolite ZSM-5 with Unique Supermicropores Synthesized Using Mesoporous Carbon as a Template, Adv. Mater., 16 (2004) 727-732.

[91] Y. Fang, H. Hu, An ordered mesoporous aluminosilicate with completely crystalline zeolite wall structure, J. Am. Chem. Soc., 128 (2006) 10636-10637.

[92] H. Li, Y. Sakamoto, Z. Liu, T. Ohsuna, O. Terasaki, M. Thommes, S. Che, Mesoporous silicalite-1 zeolite crystals with unique pore shapes analogous to the morphology, Microporous Mesoporous Mater., 106 (2007) 174-179.

[93] W. Fan, M.A. Snyder, S. Kumar, P.-S. Lee, W.C. Yoo, A.V. McCormick, R.L. Penn, A. Stein, M. Tsapatsis, Hierarchical nanofabrication of microporous crystals with ordered mesoporosity, Nature materials, 7 (2008) 984-991.

[94] H. Chen, J. Wydra, X. Zhang, P.-S. Lee, Z. Wang, W. Fan, M. Tsapatsis, Hydrothermal synthesis of zeolites with three-dimensionally ordered mesoporous-imprinted structure, J. Am. Chem. Soc., 133 (2011) 12390-12393.

[95] H.S. Cho, R. Ryoo, Synthesis of ordered mesoporous MFI zeolite using CMK carbon templates, Microporous Mesoporous Mater., 151 (2012) 107-112.

[96] K. Zhu, K. Egeblad, C.H. Christensen, Mesoporous carbon prepared from carbohydrate as hard template for hierarchical zeolites, European Journal of Inorganic Chemistry, 2007 (2007) 3955-3960.

[97] X. Wang, G. Li, W. Wang, C. Jin, Y. Chen, Synthesis, characterization and catalytic performance of hierarchical TS-1 with carbon template from sucrose carbonization, Microporous Mesoporous Mater., 142 (2011) 494-502.

[98] Y. Tao, H. Kanoh, K. Kaneko, Uniform mesopore-donated zeolite Y using carbon aerogel templating, The Journal of Physical Chemistry B, 107 (2003) 10974-10976.

[99] Y. Tao, H. Kanoh, K. Kaneko, ZSM-5 monolith of uniform mesoporous channels, J. Am. Chem. Soc., 125 (2003) 6044-6045.

[100] W.-C. Li, A.-H. Lu, R. Palkovits, W. Schmidt, B. Spliethoff, F. Schüth, Hierarchically structured monolithic silicalite-1 consisting of crystallized nanoparticles and its performance in the beckmann rearrangement of cyclohexanone oxime, J. Am. Chem. Soc., 127 (2005) 12595-12600.

[101] R.J. White, A. Fischer, C. Goebel, A. Thomas, A sustainable template for mesoporous zeolite synthesis, J. Am. Chem. Soc., 136 (2014) 2715-2718.

[102] B.T. Holland, L. Abrams, A. Stein, Dual templating of macroporous silicates with zeolitic microporous frameworks, J. Am. Chem. Soc., 121 (1999) 4308-4309.

[103] K.H. Rhodes, S.A. Davis, F. Caruso, B. Zhang, S. Mann, Hierarchical Assembly of Zeolite Nanoparticles into Ordered Macroporous Monoliths Using Core− Shell Building Blocks, Chem. Mater., 12 (2000) 2832-2834.

[104] V. Naydenov, L. Tosheva, J. Sterte, Palladium-containing zeolite beta macrostructures prepared by resin macrotemplating, Chem. Mater., 14 (2002) 4881-4885.

[105] V. Naydenov, L. Tosheva, J. Sterte, Vanadium modified AlPO-5 spheres through resin macrotemplating, Microporous Mesoporous Mater., 66 (2003) 321-329.

[106] Y. Kang, W. Shan, J. Wu, Y. Zhang, X. Wang, W. Yang, Y. Tang, Uniform nanozeolite microspheres with large secondary pore architecture, Chem. Mater., 18 (2006) 1861-1866.

[107] Y. Shi, X. Li, J. Hu, J. Lu, Y. Ma, Y. Zhang, Y. Tang, Zeolite microspheres with hierarchical structures: formation, mechanism and catalytic performance, J Mater Chem, 21 (2011) 16223-16230.

[108] H. Zhu, Z. Liu, Y. Wang, D. Kong, X. Yuan, Z. Xie, Nanosized $CaCO_3$ as hard template for creation of intracrystal pores within silicalite-1 crystal, Chem. Mater., 20 (2007) 1134-1139.

[109] B. Zhang, S.A. Davis, N.H. Mendelson, S. Mann, Bacterial templating of zeolite fibres with hierarchical structure, Chem. Commun., (2000) 781-782.

[110] A. Dong, Y. Wang, Y. Tang, N. Ren, Y. Zhang, Y. Yue, Z. Gao, Zeolitic tissue through wood cell templating, Adv. Mater., 14 (2002) 926-929.

[111] Ó. de la Iglesia, J.L. Sánchez, J. Coronas, Hierarchical silicalite-1 structures based on pyrolized materials, Mater. Lett., 65 (2011) 3124-3127.

[112] F. Ocampo, J.A. Cunha, M.R. de Lima Santos, J.-P. Tessonnier, M.M. Pereira, B. Louis, Synthesis of zeolite crystals with unusual morphology: Application in acid catalysis, Appl Catal a-Gen, 390 (2010) 102-109.

[113] V. Valtchev, M. Smaihi, A.C. Faust, L. Vidal, Biomineral-silica-induced zeolitization of Equisetum arvense, Angew. Chem. Int. Ed., 42 (2003) 2782-2785.

[114] V.P. Valtchev, M. Smaihi, A.-C. Faust, L. Vidal, Equisetum a rvense Templating of Zeolite Beta Macrostructures with Hierarchical Porosity, Chem. Mater., 16 (2004) 1350-1355.

[115] H. Katsuki, S. Furuta, T. Watari, S. Komarneni, ZSM-5 zeolite/porous carbon composite: Conventional-and microwave-hydrothermal synthesis from carbonized rice husk, Microporous Mesoporous Mater., 86 (2005) 145-151.

[116] C. Kresge, M. Leonowicz, W. Roth, J. Vartuli, J. Beck, Ordered mesoporous molecular sieves synthesized by a liquid-crystal template mechanism, nature, 359 (1992) 710-712.

[117] A. Karlsson, M. Stöcker, R. Schmidt, Composites of micro-and mesoporous materials: simultaneous syntheses of MFI/MCM-41 like phases by a mixed template approach, Microporous Mesoporous Mater., 27 (1999) 181-192.

[118] L. Huang, W. Guo, P. Deng, Z. Xue, Q. Li, Investigation of synthesizing MCM-41/ZSM-5 composites, The Journal of Physical Chemistry B, 104 (2000) 2817-2823.

[119] N. Petkov, M. Hölzl, T. Metzger, S. Mintova, T. Bein, Ordered micro/mesoporous composite prepared as thin films, The Journal of Physical Chemistry B, 109 (2005) 4485-4491.

[120] Y. Liu, W. Zhang, T.J. Pinnavaia, Steam-stable aluminosilicate mesostructures assembled from zeolite type Y seeds, J. Am. Chem. Soc., 122 (2000) 8791-8792.

[121] Y. Liu, W. Zhang, T.J. Pinnavaia, Steam-stable MSU-S aluminosilicate mesostructures assembled from zeolite ZSM-5 and zeolite beta seeds, Angew. Chem. Int. Ed., 40 (2001) 1255-1258.

[122] F.S. Xiao, L. Wang, C. Yin, K. Lin, Y. Di, J. Li, R. Xu, D.S. Su, R. Schlögl, T. Yokoi, Catalytic properties of hierarchical mesoporous zeolites templated with a mixture of small organic ammonium salts and mesoscale cationic polymers, Angew. Chem., 118 (2006) 3162-3165.

[123] T. Tang, C. Yin, L. Wang, Y. Ji, F.-S. Xiao, Good sulfur tolerance of a mesoporous Beta zeolite-supported palladium catalyst in the deep hydrogenation of aromatics, J. Catal., 257 (2008) 125-133.

[124] K. Song, J. Guan, S. Wu, Q. Kan, Synthesis and characterization of strong acidic mesoporous alumino-silicates constructed of zeolite MCM-22 precursors, Catal. Commun., 10 (2009) 631-634.

[125] L. Wang, Z. Zhang, C. Yin, Z. Shan, F.-S. Xiao, Hierarchical mesoporous zeolites with controllable mesoporosity templated from cationic polymers, Microporous Mesoporous Mater., 131 (2010) 58-67.

[126] K. Möller, B. Yilmaz, U. Müller, T. Bein, Hierarchical zeolite beta via nanoparticle assembly with a cationic polymer, Chem. Mater., 23 (2011) 4301-4310.

[127] D. Serrano, R. García, G. Vicente, M. Linares, D. Procházková, J. Čejka, Acidic and catalytic properties of hierarchical zeolites and hybrid ordered mesoporous materials assembled from MFI protozeolitic units, J. Catal., 279 (2011) 366-380.

[128] Y. Jin, Y. Li, S. Zhao, Z. Lv, Q. Wang, X. Liu, L. Wang, Synthesis of mesoporous MOR materials by varying temperature crystallizations and combining ternary organic templates, Microporous Mesoporous Mater., 147 (2012) 259-266.

[129] K. Na, C. Jo, J. Kim, K. Cho, J. Jung, Y. Seo, R.J. Messinger, B.F. Chmelka, R. Ryoo, Directing zeolite structures into hierarchically nanoporous architectures, Science, 333 (2011) 328-332.

[130] D.P. Serrano, J. Aguado, J.M. Escola, J.M. Rodríguez, Á. Peral, Hierarchical zeolites with enhanced textural and catalytic properties synthesized from organofunctionalized seeds, Chem. Mater., 18 (2006) 2462-2464.

[131] S.L. Burkett, M.E. Davis, Mechanism of structure direction in the synthesis of Si-ZSM-5: an investigation by intermolecular 1H-29Si CP MAS NMR, The Journal of Physical Chemistry, 98 (1994) 4647-4653.

[132] A. Persson, B. Schoeman, J. Sterte, J.-E. Otterstedt, The synthesis of discrete colloidal particles of TPA-silicalite-1, Zeolites, 14 (1994) 557-567.

[133] B.J. Schoeman, O. Regev, A study of the initial stage in the crystallization of TPA-silicalite-1, Zeolites, 17 (1996) 447-456.

[134] P.-P.E. de Moor, T.P. Beelen, R.A. van Santen, In situ observation of nucleation and crystal growth in zeolite synthesis. A small-angle X-ray scattering investigation on Si-TPA-MFI, The Journal of Physical Chemistry B, 103 (1999) 1639-1650.

[135] D. Serrano, J. Aguado, J. Rodriguez, A. Peral, Effect of the organic moiety nature on the synthesis of hierarchical ZSM-5 from silanized protozeolitic units, J. Mater. Chem., 18 (2008) 4210-4218.

[136] D. Serrano, J. Aguado, G. Morales, J. Rodriguez, A. Peral, M. Thommes, J. Epping, B. Chmelka, Molecular and meso-and macroscopic properties of hierarchical nanocrystalline ZSM-5 zeolite prepared by seed silanization, Chem. Mater., 21 (2009) 641-654.

[137] D. Serrano, J. Aguado, J. Escola, A. Peral, G. Morales, E. Abella, Synthesis of hierarchical ZSM-5 by silanization and alkoxylation of protozeolitic units, Catal. Today, 168 (2011) 86-95.

[138] D.P. Serrano, R.A. Garcia, M. Linares, B. Gil, Influence of the calcination treatment on the catalytic properties of hierarchical ZSM-5, Catal Today, 179 (2012) 91-101.

[139] H. Wang, T.J. Pinnavaia, MFI zeolite with small and uniform intracrystal mesopores, Angew. Chem. Int. Ed., 45 (2006) 7603-7606.

[140] D.H. Park, S.S. Kim, H. Wang, T.J. Pinnavaia, M.C. Papapetrou, A.A. Lappas, K.S. Triantafyllidis, Selective petroleum refining over a zeolite catalyst with small intracrystal mesopores, Angew. Chem., 121 (2009) 7781-7784.

[141] M. Choi, H.S. Cho, R. Srivastava, C. Venkatesan, D.-H. Choi, R. Ryoo, Amphiphilic organosilane-directed synthesis of crystalline zeolite with tunable mesoporosity, Nature materials, 5 (2006) 718-723.

[142] M. Choi, D.H. Lee, K. Na, B.W. Yu, R. Ryoo, High Catalytic Activity of Palladium (II)-Exchanged Mesoporous Sodalite and NaA Zeolite for Bulky Aryl Coupling Reactions: Reusability under Aerobic Conditions, Angew. Chem., 121 (2009) 3727-3730.

[143] D.-H. Lee, M. Choi, B.-W. Yu, R. Ryoo, Organic functionalization of mesopore walls in hierarchically porous zeolites, Chem. Commun., (2009) 74-76.

[144] A. Inayat, I. Knoke, E. Spiecker, W. Schwieger, Assemblies of Mesoporous FAU-Type Zeolite Nanosheets, Angew. Chem. Int. Ed., 51 (2012) 1962-1965.

[145] L. Meng, B. Mezari, M.G. Goesten, E.J. Hensen, One-Step Synthesis of Hierarchical ZSM-5 Using Cetyltrimethylammonium as Mesoporogen and Structure-Directing Agent, Chem Mater, 29 (2017) 4091-4096.

[146] S. Naik, A. Chiang, R. Thompson, F. Huang, Formation of silicalite-1 hollow spheres by the self-assembly of nanocrystals, Chem. Mater., 15 (2003) 787-792.

[147] B.T. Holland, Transformation of mostly amorphous mesoscopic aluminosilicate colloids into high surface area mesoporous ZSM-5, Microporous Mesoporous Mater., 89 (2006) 291-299.

[148] Z. Wang, C. Li, H.J. Cho, S.-C. Kung, M.A. Snyder, W. Fan, Direct, single-step synthesis of hierarchical zeolites without secondary templating, Journal of Materials Chemistry A, 3 (2015) 1298-1305.

[149] B. Li, Z. Hu, B. Kong, J. Wang, W. Li, Z. Sun, X. Qian, Y. Yang, W. Shen, H. Xu, Hierarchically tetramodal-porous zeolite ZSM-5 monoliths with template-free-derived intracrystalline mesopores, Chemical Science, 5 (2014) 1565-1573.

[150] X. Zhang, D. Liu, D. Xu, S. Asahina, K.A. Cychosz, K.V. Agrawal, Y. Al Wahedi, A. Bhan, S. Al Hashimi, O. Terasaki, Synthesis of self-pillared zeolite nanosheets by repetitive branching, Science, 336 (2012) 1684-1687.

[151] D. Xu, G.R. Swindlehurst, H. Wu, D.H. Olson, X. Zhang, M. Tsapatsis, On the synthesis and adsorption properties of single-unit-cell hierarchical zeolites made by rotational intergrowths, Adv. Funct. Mater., 24 (2014) 201-208.

[152] W. Schwieger, A.G. Machoke, T. Weissenberger, A. Inayat, T. Selvam, M. Klumpp, A. Inayat, Hierarchy concepts: classification and preparation strategies for zeolite containing materials with hierarchical porosity, Chem. Soc. Rev., 45 (2016) 3353-3376.

[153] E.-P. Ng, D. Chateigner, T. Bein, V. Valtchev, S. Mintova, Capturing ultrasmall EMT zeolite from template-free systems, Science, 335 (2012) 70-73.

[154] M. Khaleel, A.J. Wagner, K.A. Mkhoyan, M. Tsapatsis, On the rotational intergrowth of hierarchical FAU/EMT zeolites, Angew. Chem. Int. Ed., 53 (2014) 9456-9461.

[155] A.I. Lupulescu, J.D. Rimer, Tailoring Silicalite-1 Crystal Morphology with Molecular Modifiers, Angew. Chem., 124 (2012) 3401-3405.

[156] A. Zukal, V. Patzelova, U. Lohse, Secondary porous structure of dealuminated Y zeolites, Zeolites, 6 (1986) 133-136.

[157] D.A. Cooper, T.W. Hastings, E.P. Hertzenberg, Process for preparing zeolite Y with increased mesopore volume, Google Patents, 1997.

[158] Y. Sasaki, T. Suzuki, Y. Takamura, A. Saji, H. Saka, Structure analysis of the mesopore in dealuminated zeolite Y by high resolution TEM observation with slow scan CCD camera, J. Catal., 178 (1998) 94-100.

[159] S. Van Donk, A.H. Janssen, J.H. Bitter, K.P. de Jong, Generation, characterization, and impact of mesopores in zeolite catalysts, Catalysis Reviews, 45 (2003) 297-319.

[160] Q. Sheng, K. Ling, Z. Li, L. Zhao, Effect of steam treatment on catalytic performance of HZSM-5 catalyst for ethanol dehydration to ethylene, Fuel Process. Technol., 110 (2013) 73-78.

[161] M. Müller, G. Harvey, R. Prins, Comparison of the dealumination of zeolites beta, mordenite, ZSM-5 and ferrierite by thermal treatment, leaching with oxalic acid and treatment with SiCl 4 by 1 H, 29 Si and 27 Al MAS NMR, Micropor Mesopor Mat, 34 (2000) 135-147.

[162] J.P. Marques, I. Gener, P. Ayrault, J.M. Lopes, F.R. Ribeiro, M. Guisnet, Semi-quantitative estimation by IR of framework, extraframework and defect Al species of HBEA zeolites, Chem. Commun., (2004) 2290-2291.

[163] C. Zhang, Q. Liu, Z. Xu, K. Wan, Synthesis and characterization of composite molecular sieves with mesoporous and microporous structure from ZSM-5 zeolites by heat treatment, Microporous Mesoporous Mater., 62 (2003) 157-163.

[164] R. Otomo, T. Yokoi, J.N. Kondo, T. Tatsumi, Dealuminated Beta zeolite as effective bifunctional catalyst for direct transformation of glucose to 5-hydroxymethylfurfural, Appl Catal a-Gen, 470 (2014) 318-326.

[165] R. Barrer, M. Makki, Molecular sieve sorbents from clinoptilolite, Can. J. Chem., 42 (1964) 1481-1487.

[166] B. Meyers, T. Fleisch, G. Ray, J. Miller, J. Hall, A multitechnique characterization of dealuminated mordenites, J. Catal., 110 (1988) 82-95.

[167] G. Lee, J. Maj, S. Rocke, J. Garces, Shape selective alkylation of polynuclear aromatics with mordenite-type catalysts: A high yield synthesis of 4, 4′-Diisopropylbiphenyl, Catal. Lett., 2 (1989) 243-247.

[168] M.R. Apelian, A.S. Fung, G.J. Kennedy, T.F. Degnan, Dealumination of zeolite β via dicarboxylic acid treatment, The Journal of Physical Chemistry, 100 (1996) 16577-16583.

[169] E.F. Lee, L.V. Rees, Dealumination of sodium Y zeolite with hydrochloric acid, Journal of the Chemical Society, Faraday Transactions 1: Physical Chemistry in Condensed Phases, 83 (1987) 1531-1537.

[170] R. Giudici, H. Kouwenhoven, R. Prins, Comparison of nitric and oxalic acid in the dealumination of mordenite, Appl Catal a-Gen, 203 (2000) 101-110.

[171] M.D. González, Y. Cesteros, P. Salagre, Comparison of dealumination of zeolites beta, mordenite and ZSM-5 by treatment with acid under microwave irradiation, Microporous Mesoporous Mater., 144 (2011) 162-170.

[172] R. Dessau, E. Valyocsik, N. Goeke, Aluminum zoning in ZSM-5 as revealed by selective silica removal, Zeolites, 12 (1992) 776-779.

[173] A. Cizmek, B. Subotic, I. Smit, A. Tonejc, R. Aiello, F. Crea, A. Nastro, Dissolution of high-silica zeolites in alkaline solutions. 2. Dissolution of'activated'silicalite-1 and ZSM-5 with different aluminum content, Microporous Mater., 8 (1997) 159-169.

[174] M. Ogura, S.-y. Shinomiya, J. Tateno, Y. Nara, E. Kikuchi, M. Matsukata, Formation of uniform mesopores in ZSM-5 zeolite through treatment in alkaline solution, Chem. Lett., 29 (2000) 882-883.

[175] M. Ogura, S.-y. Shinomiya, J. Tateno, Y. Nara, M. Nomura, E. Kikuchi, M. Matsukata, Alkali-treatment technique—new method for modification of structural and acid-catalytic properties of ZSM-5 zeolites, Appl Catal a-Gen, 219 (2001) 33-43.

[176] J. Groen, L. Peffer, J. Moulijn, J. Pérez-Ramırez, Mesoporosity development in ZSM-5 zeolite upon optimized desilication conditions in alkaline medium, Colloids Surf. Physicochem. Eng. Aspects, 241 (2004) 53-58.

[177] J.C. Groen, J.A. Moulijn, J. Pérez-Ramírez, Alkaline posttreatment of MFI zeolites. From accelerated screening to scale-up, Industrial & engineering chemistry research, 46 (2007) 4193-4201.

[178] J.C. Groen, J.C. Jansen, J.A. Moulijn, J. Pérez-Ramírez, Optimal aluminum-assisted mesoporosity development in MFI zeolites by desilication, The Journal of Physical Chemistry B, 108 (2004) 13062-13065.

[179] X. Wei, P.G. Smirniotis, Development and characterization of mesoporosity in ZSM-12 by desilication, Microporous Mesoporous Mater., 97 (2006) 97-106.

[180] J.C. Groen, T. Sano, J.A. Moulijn, J. Pérez-Ramírez, Alkaline-mediated mesoporous mordenite zeolites for acid-catalyzed conversions, J. Catal., 251 (2007) 21-27.

[181] J.C. Groen, S. Abelló, L.A. Villaescusa, J. Pérez-Ramírez, Mesoporous beta zeolite obtained by desilication, Microporous Mesoporous Mater., 114 (2008) 93-102.

[182] J. Pérez-Ramírez, S. Abelló, L.A. Villaescusa, A. Bonilla, Toward Functional Clathrasils: Size-and Composition-Controlled Octadecasil Nanocrystals by Desilication, Angew. Chem. Int. Ed., 47 (2008) 7913-7917.

[183] A. Bonilla, D. Baudouin, J. Pérez-Ramírez, Desilication of ferrierite zeolite for porosity generation and improved effectiveness in polyethylene pyrolysis, J. Catal., 265 (2009) 170-180.

[184] Ł. Mokrzycki, B. Sulikowski, Z. Olejniczak, Properties of Desilicated ZSM-5, ZSM-12, MCM-22 and ZSM-12/MCM-41 Derivatives in Isomerization of α-Pinene, Catal. Lett., 127 (2009) 296.

[185] K.P. de Jong, J. Zečević, H. Friedrich, P.E. de Jongh, M. Bulut, S. Van Donk, R. Kenmogne, A. Finiels, V. Hulea, F. Fajula, Zeolite Y crystals with trimodal porosity as ideal hydrocracking catalysts, Angew. Chem., 122 (2010) 10272-10276.

[186] Z. Musilová-Pavlačková, S.I. Zones, J. Čejka, Post-synthesis modification of SSZ-35 zeolite to enhance the selectivity in p-xylene alkylation with isopropyl alcohol, Top. Catal., 53 (2010) 273-282.

[187] L. Sommer, D. Mores, S. Svelle, M. Stöcker, B.M. Weckhuysen, U. Olsbye, Mesopore formation in zeolite H-SSZ-13 by desilication with NaOH, Microporous Mesoporous Mater., 132 (2010) 384-394.

[188] D. Verboekend, J.C. Groen, J. Pérez-Ramírez, Interplay of Properties and Functions upon Introduction of Mesoporosity in ITQ-4 Zeolite, Adv. Funct. Mater., 20 (2010) 1441-1450.

[189] M. Kubů, N. Žilková, J. Čejka, Post-synthesis modification of TUN zeolite: Textural, acidic and catalytic properties, Catal. Today, 168 (2011) 63-70.

[190] Z. Qin, B. Shen, X. Gao, F. Lin, B. Wang, C. Xu, Mesoporous Y zeolite with homogeneous aluminum distribution obtained by sequential desilication–dealumination and its performance in the catalytic cracking of cumene and 1, 3, 5-triisopropylbenzene, J. Catal., 278 (2011) 266-275.

[191] D. Verboekend, A.M. Chabaneix, K. Thomas, J.-P. Gilson, J. Pérez-Ramírez, Mesoporous ZSM-22 zeolite obtained by desilication: peculiarities associated with crystal morphology and aluminium distribution, CrystEngComm, 13 (2011) 3408-3416.

[192] D. Verboekend, G. Vilé, J. Pérez-Ramírez, Hierarchical Y and USY zeolites designed by post-synthetic strategies, Adv. Funct. Mater., 22 (2012) 916-928.

[193] S. Abello, A. Bonilla, J. Perez-Ramirez, Mesoporous ZSM-5 zeolite catalysts prepared by desilication with organic hydroxides and comparison with NaOH leaching, Appl Catal a-Gen, 364 (2009) 191-198.

[194] J. Pérez-Ramírez, D. Verboekend, A. Bonilla, S. Abelló, Zeolite Catalysts with Tunable Hierarchy Factor by Pore-Growth Moderators, Adv. Funct. Mater., 19 (2009) 3972-3979.

[195] D. Verboekend, J. Pérez-Ramírez, Desilication Mechanism Revisited: Highly Mesoporous All-Silica Zeolites Enabled Through Pore-Directing Agents, Chemistry-A European Journal, 17 (2011) 1137-1147.

[196] K.H. Rhodes, S.A. Davis, F. Caruso, B. Zhang, S. Mann, Hierarchical Assembly of Zeolite Nanoparticles into Ordered Macroporous Monoliths Using Core− Shell Building Blocks, Chem. Mater., 12 (2000) 2832-2834.

[197] K. Miyake, Y. Hirota, K. Ono, Y. Uchida, S. Tanaka, N. Nishiyama, Direct and selective conversion of methanol to para-xylene over Zn ion doped ZSM-5/silicalite-1 core-shell zeolite catalyst, J. Catal., 342 (2016) 63-66.

[198] A. Ghorbanpour, A. Gumidyala, L.C. Grabow, S.P. Crossley, J.D. Rimer, Epitaxial growth of ZSM-5@ Silicalite-1: A core–shell zeolite designed with passivated surface acidity, ACS nano, 9 (2015) 4006-4016.

[199] D.R. Corbin, S. Schwarz, G.C. Sonnichsen, Methylamines synthesis: A review, Catal. Today, 37 (1997) 71-102.

[200] C.H. Bartholomew, Mechanisms of catalyst deactivation, Appl Catal a-Gen, 212 (2001) 17-60.

[201] L. Lin, T. Zhang, X. Zhang, H. Liu, K.L. Yeung, J. Qiu, New Pd/SiO$_2$@ ZIF-8 Core–Shell Catalyst with Selective, Antipoisoning, and Antileaching Properties for the Hydrogenation of Alkenes, Industrial & Engineering Chemistry Research, 53 (2014) 10906-10913.

[202] H. Yin, J. Choi, A.C. Yip, Anti-poisoning core–shell metal/ZIF-8 catalyst for selective alkene hydrogenation, Catal. Today, 265 (2016) 203-209.

[203] T. Zhang, X. Zhang, X. Yan, L. Lin, H. Liu, J. Qiu, K.L. Yeung, Core–shell Pd/ZSM-5@ ZIF-8 membrane micro-reactors with size selectivity properties for alkene hydrogenation, Catal. Today, 236 (2014) 41-48.

Chapter 3

Stacking MFI Zeolite Structures for Improved Sonogashira Coupling Reactions

3.1 Introduction

Among the array of transition-metal-catalysed C-C bond forming methods, Sonogashira coupling involves the reaction among halides, triflates and terminal alkynes; this reaction is catalysed by palladium (Pd) with or without the presence of couple (e.g. sulfonic amides in Scheme 1) and has become a powerful tool for synthesizing natural products, biologically active compounds, pharmaceuticals, agrochemicals and functionalized materials [1]. For example, in Scheme 3.1, quinols as antitumour agents **(a)**, furopyrimidinones with antiviral activity **(b)** and allosteric enhancers of an adenosine receptor **(c)** are synthesized by the couplings [2-4]. The Sonogashira reaction is traditionally conducted using a homogenous Pd catalyst such as palladium-phosphine complex [5-7]. Some ligand-free examples of Sonogashira coupling have also been successfully developed but usually require a large amount of Pd, which is not economically efficient [8, 9]. Since the 1990s, more effort has focused on the development of heterogeneous Pd catalysts to overcome the drawbacks associated with the recovery of the expensive catalyst in large-scale production, as well as the difficulty of separation of residual Pd in the final products that precludes a wide application to the food and pharmaceutical industry [10, 11].

sulfonic amides (I)　　　ethynyl dienone (II)　　　　　　　quinol derivatives (**a**)

furopyrimidinones　(**b**)

2-amino-3-(4-chlorobenzoyl)-4-neopentyl-
5-phenylethynyl thiophene　(**c**)
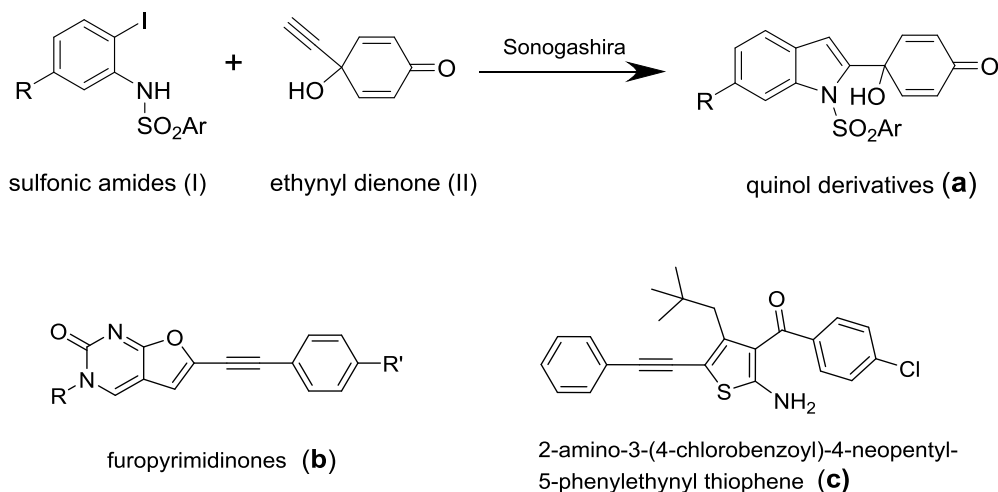
Scheme 3.1 Biologically active compounds formed through Sonogashira couplings.

Although Pd nanoparticles can catalyze Sonogashira coupling with high efficiency, they deactivate very easily due to aggregation during the reaction, which hinders further application on a large scale. In recent years, different type of zeolite-supported Pd catalysts, such as MFI, BEA, NaY zeolites, have received much attention because of both their physical and chemical stabilities in Sonogashira coupling reactions [12-14]. Zeolites are crystalline aluminosilicates with periodic arrangements of pores or channels and have experienced rapid and extensive growth since their industrial application to the Mobil methanol-to-gasoline (MTG) process [15, 16]. They are well known materials having a high specific surface area, ion-exchange capacity, good thermal/mechanical stability, and superior catalytic activity and shape-selectivity [17]. In particular, ZSM-5 (an MFI type zeolite) with interconnected 10-membered rings have been widely used in refinery and petrochemical applications, such as nitrogen oxides (NO_x) reduction [18-20], hydrocarbon conversions [21-25], along with other important industrial applications such as methanol-to-propene (MTP) conversion, N_2O decomposition, Fenton reaction and photocatalytic reactions [26-34]. Moreover, ZSM-5 zeolites have been extensively studied as support for metal catalysts for many organic transformations [35-39]. However, traditional ZSM-5 support has the drawback of easy agglomeration, leading to decreased

catalytic activity, fast deactivation and low sustainability. To improve the mechanical strength and resistance towards attrition loss, many industrial zeolite catalysts are prepared by embedding zeolite crystallites into a matrix using a binder, which is a synthetic material such as silica and alumina or a natural clay such as kaolin, bentonite, etc, [40, 41]. The binder-based matrix zeolite has shown interesting advantages in propane aromatization [41], n-butane isomerization [42] and n-octane isomerization [43]. However, the use of a binder is neither environmentally friendly nor economically efficient. The cost of kaolin is approximately USD 500/t according to Alibaba as of February 2019. Herein, we report a novel synthetic methodology for synthesizing the ZSM-5 stacking zeolite without using binders, and the as-prepared stacking ZSM-5 is used as supports for depositing Pd nanoparticles. The functionality of the Pd/stacking zeolite was demonstrated in ligand-free Sonogashira coupling reactions.

3.2 Experimental section

3.2.1 Materials

Tetraethyl orthosilicate (TEOS, 98%), aluminium isopropoxide (>98%), tetrapropylammonium hydroxide (TPAOH, 1.0 M in H_2O), palladium nitrate dehydrate (approximately 40% Pd basis), sodium borohydride (99%) and aluminium nitrate nonahydrate were purchased from Sigma-Aldrich. Sodium hydroxide was purchased from Thermo Fisher Scientific. Commercial ZSM-5 (CBV2314) was purchased from Zeolyst International. Phenyl acetylene (>97%), 4-ethylnyl anisole (>98%), bromobenzene (99%), 4-bromobenzaldehyde (99%), 2-bromobenzonitrile (>98%), 2-bromo-5-fluorobenzonitrile (>98%), triethylamine (99%), potassium carbonate (>99%), potassium tert-butoxide (99%), potassium methoxide (98%), dimethyl formamide (>99.5%) and toluene (99%) were supplied by Tansoole Company, China. Deionized (DI) water was prepared by a lab-based water-purification apparatus and was

used to prepare all required samples and solutions. All chemicals were used as received without any further treatment.

3.2.2 Sample preparation

Preparation of micro-sized ZSM-5 support

The synthesis of micro-sized ZSM-5 supports was similar to the method in our previous paper [44]. In a typical synthesis, 7.5 ml of TPAOH, 28 ml of DI water and 27.9 ml of TEOS were added sequentially to a polypropylene (PP) bottle. The resulting mixture was placed in an incubator shaker (Labnet 311DS) at 298 K for 24 h. Thereafter, a solution containing 0.25 g of NaOH, 1.02 g of aluminium isopropoxide, 28 ml of DI water and 7.5 ml of TPAOH was added to the mixture. The prepared mother gel was stirred at 298 K for 3 h, followed by crystallization at 453 K for 72 h. The molar composition of the final gel was TPAOH:NaOH:Al(O-i-Pr):SiO_2:H_2O=3:1:1:25:750. The solid products were subsequently washed 3 times with DI water and collected by centrifugation. Finally, the Na-ZSM-5 samples were obtained by calcination of the as-synthesized samples in a tube furnace at 823 K (ramping rate of 1 K/min from ambient temperature) for 10 h to remove the organic template. A similar procedure was used to make smaller micro-sized ZSM-5 crystals, except the hydrothermal treatment was performed for 42 h instead of 72 h. The synthesized micro-sized ZSM-5 was denoted Z-1 and Z-2 for the 42 h and 72 h hydrothermal treatment, respectively.

Preparation of nano-sized ZSM-5 support

The nano-sized ZSM-5 support was synthesized following the method reported by Mochizuki et al. [45]. In a typical synthesis, 15 ml of TPAOH, 16 ml of DI water and 13.68 ml TEOS were added sequentially to a PP bottle. The resulting mixture was kept in an oil bath at 353 K for 24

h. Thereafter, a solution containing 4 ml of DI water, 0.46 g of $Al(NO_3)_3 \cdot 9H_2O$ and 0.24 g of NaOH was added to the mixture. The prepared mother gel was stirred at room temperature for 30 min, followed by crystallization at 443 K for 24 h. The molar composition of the final gel was $SiO_2:Al_2O_3:TPAOH:NaOH:H_2O$ = 1:0.01:0.25:0.1:30. The solid product was subsequently washed 3 times with DI water and was collected by centrifugation. Finally, the products were calcined using the abovementioned method. The nano-sized ZSM-5 was denoted as Z-0.1 and had a crystal size of approximately 0.1 µm (or 100 nm). The H-type ZSM-5 (H-ZSM-5) samples were obtained as follows. The calcined Na-ZSM-5 samples (micron- and nano-sized) were treated with 1 M NH_4NO_3 aq. at 353 K for 5 h followed by calcination at 823 K for 10 h to exchange Na^+ ions for protons.

Synthesis of stacking ZSM-5

The stacking ZSM-5 samples were obtained as follows. The H-ZSM-5 samples were embedded into a pill disc of 3 mm thickness and 20 mm diameter using hydraulic pressing followed by programmed temperature calcination at 1073 K for 5 h. Thereafter, the calcinated pill discs were crushed into fine powders before being transferred to a laboratory test sieve (Endecotts Ltd.). Those samples with particle sizes between 45 and 63 µm were screened out. The synthesized stacking ZSM-5 was denoted HZ, and thus HZ-X (where X = 2, 1 and 0.1) for stacking ZSM-5 made from the corresponding micro- and nano-sized ZSM-5.

Preparation of Pd/ZSM-5 catalysts

The Pd/ZSM-5 samples containing approximately 0.03 wt.% palladium were obtained by adding a 10 ml $Pd(NO_3)_2$ aqueous solution to the ZSM-5 suspension (1 g of ZSM-5 immersed in 10 ml DI water) and the mixture was stirred at 353 K for 24 h. Subsequently, a 0.1-mmol/ml sodium borohydride aqueous solution was added to the Pd^{2+}/ZSM-5 mixture under vigorous

stirring for 1 h at ambient temperature. The resulting products were washed, collected by centrifugation, and then dried overnight in a vacuum oven at 353 K. The synthesized Pd/ZSM-5 catalysts were denoted PZ-X and PHZ-X (where X = 2, 1 and 0.1) for unmodified ZSM-5 and modified stacking ZSM-5, respectively, where P, H and Z represent palladium, the stacking structure and ZSM-5, respectively.

3.2.3 Characterization

The X-ray diffraction (XRD) patterns of the samples were recorded using a Philips PW1700 XRD instrument equipped with a Co-$K\alpha$ radiation source. The specific surface area was measured via N_2 adsorption/desorption measurements at 77 K using a Gemini VI surface area and pore size analyser. The metal dispersion on the catalysts was measured via CO chemisorption using a BELCAT II. Scanning electron microscopic (SEM) imaging and energy-dispersive X-ray spectroscopy (EDS) analysis were performed using a JEOL 700F scanning electron microscope. The chemical compositions of Al, Si and Pd were measured with a Varian 720 inductively coupled plasma optical emission spectrometry (ICP-OES) using an acid digestion method. ^1H NMR and ^{13}C NMR spectra were recorded in $CDCl_3$ on a Bruker BioSpin GmbH 400 (400 MHz) spectrometer. The chemical shifts were referenced to residual chloroform (7.24 ppm) and reported in ppm. The consumption of starting material was monitored by thin layer chromatography (TLC) analysis on silica gel plates (GF254) visualized under UV light (254 and 365 nm).

3.2.4 Catalytic Sonogashira coupling reaction

Bromobenzene (0.3 mmol), phenyl acetylene (0.3 mmol), K_2CO_3 (0.33 mmol), solid catalyst (8 mg) and solvent (2 mL) were added to a round-bottom flask equipped with a magnetic stirring bar. The mixture was heated at 373 K in an oil bath with vigorous stirring for 24 h until

the starting materials were consumed completely as monitored by TLC. The reaction mixture was diluted with ethyl acetate and water, and then the organic layer was separated and washed with brine, dried over $MgSO_4$, and concentrated in vacuum. The residue was purified on preparative TLC. The identification of products was conducted by using NMR measurements. For recycling, the Sonogashira coupling was conducted with phenylacetylene and bromobenzene under the same reaction conditions except using the recovered catalyst. The heterogeneous catalyst was recovered by filtration after reaction and washed with water and ethanol successively. The recovered catalyst was dried at 358 K overnight in an oven and ready for the next run. The turnover number (TON) was calculated based on GC analysis.

3.3 Results and discussion

3.3.1 Characterization of the synthesized samples

The Si/Al ratios of the as-prepared ZSM-5 samples (Z-2, Z-1 and Z-0.1) are 26 to 31 based on the EDS measurements (Table 3.1). The XRD patterns of commercial zeolites with similar Si/Al ratios are compared in Fig. 3.1 (a). These patterns show that common ZSM-5 can withstand up to 1273 K calcination without significant loss of crystallinity, indicating that 1073 K is an acceptable temperature for the synthesis of stacking ZSM-5. Fig. 3.1 (b) shows the XRD patterns of the synthesized Pd/stacking zeolite samples and their unmodified counterparts. The results confirm the phase purity and retention of crystallinity after hydraulic pressing and high temperature treatment. All samples consist of a crystalline MFI phase (refer to the ZSM-5 simulated patterns). The XRD patterns also confirm that the Pd contents in all samples were very small and bulky Pd species were not present. It is noted that the intensity of sample PHZ-0.1 is decreased compared with that of PZ-0.1, probably due to the lower thermal stability of nano-sized ZSM-5 particles compared to that of the micro-sized particles in PZ-1 and PZ-2. This result agrees with the conclusion reported by Wang et al. [46] that heat treatment at a

relatively low temperature has a negligible effect on the pore structure of zeolite samples, whereas the pore structure of zeolite significantly changes at relatively high temperatures.
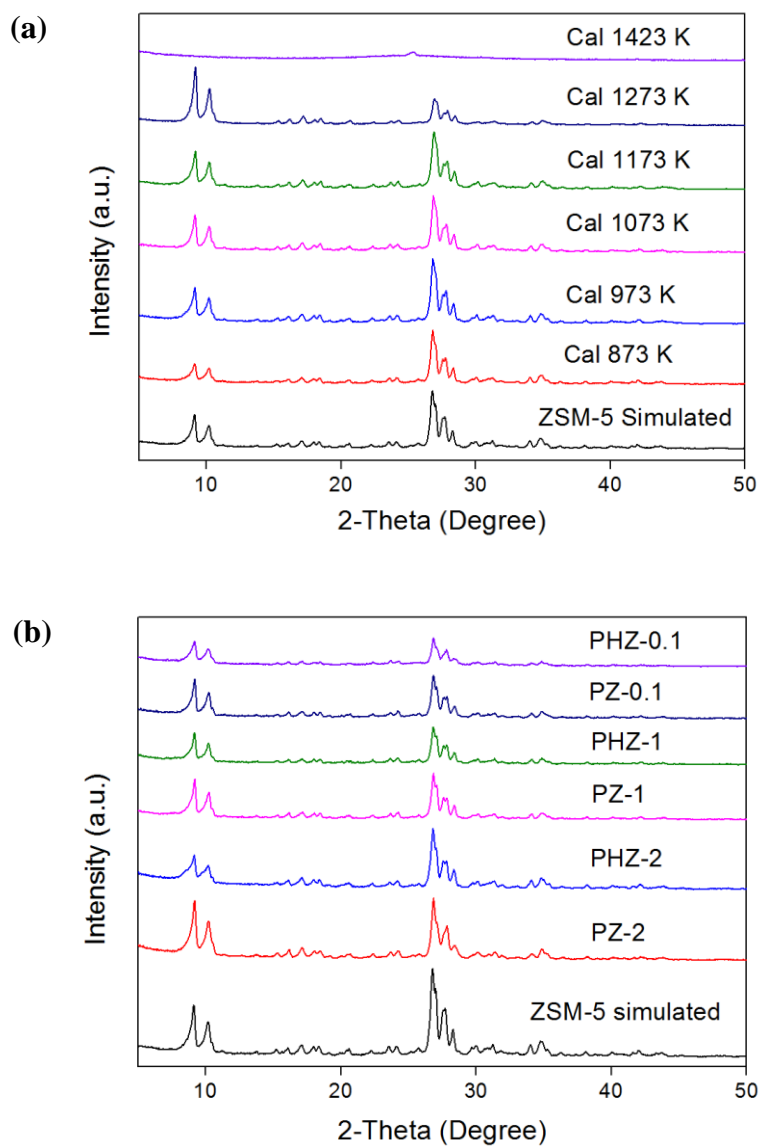
Fig. 3.1 XRD patterns of (a) commercial zeolites calcined from 873 to 1423 K and (b) the synthesized PZ-2, PHZ-2, PZ-1, PHZ-1, PZ-0.1 and PHZ-0.1 samples.

Table 3.1 The BET surface areas and Si/Al ratios of the stacking ZSM-5 and their counterparts.

Samples	$S_{BET}(m^2/g)^a$	$V_p(cm^3/g)^b$	Si/Al(-)^c
Z-2	318	0.17	26
HZ-2	294	0.16	28
Z-1	303	0.16	26
HZ-1	268	0.15	27
Z-0.1	331	0.22	31
HZ-0.1	118	0.08	37

^{a} BET surface area

^{b} pore volume calculated by t-plot.

^{c} measure by EDS

Fig. 3.2 shows the SEM images of ZSM-5 units and their stacking counterparts. Images (a), (c) and (e) confirm that samples Z-2, Z-1 and Z-0.1 have a particle size of approximately 2 µm, 1 µm and 0.1 µm, respectively. Images (b), (d) and (f) show the stacking ZSM-5 samples of HZ-2, HZ-1 and HZ-0.1, which have a sponge-like topography consisting of a dimension of approximately 30 µm × 40 µm. Stacking zeolites are clearly displayed in images (b), (d) and (f), indicating that the stacking structure was successfully synthesized. Images (b) and (d) clearly show the micro-sized zeolite units that generated the "sponge stacking", whereas image (f) shows that the stacking ZSM-5 that was made from nano-sized units has a rock shape topography, probably due to the partial damage to the nanoparticles, which caused some of them to collapse together.
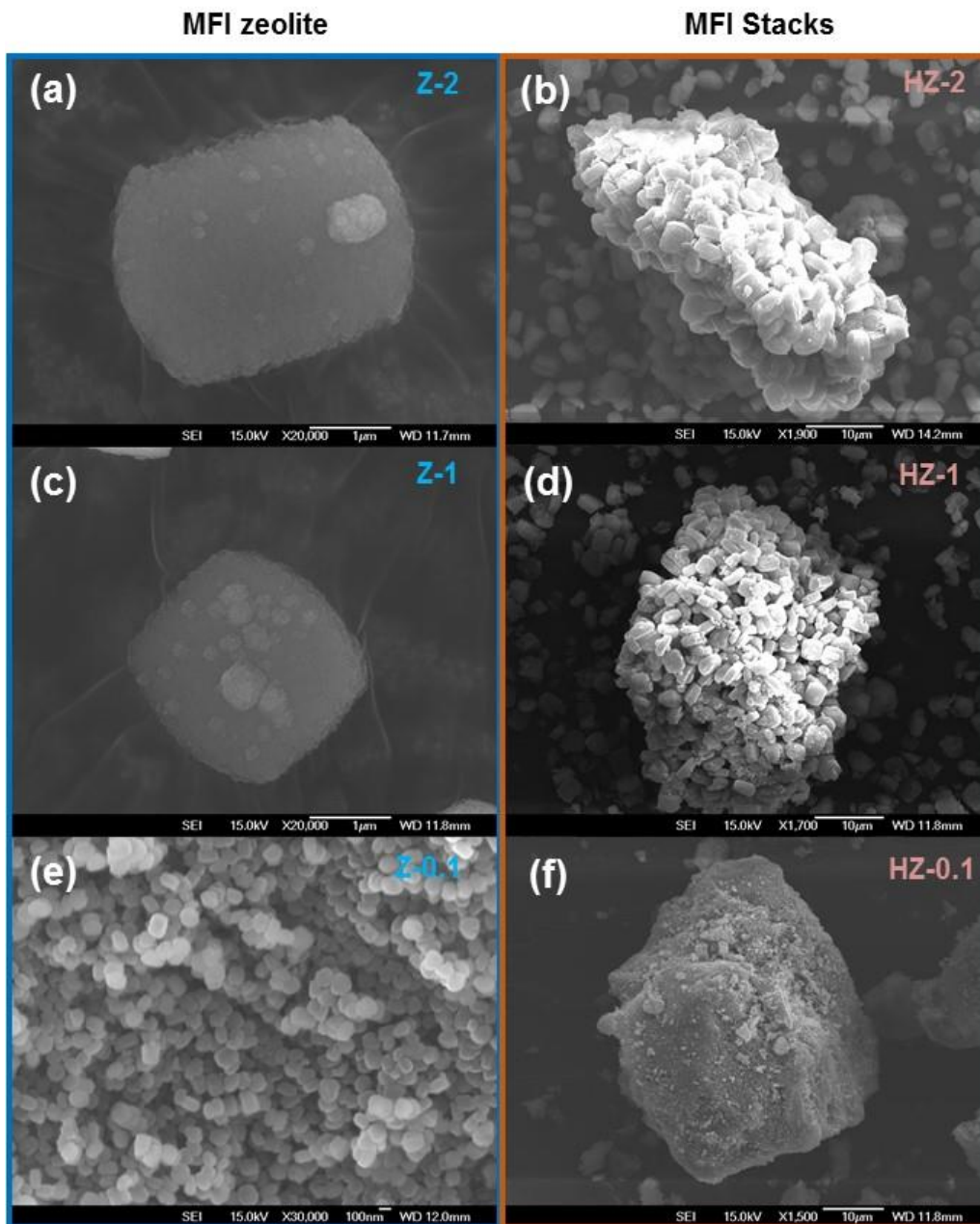
Fig. 3.2 SEM images of (a), (c) and (e) are Z-2, Z-1 and Z-0.1, respectively; images (b), (d) and (f) are HZ-2, HZ-1 and HZ-0.1, respectively.

The BET surface area and pore volume (Table 3.1) were generally comparable in all unmodified samples (Z-2, Z-1 and Z-0.1), among which the nano-sized Z-0.1 sample has the highest surface area of 331 m^2/g. However, HZ-0.1 has the lowest surface area of 118 m^2/g after the stacking modification, possibly due to the partial damage to the structure during

calcination at high temperature. This result is consistent with the XRD patterns which indicate that smaller particles are structurally less stable under high temperature. Moreover, the EDS results show that all stacking ZSM-5 samples underwent an increase in the Si/Al ratio. The increase in the Si/Al ratio is greater for nano-sized units than for micro-sized units, confirming that there is more leaching of Al species from nano-sized units than from micro-sized units during the high temperature treatment.

The amount and strength of acidic sites of the stacking zeolites and their unit counterparts were characterized using the NH_3-TPD method (Fig. 3.3). All NH_3-TPD profiles except that of HZ-0.1 exhibited two well-resolved NH_3 desorption peaks, one at low temperature (near 483 K) and the other at high temperature (near 700 K). The low-temperature peak is ascribed to ammonia adsorbed on weak acid sites, and the high-temperature peak is attributed to the strong adsorption sites of ammonia [47]. The patterns show that all the unmodified zeolites (Z-2, Z-1 and Z-0.1) contributed two peaks over a similar temperature range, which agrees with the finding that the crystal size of H-ZSM-5 zeolites has an insignificant influence on the acidic properties [48]. The patterns also show that both stacking ZSM-5s made from micro-sized units retained the acidic properties after modification, and even the intensity of the peaks was slightly decreased. However, for stacking ZSM-5 made from nano-sized units, no distinctive peaks are apparent; this outcome is consistent with the previous finding that the structure of nano-sized ZSM-5 was partially damaged during the high temperature process. The severe structural deterioration observed in HZ-0.1 (compared with HZ-2 and HZ-1) could be due to the lower crystallinity of nano-sized zeolite during the beginning stage of crystal growth, which results in a less stable structure that is more sensitive to heat treatment. In contrast, the micro-sized samples (HZ-2 and HZ-1) possess a relatively mature crystalline structure with higher thermal-structural stability. Moreover, the lower acidity of nano-sized zeolites compared with that of micro-sized ones is probably due to the higher Si/Al ratio.
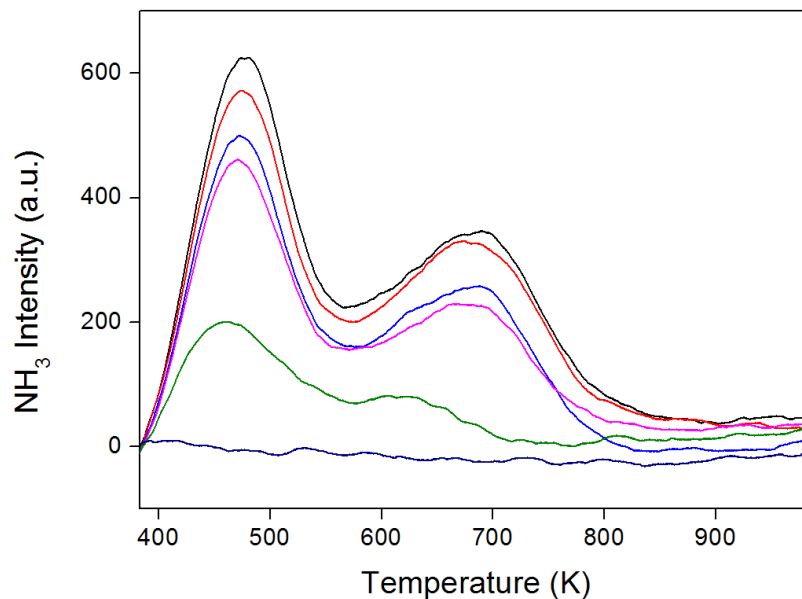
Fig. 3.3 NH$_3$-TPD results of Z-2, Z-1, and Z-0.1 and their stacking counterparts.

CO-chemisorption (Table 3.2) results show that Pd particles that were loaded on stacking ZSM-5 and their counterpart units have particle sizes ranging from 4.12 to 6.02 nm. Given the pore size of ZSM-5 is much smaller than 2 nm, most Pd particles are likely located on the surface of the ZSM-5 particles. The results also show that PHZ-2 and PHZ-1 undergo an obvious increase in metal dispersion and adsorption amount, whereas the particle size of the Pd that was loaded on them decreases, which can be ascribed to the hierarchical-resemblance properties generated during the stacking process. However, PHZ-0.1 showed the opposite results, which can be ascribed to the partial damage to the structure.

Table 3.2 CO-chemisorption of synthesized Pd/stacking ZSM-5 and their unit counterparts.

Catalysts	Metal dispersion (%)	Adsorption amount (cm^3/g)	Particle size (nm)
PZ-2	20.26	0.14	5.53
PHZ-2	27.21	0.21	4.12
PZ-1	20.99	0.13	5.34
PHZ-1	26.24	0.19	4.27
PZ-0.1	23.98	0.19	4.68
PHZ-0.1	18.62	0.15	6.02

3.3.2 Catalytic performance in Sonogashira reactions

Samples PHZ-1 and PHZ-2 showed an increased TON compared to their unmodified counterparts (Table 3.3). Specifically, the TON of the reaction increased more than 3-fold using PHZ-2 instead of PZ-2 and more than 2-fold using PHZ-1 instead of PZ-1. The large increase in the TON can be ascribed to the increase in the stability of the zeolite particle units associated with the stacking ZSM-5. The uniform stacking ZSM-5 is structurally stable and is able to immobilize Pd nanoparticles within the hierarchical structure, thereby preventing the active Pd nanoparticles from leaching during the reaction. In contrast, unstacked ZSM-5 particles tend to become large and irregular agglomerates during vigorous stirring in the liquid phase, which increased diffusion limitations and decreased accessibility to the Pd sites. Moreover, the higher catalytic performance of PHZ-2 than PHZ-1 agrees with the previous results that larger ZSM-5 particle is structurally more stable at high temperature treatment during the stacking process, despite both micro-sized ZSM-5 units produced stacking structures that increased the TON greatly. Interestingly, nano-sized PZ-0.1 has the highest TON among the unmodified samples

(PZ-2, PZ-1 and PZ-0.1), but this value decreased by more than one half after the stacking

modification, due to the partial damage to the structure during the high temperature calcination.

Table 3.3 Reaction optimization and catalyst screening for the Sonogashira reaction of (I) phenyl acetylene with (II) bromobenzene.[a]
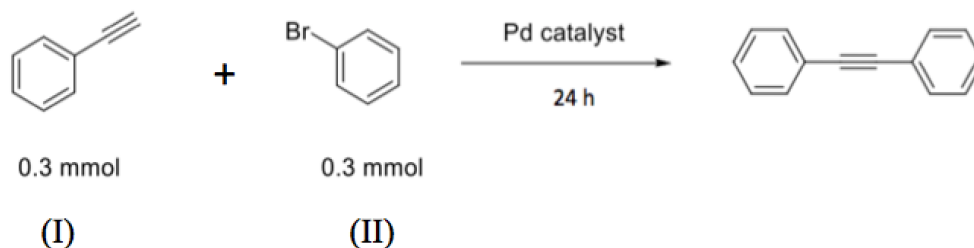
Entry	Catalyst	Pd loading (μg/g)[b]	Base	Temp. (K)	Solvent	TON
1	PZ-2	317.1	K_2CO_3	373	DMF	103
2	PHZ-2	361.3	K_2CO_3	373	DMF	369
3	PZ-1	287.0	K_2CO_3	373	DMF	61
4	PHZ-1	335.1	K_2CO_3	373	DMF	151
5	PZ-0.1	381.2	K_2CO_3	373	DMF	117
6	PHZ-0.1	371.6	K_2CO_3	373	DMF	45

[a] Reaction conditions: 8 mg of each catalyst, bromobenzene (0.3 mmol), phenyl acetylene (0.3 mmol), K_2CO_3 (0.33 mmol), solvent (2 mL) at 373 K for 24 h.

[b] Measured using ICP.

In Table 3.4, the substrate scope and functional group tolerance of PHZ-2 is examined (the NMR data are given in Appendix A). As demonstrated, neutral phenyl acetylene can react efficiently with electro-neutral and electron-deficient aryl bromides under the standard reaction conditions (Entry 1-4, Table 3.4). Apparently, aryl bromide with an electron-withdrawing group gave a better TON (Entry 2, Table 3.4). The *o*-substituted groups on aryl bromides

slightly decreased the yields of the desired products (Entry 3-4, Table 3.4) due to the steric effect. In contrast, cross coupling with electron-rich aryl bromides were not observed. Notably, the alkyne with an electron-donating group was also effectively transformed under these conditions (Entry 5, Table 3.4). These results indicate that the Pd/stacking ZSM-5 catalyst is applicable to Sonogashira reactions with a wide range of substrates involving different functional groups.

Table 3.4 PHZ-2 catalyzed Sonogashira reaction of aromatic bromides with alkynes[a].

Entry	Substrate	Product	TON
1			369
2			422
3			309
4			286
5			390
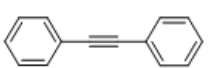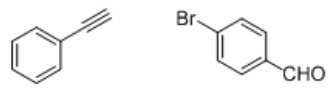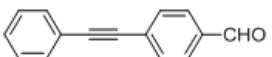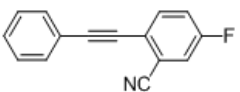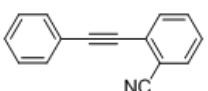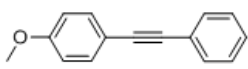
[a]Reaction conditions: alkyne (0.3 mmol), phenyl bromide (0.3 mmol), K_2CO_3 (0.33 mmol) and solid catalyst (8 mg) in DMF (2 mL) at 373 K for 24 h.

To check the reusability of the catalysts, the reaction of bromobenzene with phenyl acetylene was performed under the optimized reaction conditions. Fig. 3.4 shows the TON of each run for PHZ-2 (best performance among stacking ZSM-5 samples) and PZ-0.1 (best performance among unmodified ZSM-5 units). After each run, the samples were separated through a funnel, washed with water and ethyl acetate and dried in an oven at 358 K. The recovered samples

were used in the sample reaction for the following runs. Sample PHZ-2 retained a 70% activity after 4 runs, whereas the activity of PZ-0.1 decreased more than 50% after 4 runs, indicating the better stability and durability of the stacking ZSM-5 structure. The slightly decreased activity of PHZ-2 sample could be attributed to undesired by-products possibly generated during the reaction which either inhibit the coupling reactions or deactivate the Pd sites through irreversible adsorption under the tested conditions. However, it can be clearly seen that the inhibiting by-products have less influence on the performance of the reused stacking zeolite compared with the unstacked ones. The results clearly indicate that the stacking modification gives a robust hierarchical structure to zeolite that is reusable and can be separated readily from the liquid phase. In addition, the catalytic performance of the reused catalyst, such as PHZ-2, is expected to be fully recovered by high temperature calcination before each recycling. Notably, during the recovery process, PZ-0.1 samples were clearly seen to agglomerate, whereas no obvious change for PHZ-2 was observed, which can be ascribed to the more stable structure generated by the stacking modification. Fig. 3.5 shows the XRD patterns of the PHZ-2 samples before and after 4 runs. The results show that there is no obvious change of crystallinity for sample PHZ-2 even after 4 reactions, indicating an excellent recyclability of PHZ-2 samples.
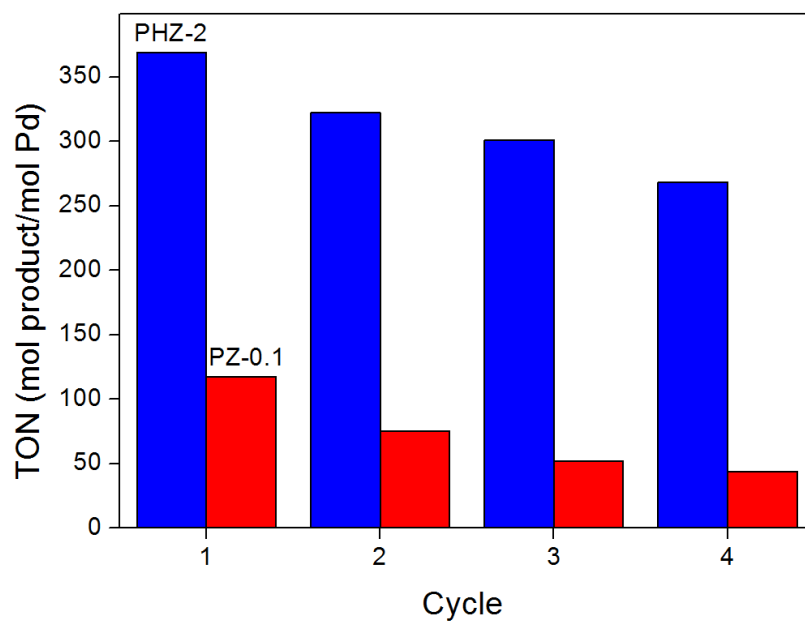
Fig. 3.4 Sonogashira reaction of phenyl acetylene with bromobenzene over PHZ-2 and PZ-0.1 for 4 runs. Reaction conditions: bromobenzene (1.5 mmol), phenyl acetylene (1.5 mmol), solid catalyst (40 mg), K_2CO_3 (1.65 mmol) and DMF (10 mL) stirred at 373 K for 24 h.
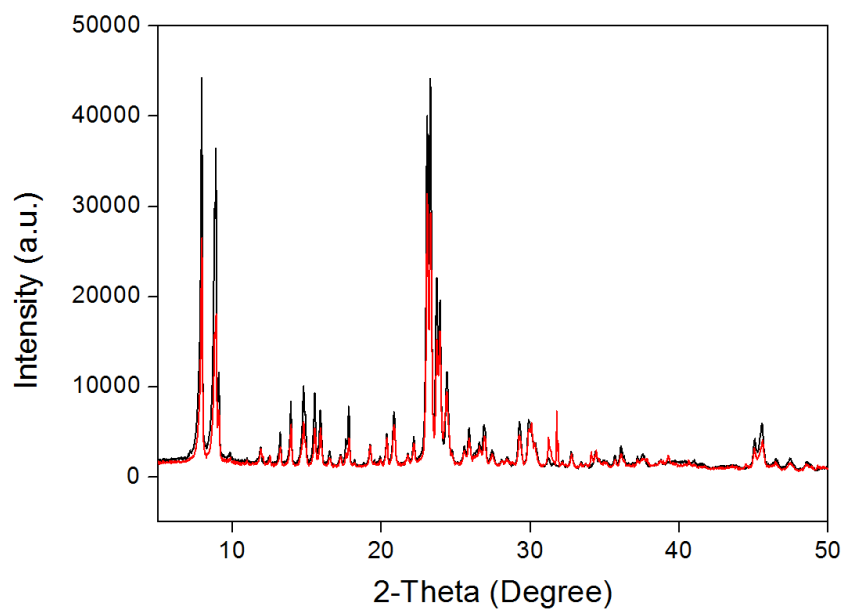
Fig. 3.5 XRD patterns of the PHZ-2 samples before (black colour) and after 4 runs (red colour).

3.4 Conclusions

A new type of stacking MFI consisting of Pd/stacking ZSM-5 was successfully synthesized. Three stacking zeolites were synthesized from ZSM-5 units with particle sizes of 100 nm, 1 µm and 2 µm. These stacking zeolites and their unit counterparts were used as supports for loading Pd nanoparticles. The effectiveness of the as-prepared Pd/stacking ZSM-5 catalysts was probed in Sonogahsira coupling reactions. The Pd/stacking ZSM-5 synthesized from micro-sized units exhibited a 2- to 3-fold increase in Sonogashira coupling yield compared to that of their unit counterparts (the TON increased from 103 to 369 and 61 to 151 for samples HZ-2 and HZ-1, respectively), whereas the stacking made from nano-sized units exhibited a decrease in yield (the TON decreased from 117 to 45) due to partial damage caused by high temperature. The results also show that nano-sized ZSM-5 particles are structurally less stable than a micro-sized ones under a high temperature (>1073 K) environment, resulting in greater structure damage. The recycle tests showed improved durability for stacking ZSM-5 synthesized from micro-sized particles than their unmodified counterparts, as sample PHZ-2 retained more than 70% activity after 4 runs. The novel process of synthesizing stacking zeolites in this work sheds light on new routes for producing zeolite matrix on an industrial scale, which would greatly decrease the cost for binders that are used to link zeolite particles conventionally. The improved mass transfer properties due to the hierarchical-resemblance structure, the recyclability and the prolonged catalyst lifetime given by the stacking zeolite may enable scale-up of other liquid phase zeolite-catalyzed reactions in general.

3.5 References

[1] R. Chinchilla, C. Nájera, The Sonogashira reaction: a booming methodology in synthetic organic chemistry, Chem. Rev., 107 (2007) 874-922.

[2] A.J. McCarroll, T.D. Bradshaw, A.D. Westwell, C.S. Matthews, M.F. Stevens, Quinols As Novel Therapeutic Agents. 7. Synthesis of Antitumor 4-[1-(Arylsulfonyl-1 H-indol-2-yl)]-4-hydroxycyclohexa-2, 5-dien-1-ones by Sonogashira Reactions, J. Med. Chem., 50 (2007) 1707-1710.

[3] M.J. Robins, I. Nowak, V.K. Rajwanshi, K. Miranda, J.F. Cannon, M.A. Peterson, G. Andrei, R. Snoeck, E. De Clercq, J. Balzarini, Synthesis and Antiviral Evaluation of 6-(Alkyl-heteroaryl) furo [2, 3-d] pyrimidin-2 (3 H)-one Nucleosides and Analogues with Ethynyl, Ethenyl, and Ethyl Spacers at C6 of the Furopyrimidine Core, J. Med. Chem., 50 (2007) 3897-3905.

[4] R. Romagnoli, P.G. Baraldi, A.P. IJzerman, A. Massink, O. Cruz-Lopez, L.C. Lopez-Cara, G. Saponaro, D. Preti, M. Aghazadeh Tabrizi, S. Baraldi, Synthesis and biological evaluation of novel allosteric enhancers of the A1 adenosine receptor based on 2-amino-3-(4′-chlorobenzoyl)-4-substituted-5-arylethynyl thiophene, J. Med. Chem., 57 (2014) 7673-7686.

[5] B.H. Lipshutz, D.W. Chung, B. Rich, Sonogashira couplings of aryl bromides: room temperature, water only, no copper, Org. Lett., 10 (2008) 3793-3796.

[6] P.R. Verma, S. Mandal, P. Gupta, B. Mukhopadhyay, Carbohydrate derived thiosemicarbazone and semicarbazone palladium complexes: homogeneous catalyst for C–C cross coupling reactions, Tetrahedron Lett., 54 (2013) 4914-4917.

[7] A.R. Hajipour, F. Rafiee, (BeDABCO) 2Pd2Cl6 as an efficient homogeneous catalyst for copper-free Sonogashira cross-coupling reaction, Appl. Organomet. Chem., 28 (2014) 595-597.

[8] A.R. Gholap, K. Venkatesan, R. Pasricha, T. Daniel, R.J. Lahoti, K.V. Srinivasan, Copper- and ligand-free Sonogashira reaction catalyzed by Pd (0) nanoparticles at ambient conditions under ultrasound irradiation, J. Org. Chem., 70 (2005) 4869-4872.

[9] L. Yu, Z. Han, Y. Ding, Gram-Scale Preparation of Pd@ PANI: A Practical Catalyst Reagent for Copper-Free and Ligand-Free Sonogashira Couplings, Organic Process Research & Development, 20 (2016) 2124-2129.

[10] P. Wang, G.-Y. Wang, W.-L. Qiao, Y.-S. Feng, Mesoporous Carbon Supporting Pd (0) as a Highly Efficient and Stable Catalyst for Sonogashira Reaction in Aqueous Media, Catal. Lett., 146 (2016) 1792-1799.

[11] A. Elhage, A.E. Lanterna, J.C. Scaiano, Light-Induced Sonogashira C–C Coupling under Mild Conditions Using Supported Palladium Nanoparticles, ACS Sustain. Chem., 6 (2018) 1717-1722.

[12] K. Okumura, K. Okazaki, H. Yamashita, Y. Koga, Direct inclusion of phosphine derivatives in the pores of zeolite β, Microporous Mesoporous Mater., 268 (2018) 285-292.

[13] L. Djakovitch, P. Rollet, Sonogashira cross-coupling reactions catalysed by heterogeneous copper-free Pd-zeolites, Tetrahedron Lett., 45 (2004) 1367-1370.

[14] R. Kore, M. Tumma, R. Srivastava, Syntheses and catalytic activities of homogenous and hierarchical ZSM-5 grafted Pd(II) dicarbene complex of imidazole based ionic liquids, Catal. Today, 198 (2012) 189-196.

[15] C.D. Chang, A. Silvestri, MTG-origin, evolution, operation, Chem. Tech., 17 (1987) 624-631.

[16] I. Maxwell, W. Stork, Hydrocarbon processing with zeolites, Stud. Surf. Sci. Catal., Elsevier1991, pp. 571-630.

[17] J. Weitkamp, Zeolites and catalysis, Solid State Ionics, 131 (2000) 175-188.

[18] F. Bin, C. Song, G. Lv, J. Song, S. Wu, X. Li, Selective catalytic reduction of nitric oxide with ammonia over zirconium-doped copper/ZSM-5 catalysts, Appl. Catal. B-Environ., 150 (2014) 532-543.

[19] A. De Lucas, J. Valverde, F. Dorado, A. Romero, I. Asencio, Influence of the ion exchanged metal (Cu, Co, Ni and Mn) on the selective catalytic reduction of NOx over mordenite and ZSM-5, J. Mol. Catal. A: Chem., 225 (2005) 47-58.

[20] M. Salazar, R. Becker, W. Grünert, Hybrid catalysts—an innovative route to improve catalyst performance in the selective catalytic reduction of NO by NH_3, Appl. Catal. B Environ., 165 (2015) 316-327.

[21] C.D. Chang, S.S. Grover, Conversion of methanol to gasoline components, Google Patents, 1977.

[22] A. Corma, Inorganic solid acids and their use in acid-catalyzed hydrocarbon reactions, Chem. Rev., 95 (1995) 559-614.

[23] H.S. Lacheen, E. Iglesia, Stability, structure, and oxidation state of Mo/H-ZSM-5 catalysts during reactions of CH_4 and CH_4–CO_2 mixtures, J. Catal., 230 (2005) 173-185.

[24] X. Li, D. Han, H. Wang, G. Liu, B. Wang, Z. Li, J. Wu, Propene oligomerization to high-quality liquid fuels over Ni/HZSM-5, Fuel, 144 (2015) 9-14.

[25] X. Li, B. Shen, C. Xu, Interaction of titanium and iron oxide with ZSM-5 to tune the catalytic cracking of hydrocarbons, Appl. Catal. A-Gen., 375 (2010) 222-229.

[26] G. Centi, S. Perathoner, T. Torre, M.G. Verduna, Catalytic wet oxidation with H2O2 of carboxylic acids on homogeneous and heterogeneous Fenton-type catalysts, Catal. Today, 55 (2000) 61-69.

[27] Z.M. El-Bahy, M.M. Mohamed, F.I. Zidan, M.S. Thabet, Photo-degradation of acid green dye over Co–ZSM-5 catalysts prepared by incipient wetness impregnation technique, J. Hazard. Mater., 153 (2008) 364-371.

[28] N. Hadi, A. Niaei, S. Nabavi, M.N. Shirazi, R. Alizadeh, Effect of second metal on the selectivity of Mn/H-ZSM-5 catalyst in methanol to propylene process, J. Ind. Eng. Chem., 29 (2015) 52-62.

[29] M. Kögel, V. Sandoval, W. Schwieger, A. Tissler, T. Turek, Catalytic Activity and Hydrothermal Stability of Cu-ZSM-5 Used for the Decomposition of N_2O, Chemical Engineering & Technology: Industrial Chemistry-Plant Equipment-Process Engineering-Biotechnology, 21 (1998) 655-658.

[30] B. Palella, M. Cadoni, A. Frache, H. Pastore, R. Pirone, G. Russo, S. Coluccia, L. Marchese, On the hydrothermal stability of CuAPSO-34 microporous catalysts for N_2O decomposition: a comparison with CuZSM-5, J. Catal., 217 (2003) 100-106.

[31] R. Qi, T. Fu, W. Wan, Z. Li, Pore fabrication of nano-ZSM-5 zeolite by internal desilication and its influence on the methanol to hydrocarbon reaction, Fuel Process. Technol., 155 (2017) 191-199.

[32] M.-L. Tsai, R.G. Hadt, P. Vanelderen, B.F. Sels, R.A. Schoonheydt, E.I. Solomon, $[Cu_2O]$ 2+ Active Site Formation in Cu–ZSM-5: Geometric and Electronic Structure Requirements for N2O Activation, J. Am. Chem. Soc., 136 (2014) 3522-3529.

[33] J. Wang, N. Mizuno, M. Misono, Comparison of catalytic decomposition of dinitrogen oxide and nitrogen monoxide over Cu/ZSM-5 and Cu/Y zeolites, Bull. Chem. Soc. Jpn., 71 (1998) 947-954.

[34] W. Zou, P. Xie, W. Hua, Y. Wang, D. Kong, Y. Yue, Z. Ma, W. Yang, Z. Gao, Catalytic decomposition of N_2O over Cu-ZSM-5 nanosheets, J. Mol. Catal. A: Chem., 394 (2014) 83-88.

[35] C.M. Parlett, K. Wilson, A.F. Lee, Hierarchical porous materials: catalytic applications, Chem. Soc. Rev., 42 (2013) 3876-3893.

[36] M. Choi, K. Na, J. Kim, Y. Sakamoto, O. Terasaki, R. Ryoo, Stable single-unit-cell nanosheets of zeolite MFI as active and long-lived catalysts, Nature, 461 (2009) 246.

[37] Y. Nishina, K. Takami, Bromination of aromatic compounds using an Fe_2O_3/zeolite catalyst, Green Chem., 14 (2012) 2380-2383.

[38] A. Kumbhar, S. Kamble, A. Mane, R. Jha, R. Salunkhe, Modified zeolite immobilized palladium for ligand-free Suzuki–Miyaura cross-coupling reaction, J. Organomet. Chem., 738 (2013) 29-34.

[39] G. Ye, Y. Sun, Z. Guo, K. Zhu, H. Liu, X. Zhou, M.-O. Coppens, Effects of zeolite particle size and internal grain boundaries on Pt/Beta catalyzed isomerization of n -pentane, J. Catal., 360 (2018) 152-159.

[40] M.J. Ramos, A. Casas, L. Rodríguez, R. Romero, A. Perez, Transesterification of sunflower oil over zeolites using different metal loading: a case of leaching and agglomeration studies, Appl Catal a-Gen, 346 (2008) 79-85.

[41] V. Choudhary, P. Devadas, A. Kinage, M. Guisnet, Influence of binder on the acidity and performance of H-Gallosilicate (MFI) zeolite in propane aromatization, Appl Catal a-Gen, 162 (1997) 223-233.

[42] F. Dorado, R. Romero, P. Cañizares, Influence of Clay Binders on the Performance of Pd/HZSM-5 Catalysts for the Hydroisomerization of n-Butane, Industrial & engineering chemistry research, 40 (2001) 3428-3434.

[43] P. Sánchez, F. Dorado, A. Fúnez, V. Jiménez, M.J. Ramos, J.L. Valverde, Effect of the binder content on the catalytic performance of beta-based catalysts, J. Mol. Catal. A: Chem., 273 (2007) 109-113.

[44] X. Jia, Y. Jeong, H. Baik, J. Choi, A.C. Yip, Increasing Resolution of Selectivity in Alkene Hydrogenation via Diffusion Length in Core-shell MFI zeolite, Catal. Today, (2018).

[45] H. Mochizuki, T. Yokoi, H. Imai, R. Watanabe, S. Namba, J.N. Kondo, T. Tatsumi, Facile control of crystallite size of ZSM-5 catalyst for cracking of hexane, Microporous Mesoporous Mater., 145 (2011) 165-171.

[46] C. Wang, L. Cao, J. Huang, Influences of acid and heat treatments on the structure and water vapor adsorption property of natural zeolite, Surf. Interface Anal., 49 (2017) 1249-1255.

[47] T. Miyamoto, N. Katada, J.-H. Kim, M. Niwa, Acidic property of MFI-type gallosilicate determined by temperature-programmed desorption of ammonia, J. Phys. Chem. B, 102 (1998) 6738-6745.

[48] L. Yang, Z. Liu, Z. Liu, W. Peng, Y. Liu, C. Liu, Correlation between H-ZSM-5 crystal size and catalytic performance in the methanol-to-aromatics reaction, Chin. J. Catal., 38 (2017) 683-690.

Chapter 4

Structure-performance relationships of functionalized zeolites and green solvents for microwave-assisted dehydration of fructose to 5-hydroxymethylfurfural

4.1 Introduction

The production of 5-hydroxymethylfurural (HMF) from biomass has attracted considerable research interest in recent decades because HMF is regarded as one of most promising platform compounds. HMF can be transformed to various derivatives, such as ethoxymethylfurfural, 2,5-furandicarboxylic acid, furfuryl alcohol, dimethylfuran and 2,5-diformylfuran [1-3], which can be further upgraded into an extensive spectrum of commodity chemicals and products, i.e., medicines, polymers, resins, fungicides, and biofuels [4], The high market potential of HMF can be reflected by the forecasted increase in the global sales of biobased products from 75.4 billion euros in 2010 to 431.8 billion euros in 2020 [5], This increase encourages the development of cost-effective systems for HMF production from fructose dehydration.

Carbohydrates such as starch and cellulose can be converted to HMF via three steps, which are typically catalyzed by two type of acids, i.e., Brønsted acid and Lewis acid. These steps include (1) hydrolysis of glucan to glucose catalyzed by Brønsted acid; (2) isomerization of glucose to fructose mediated by Lewis acid; and (3) dehydration of fructose to HMF facilitated by Brønsted acid. In addition, side reactions such as HMF rehydration to levulinic acid and formic acid, polymerization among the intermediates, and over-reacting HMF to heterogeneous humins can simultaneously occur [6]. These side reactions inevitably decrease the yield and selectivity of HMF. The undesirable side reactions promoted by Brønsted and Lewis acids may vary depending on the acid strength and quantity [7-9]. Therefore, the key to achieving high HMF production is to promote the desirable reactions and suppress the undesirable pathways by adjusting the involved system components [4, 10].

Different homogenous and heterogeneous catalysts have been reported for carbohydrates dehydration, i.e., mineral acids [11], metal salts [12], phosphates [13], resins [14], biochars [15], graphene oxide [16], and zeolites [17-19]. Despite their excellent performance,

homogeneous acids have drawbacks, such as equipment corrosion, environmental pollution, and post-products purification, whereas heterogeneous catalysts have demonstrated promising merits, such as easy separation and reusability, which render them feasible for upscaled industry application. Resins usually struggle with poor thermal stability [20], while biochars have limited surface area to accommodate acid sites [15]. Using zeolite as a catalyst support may offer advantages including high hydrothermal stability, high surface area, tunable porosity, and easy regeneration from thermal treatment [14, 17]. Recent studies show that the modification of ZSM-5 achieved approximately 29% of HMF yield from catalytic conversion of standard glucose at 195 °C after 30 min, which was significantly higher than the 8% achieved by classic ZSM-5 without modification [17]. Similarly, acidic zeolite L has shown high efficiency for producing HMF from fructose in ionic liquid as the medium and it can be reused four times without a significant decrease in activity [18].

While tailoring the active sites in catalysts presents a possible way, engineering of the reaction medium shares equal importance for the selective promotion of desirable reactions. Although water and alcohols as a polar solvent and protic solvents, respectively, have been attempted for HMF production, the significant occurrence of side reactions including rehydration and polymerization substantially limit the HMF yield and selectivity. Studies have reported that water as the reaction medium promotes dehydration of HMF to acids and oligomeric products [21]. The use of alcohols facilitates the formation of fuel chemicals by consuming HMF via esterification [22]. As an economically viable and relative safe alternative, polar aprotic solvents enable selective production of HMF with a promising yield. For example, the HMF yield has been reported to substantially increase from $10 <$ to 31.6% during glucose conversion upon the addition of dimethyl sulfoxide (DMSO) at a molar fraction of 0.5 in the presence of $CrCl_3$ as the catalyst [23]. The use of tetrahydrofuran (THF) as a cosolvent improved the HMF yield from 22 to 52-61% over $AlCl_3$ catalyzed glucose conversion [24]. These solvents

competed with water to solvate the substrates and products in the immediate vicinity of the reactive function groups, which inhibits them from undesirable side reactions, according to the previous computational studies [25-26].

Although polar aprotic solvent-containing reaction media have been evaluated for catalytic production of HMF, the majority of previous studies focused on homogenous catalytic systems [23-24, 27-28]. Few studies on zeolite-based catalysts reported the use of one specific solvent, such as methyl isobutyl ketone (MIBK) [29], or one particular type of zeolites, such as BEA [30], with minimal focus on the catalyst-solvent interactions. Given that the understanding of the interplay between the solvent and the zeolite catalysts is important for process scale-up, we investigate and elucidate the effect of polar aprotic-water solvent systems on the fructose dehydration over zeolites with different functional features (i.e., structure, acidity and water affinity). The substrate concentration in this study resembled that obtained from food waste dollarization, which is suggested to be effective in previous studies. Four types of polar aprotic solvent, i.e., dimethyl sulfoxide (DMSO), acetone, γ-valerolactone (GVL), and propylene carbonate (PC), were selected as the organic phase based on their satisfactory performance based on recent reports [4, 28].

4.2 Experimental

4.2.1 Materials

Tetraethyl orthosilicate (TEOS, 98%), aluminum isopropoxide (>98%), tetrapropylammonium hydroxide (TPAOH, 1.0 M in H_2O), sucrose (98%), ammonium hydroxide solution (28% NH_3 in H_2O), and aluminum nitrate nonahydrate were purchased from Sigma-Aldrich Chemical Co. Sodium hydroxide and ethanol (EtOH, 99.5%) were purchased from Thermo Fisher Scientific. Sodium hypochlorite solution (12.5%) was purchased from Jasol. These chemicals were used

to synthesize zeolites and carbon black, which were employed for making hierarchical zeolites. PC (99%) and GVL (98%) were purchased from Alfa Aesar and Acros Organics, respectively. Acetone (99.5%) and DMSO (99.9%)—two common industrial solvents—were obtained from Duksan Pure Chemicals and RCI labscan, respectively. These chemicals were used to prepare the solvent-water mixture as a reaction medium. All chemicals were used as received. Zeolites of ZSM-5 (CBV2314), BEA (CP814E), hydrophilic Y (CBV300) and hydrophobic Y (CBV780) were supplied by Zeolyst International; they were denoted as Z5, BEA, Y_{phi}, and Y_{pho}, respectively. Z5, BEA, and Y_{phi} were heat-treated at 550 °C for 10 h to generate acid sites from their ammonium forms.

4.2.2 Sample preparations

Synthesis of ZSM-5 with different particle sizes

The synthesis of microsized ZSM-5 supports was similar to the reported method [31]. In a typical synthesis, 7.5 ml of TPAOH, 28 ml of DI water, and 27.9 ml of TEOS were sequentially added to a polypropylene (PP) bottle. The resulting mixture was placed in an incubator shaker (Labnet 311DS) at 25 °C for 24 h. A solution that contains 0.25 g of NaOH, 1.02 g of aluminum isopropoxide, 28 ml of DI water, and 7.5 ml of TPAOH were added to the mixture. The prepared mother gel was stirred at 25 °C for 3 h, followed by crystallization at 180 °C for 72 h. The molar composition of the final gel was TPAOH:NaOH:Al(O-i-Pr):SiO$_2$:H$_2$O=3:1:1:25:750. The solid product was subsequently washed 3 times with DI water and collected by centrifugation. The Na-ZSM-5 samples were obtained by calcination of the as-synthesized samples in a tube furnace at 550 °C (ramping rate of 1 °C/min from ambient temperature) for 10 h to remove the organic template. A similar procedure was used to make smaller-sized ZSM-5 crystals, with the exception that the hydrothermal treatment was performed for 42 h instead of 72 h. The synthesized ZSM-5 is denoted as SZ5-X (where X is

the particle size in micrometers, e.g., SZ5-2 and SZ5-1 are synthesized ZSM-5 samples with particle sizes of 2 µm and 1 µm, respectively.

The nanosized ZSM-5 support was synthesized following the method reported by Mochizuki et al [32]. In a typical synthesis, 15 ml of TPAOH, 16 ml of DI water and 13.68 ml TEOS were sequentially added to a PP bottle. The resulting mixture was kept in an oil bath at 80 °C for 24 h. A solution that contains 4 ml of DI water, 0.46 g of $Al(NO_3)_3{\cdot}9H_2O$ and 0.24 g of NaOH was added to the mixture. The prepared mother gel was stirred at room temperature for 30 min, followed by crystallization at 170 °C for 24 h. The molar composition of the final gel was $SiO_2{:}Al_2O_3{:}TPAOH{:}NaOH{:}H_2O{=}1{:}0.01{:}0.25{:}0.1{:}30$. The solid product was subsequently washed 3 times with DI water and collected by centrifugation. The products were calcined using the previously mentioned method. The nanosized ZSM-5 was denoted as SZ5-0.1 (where -0.1 indicates that the average particle size is approximately 0.1 µm or 100 nm).

Synthesis of hierarchical ZSM-5 by using hard template

Carbon blacks as a hard template is well known for producing hierarchical zeolite with controlled porosity independent of their composition and structure [33]. The carbon black particles were synthesized following the method reported by Zhu et al [34]. In a typical experiment, 13.1 g of sucrose were dissolved in a mixture of ethanol, DI water and ammonium hydroxide solution. After stirring at 50 °C for 1.5 h, the mixed solution was hydrothermally treated at 180 °C for 2 d. The generated brown solid was crushed and treated in an N_2 environment at 850 °C for 5 h. The as-prepared carbon black was treated with sodium hypochlorite solution to obtain the hydrophilic property, as reported by Han et al [35]. Subsequently, 1 g of carbon black was added to 42 ml sodium hypochlorite solution, and the mixture was stirred under room temperature for 24 h, followed by centrifugation, washing and drying at 80 °C for 12 h.

The hierarchical ZSM-5 was synthesized by adding 1.8 g of as-prepared hydrophilic carbon black to ZSM-5 precursor solution that was used to synthesize the previously mentioned SZ5-2. The mixture was stirred at room temperature for 24 h before being transferred to an autoclave. The remaining procedures were equivalent to the procedures for SZ5-2. The product is denoted as SZ5-2H (H represents the hierarchical structure). The produced samples, i.e., SZ5-0.1, SZ5-1, SZ5-2, and SZ5-2H, were treated with 1 M NH_4NO_3 aq. at 80 °C for 5 h, followed by calcination at 550 °C for 10 h to generate H form ZSM-5 [36].

4.2.3 Characterization

The X-ray diffraction (XRD) patterns of the samples were recorded using a Philips PW1700 XRD instrument equipped with a Co-Kα radiation source. The specific surface area was measured via N_2 adsorption/desorption measurements at -196 °C using a Gemini VI surface area and pore size analyzer. The samples were degassed at 200 °C for 12 h before analysis. Scanning electron microscopic (SEM) imaging and energy-dispersive X-ray spectroscopy (EDS) analysis were performed using a JEOL 700F scanning electron microscope. Transmission electron microscopy (TEM) images were recorded using a Philips CM-200. Temperature programmed desorption of ammonia (NH_3-TPD) curves were obtained in the range of 100 - 750 °C with a ramping rate of 10 $°C \cdot min^{-1}$ (BELCAT II). The adsorption of ammonia of the samples was performed at 100 °C, followed by ammonia removal in a flow of pure helium.

4.2.4 Microwave-assisted Catalytic conversion

The conditions of catalytic conversion of glucose and fructose were determined based on previous studies [27, 37]. Model sugar substrate (i.e., glucose or fructose) of 5 wt/v% was added to a mixture of organic solvent (DMSO, acetone, GVL, or PC) and water (1:1 v/v, 10 ml

in total) that contained 0.2 g zeolite samples. Mixtures without the addition of zeolites were also prepared as the control. For the catalytic reaction, the mixture was placed in a sealed vessel and heated to 160 °C with a ramp time of 5 min in the Ethos Up Microwave Reactor (Milestone, maximum power 1900 W). The same temperature was maintained for the catalytic reaction for 1-40 min with magnetic stirring to achieve mixture homogeneity. After the conversion process, the vessel was cooled for 40 min with the assistance of mechanical ventilation, followed by centrifugation to separate the liquid and solid phases. The liquid phase was diluted with deionized (DI) water (1:3 v/v) and filtered through a mixed cellulose ester filter (0.45 µm) before product analysis. All trials were conducted in duplicate.

4.2.5 Product analysis

High-performance liquid chromatography (HPLC) was performed using the Chromaster (Hitachi) with a 5110 pump, 5210 autosampler, 5310 column oven, and 5450 refractive index (RI) detector. The HPLC system was equipped with an Aminex HPX-87H column (biorad) that operates at 50 °C. The mobile phase was 0.01 M H_2SO_4 at a flow rate of 0.5 ml·min^{-1}. Blank and spiked samples (i.e., standard compounds in DI water with known concentrations) were injected in each series of the HPLC analysis for quality assurance. The product yield and selectivity were calculated based on the carbon number (mol) as follows:

$$Product\ yield\ (mol\%) = \frac{P_f (mg\ ml^{-1}) \times n_p/MW_p}{S_i (mg\ ml^{-1}) \times n_s/MW_s} \times 100 \tag{1}$$

$$Product\ selectivity\ (mol\%) = \frac{P_f (mg\ ml^{-1}) \times n_p/MW_p}{(S_i - S_f)(mg\ ml^{-1}) \times n_s/MW_s} \times 100 \tag{2}$$

where P_f is the concentration of the final products, i.e., fructose, glucose, HMF, levoglucosan, levulinic acid and formic acid; S_i and S_f are the initial concentration and final concentration, respectively, of sugars, i.e., fructose and glucose; n_p and n_s are the numbers of carbon in the

corresponding product and the substrate, respectively; and MW is the molecular weight of the compound.

4.3 Results and discussion

4.3.1 Physicochemical properties of catalysts

The physical properties of the commercial zeolites and synthesized zeolites are listed in Table 4.1 and Table 4.2, respectively. As shown in Table 4.1, all zeolites in this study have a three-dimensional pore structure, and the BET surface area and large pore size of these zeolites decreased as the order of zeolite Y > BEA > MFI. This finding is partly attributed to the larger ring size of Y and BEA (i.e., 12) than that of MFI (i.e., 10). Although both zeolite Y and BEA are 12-membered ring zeolites, zeolite Y (7.35 × 7.35 × 7.35 Å) has a slightly larger pore size than BEA (5.95 × 5.95 × 5.95 Å) due to different ring connectivities and arrangements in the framework [38]. The Si/Al ratio between Z5 and BEA are comparable (Table 4.1) although they have different structures. Even though Y_{pho} shares the same pore structure with Y_{phi}, Y_{pho} has a substantially higher Si/Al ratio than Y_{phi}, which produces a higher water affinity of Y_{phi} than Y_{pho} [39], i.e., Y_{phi} and Y_{pho} are hydrophilic in nature and hydrophobic in nature, respectively. The Si/Al ratio is comparable in all synthesized SZ5 zeolites (Si/Al ~ 26-31 in Table 4.2). The slight increase in the Si/Al ratio of SZ5-2H compared with that of SZ5-2 may be attributed to the inevitable loss of Al atoms (and Si atoms to a lesser extent) from the framework after incorporation of mesopores by carbon templating. SZ5-2H has a higher external surface area (101 m^2/g) and lower value of V_{micro}/V_{total} (0.56) compared with SZ5-2 (81 m^2/g and 0.69), which indicates that the macro/meso porosity were successfully created in SZ5-2H by the use of carbon template during synthesis [34]. Note that the SZ5-0.1 has more mesopores observed than SZ5-2H, which is likely attributed to the formation of intracrystalline mesopores due to the random agglomeration among SZ5-0.1 particles.

Table 4.1 Physical properties of commercial zeolites tested in this study.

Catalysts	Type	Ring size (# T-atoms)[a]	Large pore size (Å)[b]	S_{BET} (m^2/g)[c]	Si/Al ratio (-)[d]
Z5	MFI	10	4.7	425	11.5
BEA	BEA	12	5.95	680	12.5
Y$_{phi}$	Y	12	7.35	925	2.6
Y$_{pho}$	Y	12	7.35	780	40

[a,b] According to the International Zeolite Association database.

[c,d] Data are referred to SDS provided by Zeolyst International Co.

Table 4.2 Physical properties of synthesized ZSM-5 zeolites.

Catalysts	Si/Ai ratio (-)[a]	S_{ext} (m^2/g)[b]	V_{micro}/V_{total} (-)[c]
SZ5-0.1	31	106	0.51
SZ5-1	26	99	0.65
SZ5-2	26	81	0.69
SZ5-2H	28	101	0.56

[a] Measured by EDS

[b] BET external surface area calculated by t-plot.

[c] Micropore volume calculated by t-plot.

The XRD patterns of the synthesized zeolites, i.e., SZ5-0.1, SZ5-1, SZ5-2, and SZ5-2H, were illustrated in Fig. 4.1. The results confirmed that all synthesized samples have well-resolved peaks in the 5-35° characteristic for the MFI structure [40], which indicates that no bulky

carbon black templates were left inside the secondary porosities and the crystallinity was well preserved for SZ5-2H. Note that the first two peaks (approximately $2\Theta = 9.2°$ and $10.3°$) of SZ5-2H was slightly weaker than that of the SZ5-2, which suggests the loss of microporous channels due to the presence of meso/macro porosities [41].
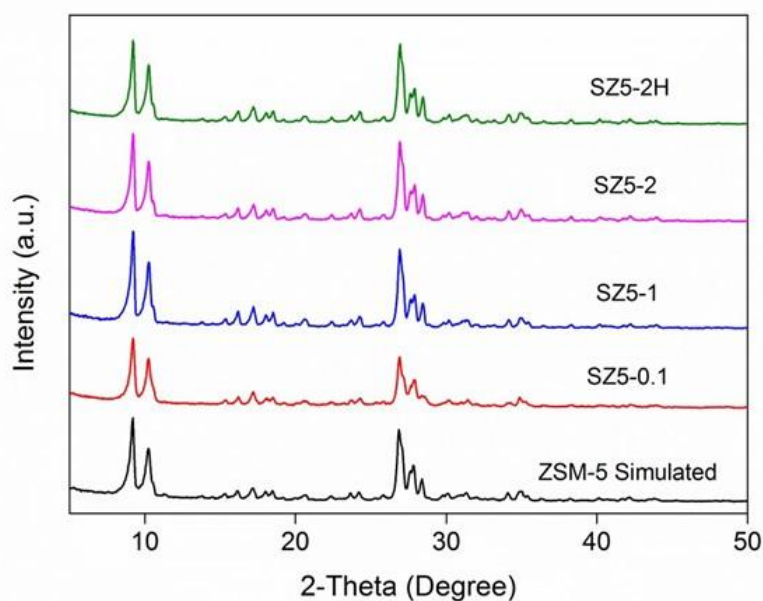
Fig. 4.1 XRD patterns of the synthesized SZ5-0.1, SZ5-1, SZ5-2, and SZ5-2H samples.

Fig. 4.2 shows the results of SEM analysis of the synthesized zeolites (SZ5-0.1, SZ5-1, SZ5-2, and SZ5-2H) and the commercial zeolites (Z5, BEA, Y_{phi}, and Y_{pho}). Figs. 4.2a to c confirmed that the particle size of the samples (along the b direction) is in ascending order: SZ5-0.1 (0.1 µm) < SZ5-1 (1 µm) < SZ5-2 (2 µm). Fig. 4.2a also shows the agglomeration of SZ5-0.1 particles. Conversely, Figs. 4.2b and c clearly show isolated particles, which indicates that the hierarchical channels were most likely generated inside the particles of SZ5-2H. As shown in Fig. 4.2d, SZ5-2H has a particle size similar to SZ5-2, while a distinct sponge-like topography was observed on the SZ5-2H particles, which is a characteristic feature of hierarchical zeolites [34]. The hierarchical single crystal exhibited coffin-like morphology that is typical of MFI

structured crystals and amorphous structures are not observed, which is consistent with the XRD patterns (Fig. 4.1). The morphology of SZ5-2H in this study was similar to that previously reported by Jacobsen et al. [33], which utilized commercial carbon black as a solid template. Fig. 4.3 shows the TEM images of the crystals in SZ5-2 (Figs. 4.3a and b) and SZ5-2H (Figs. 4.3c and d). Compared with SZ5-2, where an intact particle is observed, SZ5-2H that was produced using a carbon template shows blur bulk body and fringe with more light penetration, which can indicate the formation of a cavity, i.e., pores and/or channels. The morphology of SZ5-2H resembles that of the previously reported hierarchical zeolite Y prepared from acid/base-treated zeolites [42]. The commercial zeolites of Figs. 4.2e to h show less regular topography, while Y_{phi} (Fig. 4.2g) and Y_{pho} (Fig. 4.2h) show relatively smoother surfaces than those of Z5 (Fig. 4.2e) and BEA (Fig. 4.2f) and have heterogeneous particle sizes in the range between 0.5 to 1 µm.
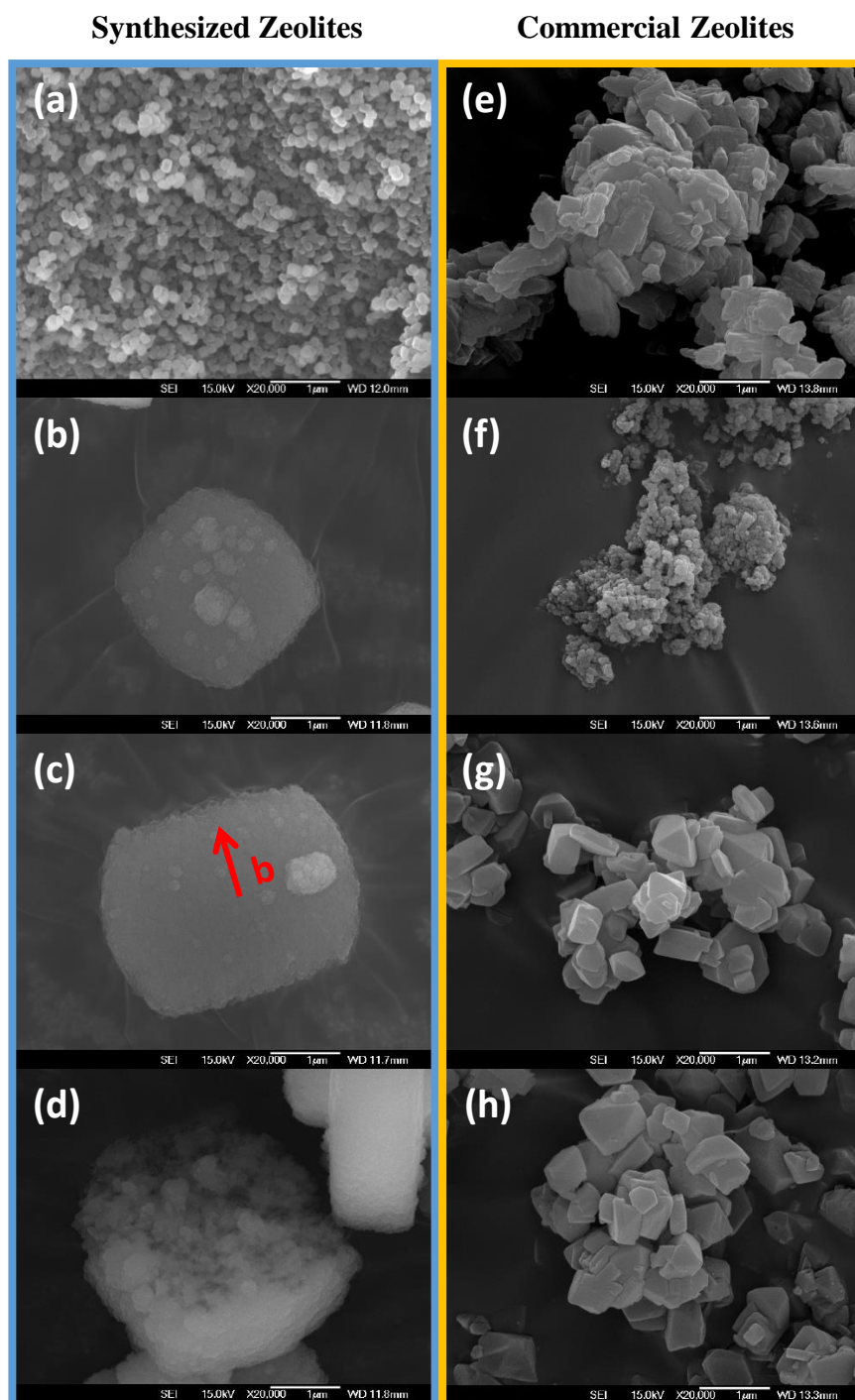
Fig. 4.2 SEM images of synthesized zeolites, (a) SZ5-0.1, (b) SZ5-1, (c) SZ5-2, and (d) SZ5-2H; commercial zeolites (e) Z5, (f) BEA, (g) Y_{phi}, and (h) Y_{pho}.
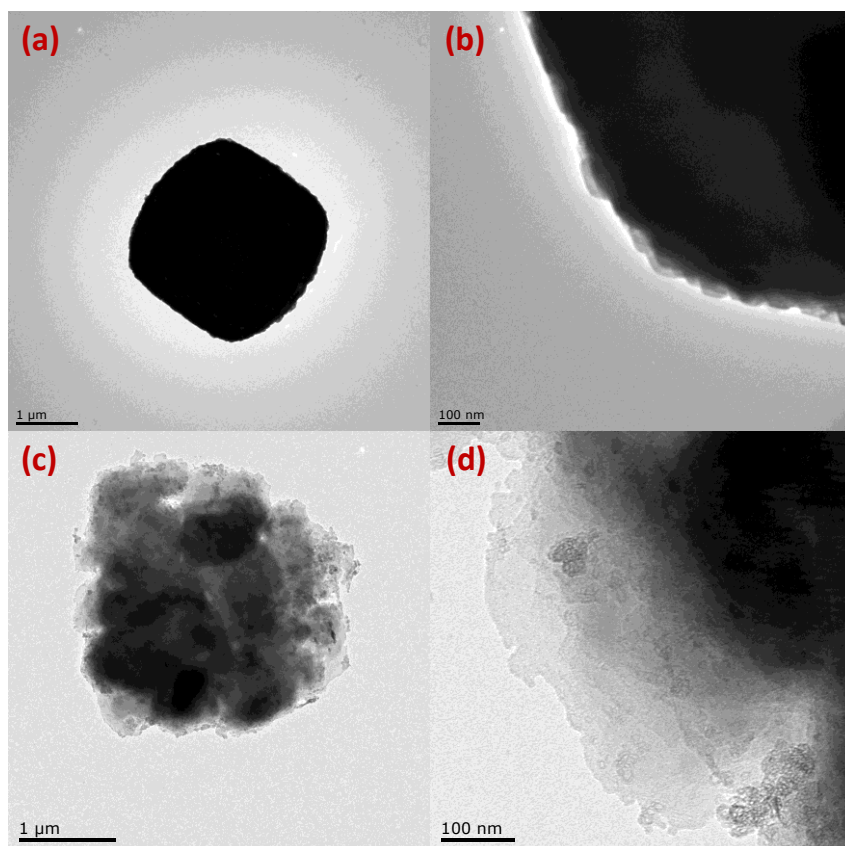
Fig. 4.3 TEM images of (a) and (b) SZ5-2; (c) and (d) SZ5-2H.

NH_3-TPD analysis of the synthesized and commercial zeolites revealed that they possessed three types of acid sites: acid site type 1 was detected between 100 to 290 °C, acid site type 2 was detected between 290 to 550 °C, and acid site type 3 was detected between 550 to 730 °C, as shown in Table 4.3. The peak at high temperature was assigned as the desorption of ammonia adsorbed on Brønsted acids and/or Lewis acids, whereas the peak at low temperature is assigned as that of ammonia adsorbed on non-acidic -OH groups or ammonium cations [43]. Since stronger acidity is associated with a higher desorption temperature [18], type 3 acidity is expected to be more effective for acid catalysis. A smaller amount of type 3 acidity for MFI zeolites, i.e., synthesized SZ5 samples and commercial Z5 (0.022 to 0.085 mmol $NH_3 \cdot g^{-1}$), compared with that for BEA (0.107 $NH_3 \cdot g^{-1}$) and Y (0.209 to 0.421 $NH_3 \cdot g^{-1}$). The total acidity of the zeolite samples generally increases with a decrease in the Si/Al ratio (Appendix B; Fig.

S1), which is consistent with the results reported by [44]. The lower total acidity of SZ5-0.1 (Si/Al = 31) than that of Y_{pho} (Si/Al = 40) is likely due to the agglomerations (Fig. 4.2a) that randomly blocked pore entrances. The total acidity of SZ5-2H is slightly lower than that of SZ5-2, which is likely attributed to the generation of macro/meso porosity, which was evident by the previous study by Han et al. [35], which indicated that the acid properties of hierarchical ZSM-5 can be simply regulated by introducing carbon black. Although the total acidity of Y_{pho} was lower than that of BEA, the type 3 acid sites of Y_{pho} was two times higher than that of BEA, which indicates that the acid strength of Y_{pho} was potentially stronger than that of BEA. The total strong acidity (type 3 in Table 4.3) of the commercial zeolites descends the order as $Y_{phi} > Y_{pho} > BEA > Z5$.

Table 4.3 Acidity measurements from NH_3-TPD.

Catalyst	Si/Al ratio	Acid sites type 1 (100-290 ºC) (mmol $NH_3 \cdot g^{-1}$)	Acid sites type 2 (290-550 ºC) (mmol $NH_3 \cdot g^{-1}$)	Acid sites type 3 (550-730 ºC) (mmol $NH_3 \cdot g^{-1}$)	Total acid sites (mmol $NH_3 \cdot g^{-1}$)
SZ5-0.1	31	0.074	0.027	0.022	0.123
SZ5-1	26	0.196	0.195	0.043	0.434
SZ5-2	26	0.221	0.248	0.080	0.549
SZ5-2H	28	0.230	0.222	0.085	0.537
Z5	11.5	0.412	0.251	0.084	0.747
BEA	12.5	0.404	0.166	0.107	0.677
Y_{phi}	2.6	0.788	0.394	0.421	1.603
Y_{pho}	40	0.019	0.088	0.209	0.316

4.3.2 Dehydration of fructose

Conversion of glucose/fructose over zeolites in aqueous phase

The conversion of glucose was examined for all zeolite samples in water singular solvent. Fig. 4.4 shows that the conversion of glucose over all zeolites was limited, and only a small amount of fructose was produced, which was likely attributed to the lack of Lewis acid that was reported to catalyze the isomerization of glucose to fructose [45], even though water can facilitate this reaction by acting as a proton shuttle [46]. Note that the glucose conversion for SZ5-2H was approximately 9.0% higher than that for SZ5-2, while the fructose yield was similar, which indicates that more byproducts were generated for hierarchical SZ5-2H compared with microporous SZ5-2. This outcome is likely due to the meso/macro porosity of SZ5-2H, which enabled larger molecules to be produced inside the channels of SZ5-2H. BEA showed the highest glucose conversion and fructose yield among all commercial zeolites and synthesized zeolites. The notable formation of fructose suggested the possible presence of Lewis acid in BEA, which catalyzes the isomerization of glucose to fructose. Jacob et al. [30] reported that the robust performance of H-BEA-18 catalyzed glucose-to-fructose isomerization and its reverse were caused by the octahedral aluminum atoms that act as Lewis acids either within the framework at lattice defect sites or as extraframework Al, that these sites were formed during calcination and were stable under reaction conditions and that they were capable of catalyzing some unknown side products. The HMF was produced over Y_{phi} zeolite for glucose conversion, which indicates that more Brønsted acidity was present of Y_{phi} zeolites than that of the remaining zeolites (Z5, BEA, Y_{pho}), which was consistent with the results of the NH_3 adsorption test in Table 4.3, where Y_{phi} had the largest amount of type 3 acid sites. However, the hydrophilic nature of Y_{phi} likely inhibited glucose conversion to some extent due to competition between water and glucose molecules for the acid sites during the reaction [47], which causes less total conversion over Y_{phi} than that of BEA.
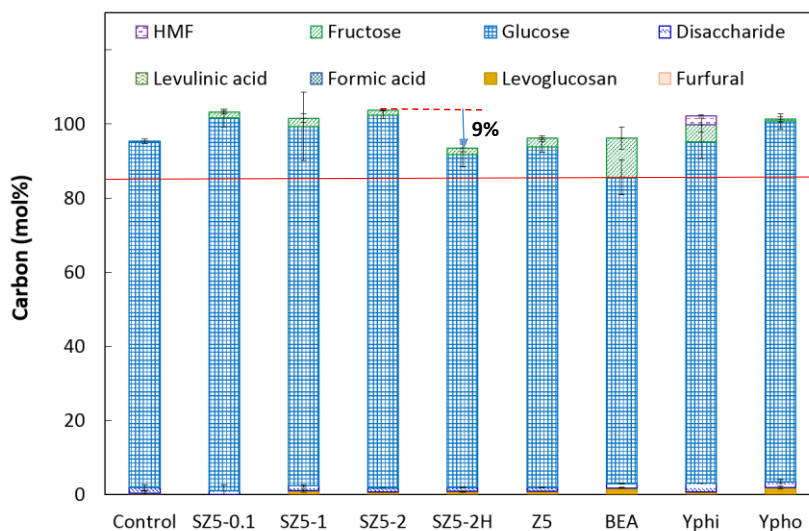
Fig. 4.4 Carbon distribution of glucose conversion in the presence of synthesized and commercial zeolites (conditions: 5 wt/v% glucose and 0.2 g zeolite catalyst in DI H_2O at 160 °C for 20 min; the red solid line represents the highest glucose conversion).

The conversion of fructose was conducted over all synthesized and commercial zeolites for the same condition as the glucose conversion. As shown in Fig. 4.5, all samples showed an increase in fructose conversion from 10.5 to 76.6%, while the HMF yield ranged from 2.4 to 16.1%. These results showed that the dehydration of fructose was substantially more active than isomerization of glucose, which suggests that Brønsted acid was the dominated acid for all tested zeolites, due to the well-known mechanism in which Lewis acid catalyzes glucose isomerization, while Brønsted acid catalyzes fructose dehydration [4]. The fructose conversion over the SZ5-0.1, SZ5-1 and SZ5-2 samples showed a similar HMF yield (2.4 to 3.0%), which indicates that the particle size of zeolites was an insignificant factor for HMF production. However, the fructose conversion over SZ5-0.1, SZ5-1 and SZ5-2 was different from 10.5 to 24.6%, which was consistent with their acidity, especially for type 3 acidity in Table 4.3, i.e.,

the higher amount of strong acidity facilitated more fructose conversion. In addition, fructose conversion over SZ5-2H (28.9%) was greater than that of SZ5-2 (22.4%), while the HMF yield was slightly changed from SZ5-2 (2.9%) to SZ5-2H (4.2%), which indicates that a larger number of side products were produced from hierarchical zeolites that have meso/macro porosities; this result was consistent with glucose conversion (Fig. 4.4) and the observation reported by [48]. Note that BEA had a fructose conversion of 76.6%, which was the maximum of all tested zeolites, while the HMF yield was only 16.1%. This finding indicates that the side reactions (i.e., rehydration and polymerization) were dominated over BEA zeolites, which can be evidenced by the formation of levulinic acid, formic acid and furfural; they have a total yield of 13.0%, which was the largest among all tested zeolites. These results were consistent with the previous report that Brønsted acid and Lewis acid promote these undesirable side reactions to various extents depending on their strength [7]. Y_{phi} and Y_{pho} showed a comparable fructose conversion of 29.2% and 25.3%, respectively. However, the HMF yield over Y_{pho} (10.1%) was almost twice that of Y_{phi} (6.4%), which indicates that the hydrophilicity of Y_{phi} inhibited the HMF yield in water. Even though Y_{phi} had the strongest acidity (Table 4.3), the existence of abundant water may isolate the effective interaction between the substrate and acid sites. Since the synthesized zeolites showed a lower glucose/fructose conversion when compared with commercial ones, the tests on binary solvent systems will mainly focus on commercial zeolites.
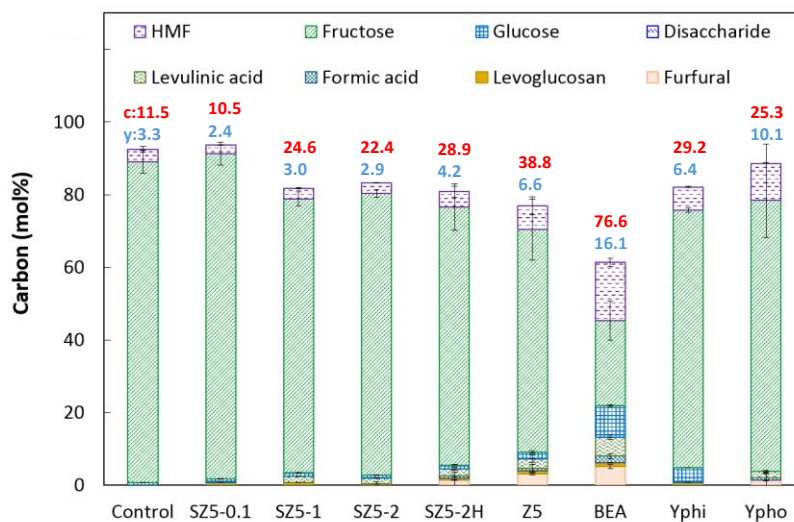
Fig. 4.5 Carbon distribution of fructose conversion in the presence of synthesized and commercial zeolites (conditions: 5 wt/v% fructose and 0.2 g zeolite catalyst in DI H_2O at 160 °C for 20 min; c in red represents fructose conversion, y in blue represents HMF yield).

Dehydration of fructose over zeolites in polar aprotic-water system

To investigate the effect of binary solvents, especially polar aprotic solvent and properties of zeolites (structure, acidity, and water affinity), on fructose conversion and HMF yield, the fructose conversion was conducted over commercial zeolites (Z5, BEA, Y_{phi}, and Y_{pho}) in four polar aprotic solvent mixtures, as shown in Fig. 4.6. The highest fructose conversion, HMF yield and HMF selectivity was obtained over Y_{pho} zeolite in DMSO/H_2O medium, which were 72.4%, 49.2% and 68.0%, respectively (Fig. 4.6a). In addition, the highest HMF yield over Y_{pho} was attained in the medium of acetone/H_2O and PC/H_2O, which was 11.2% and 24.5%, respectively, and the highest HMF selectivity was attained in these solvent mixtures, which were 47.6% for acetone/H_2O and 40.0% for PC/H_2O, as shown in Figs. 4.6b and d. When using GVL/H_2O as the medium, the HMF yield over Y_{pho} (18.1%) was comparable with that of Y_{phi}

(21.0%), while Y_{pho} (55.2%) had considerably higher HMF selectivity than that of Y_{phi} (37.3%), as shown in Fig. 4.6c. These results revealed that Y_{pho} had the most stable and active performance among all tested mixtures, which was likely attributed to its strong acidity (type 3 acidity from Table 4.3) and hydrophobic nature. Even though Y_{phi} (0.421 mmol $NH_3 \cdot g^{-1}$) has twice the strong acidity (type 3 acid sites from Table 4.3) than that of Y_{pho} (0.209 mmol $NH_3 \cdot g^{-1}$), Y_{pho} showed a better total HMF yield and selectivity than that of Y_{phi}, indicting the hydrophilic nature of Y_{phi}, which impeded the HMF formation due to a better affinity of water to the acid sites compared with the organic phase. This impedance limited the interactions between the acid sites and the organic solvents, where the fructose can dissolve more readily in the organic phase than in the water phase [29]. Z5 showed the lowest fructose conversion in the mixtures of acetone/H_2O (11.1%), GVL/H_2O (26.2%) and PC/H_2O (27.8%), as shown in Figs. 4.6b, c and d, while it showed the second lowest fructose conversion (23.3%) in the DMSO/H_2O medium, which is likely attributed to the smaller porosity of Z5 ($4.7 \times 4.46 \times 4.46$ Å) than that of BEA ($5.95 \times 5.95 \times 5.95$ Å) and Y ($7.35 \times 7.35 \times 7.35$ Å). Despite the similar Si/Al ratio (11.5-12.5, Table 4.1) and comparable strong acidity (0.084-0.107 mmol $NH_3 \cdot g^{-1}$, Table 4.3) between Z5 and BEA, the fructose conversion over BEA was 8-41% higher than Z5 depending on the reaction mixtures. This result suggested that the acid sites in Z5 may not be accessible due to the unfavorable porosity, which highlights the latter as a prerequisite for high catalytic activity. These results were consistent with the research findings that indicated that fructose conversion can occur inside the microspores of zeolites but zeolites with smaller pore sizes tended to have more initial diffusion limitations [29]. Z5 showed high HMF selectivity in all mixtures, i.e., 55.3% in DMSO/H_2O, 30.8% in acetone/H_2O, 55.4% in GVL/H_2O, and 34.7% in PC/H_2O, which may be attributed to the smallest porosity of Z5 and caused the reaction that occurred on the external surface at initial stage over Z5. This reaction decreased the reaction time between the fructose molecules and zeolites and limited the further secondary

transformations that would consume HMF to undesired side products [48]. The total catalyst activity and stability in the tested conditions were increased on the order of Z5 < BEA < Y_{phi} < Y_{pho}.

In addition to the catalyst—the fructose conversion—solvent characters may have an important role on HMF yield and HMF selectivity to various extents. Recent studies suggested that solvents can promote the formation of reactive tautomer of fructose and xylose for enhancing the dehydration reaction [49-50]. Among the investigated binary solvents, the fructose conversion was the lowest in acetone/H_2O, in which heat transfer can be hindered due to the particular low dielectric constant and dipole moment of acetone that disfavored microwave adsorption (Table 4.4). The HMF yield significantly increased when DMSO/H_2O was employed compared with water singular solvent over Z5, BEA, and Y_{pho} zeolites. In particular, the HMF yield was increased by 6.3%, 18.9% and 39.1% for Z5, BEA and Y_{pho}, respectively (Fig. 4.6a). However, the HMF yield over Y_{phi} remained constant as before (6.4%) and after the DMSO addition (5.8%), which was likely due to the water layer that separated the organic phase from the active sites of Y_{phi} zeolites [29]. The HMF yield has increased over Y_{phi} by the addition of acetone, GVL and PC when compared with water singular solvent by 4.8%, 14.6% and 11.7%, respectively (Fig. 4.6b, c and d), which can be ascribed to the lower polarity of these solvents than that of DMSO (Table 4.4). The HMF selectivity was considerably increased after the addition of organic solvents, especially in the presence of DMSO, which increased the HMF selectivity by 38.3%, 34.7%, 12.2%, and 27.9% for Z5, BEA, Y_{phi}, and Y_{pho} when compared with their performance in singular water. These results were consistent with the research that revealed that the addition of organic solvent promoted the HMF selectivity and suppressed byproducts formation to different extents in the presence of $SnCl_4$ as the homogenous catalysts [27-28]. The total solvent performance in terms of HMF yield and HMF selectivity increased from acetone < PC < GVL < DMSO in the tested conditions. The relative

significance should be evaluated via spectroscopic analysis and modeling to acquire detailed understanding on the local environmental of the substrate and the catalyst in different solvent systems.
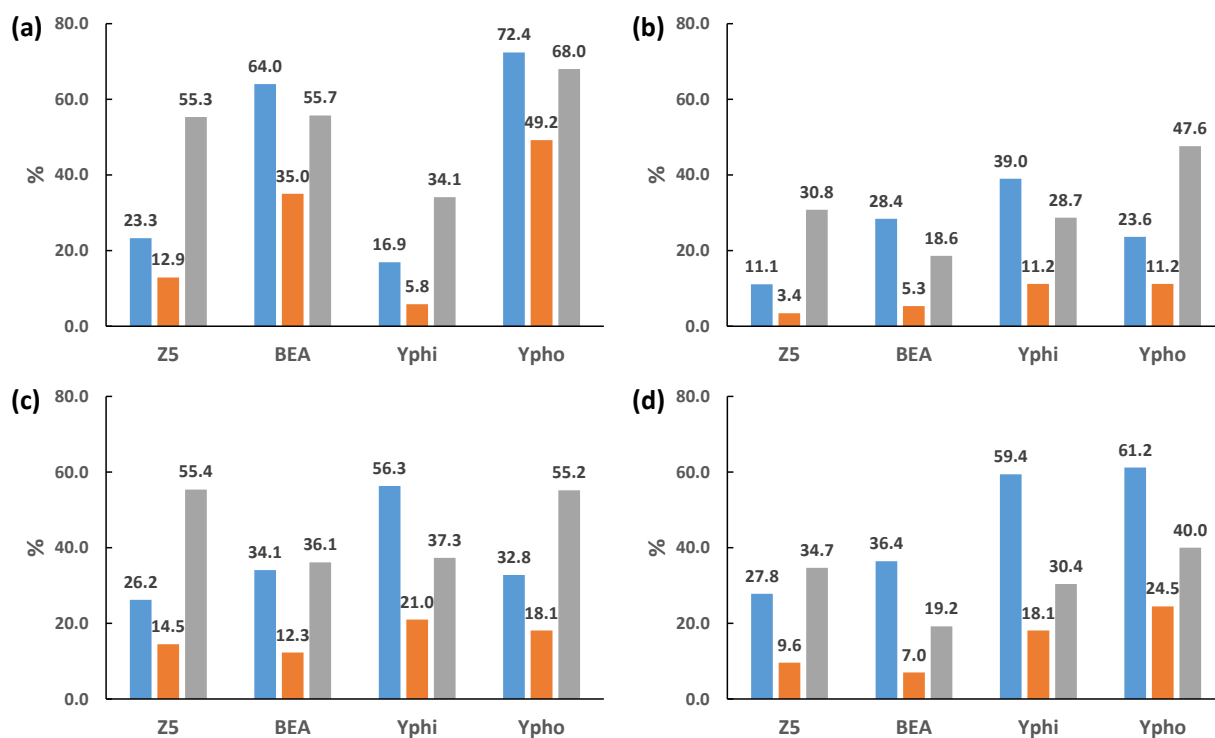
Fig. 4.6 Fructose conversion (blue), HMF yield (orange) and HMF selectivity (grey) for the commercial zeolites in polar aprotic-water binary solvent systems of (a) DMSO/H_2O, (b) acetone/H_2O, (c) GVL/H_2O, and (d) PC/H_2O. (Conditions: 5 wt/v% fructose and 0.2 g zeolite catalyst in solvent mixture (1:1 v/v) at 160 °C for 20 min)

Table 4.4 Physicochemical properties[a] of different solvents.

Solvent	Density (g/ml)	DE[b]	DM[c]	Polarity (π*)[d]
Acetone	0.78	20.7	2.91	0.71
DMSO	1.09	46.7	3.96	0.94
GVL	1.04	36.4	5.3	0.83
PC	1.2	64	4.9	0.83
Water	1	78.5	1.85	1.09

[a]Extracted from [28, 51, 52].

[b]Dielectric constant (DE).

[c]Dipole moment (DM) in D units.

[d]Kamlet-Taft solvatochromic π* scale.

Conversion over zeolites in the DMSO-water system

The kinetic study was conducted for Z5, BEA, Y_{phi}, and Y_{pho} in the medium of DMSO/H_2O due to the most robust performance of DMSO among the tested organic solvents that were observed in the last section. DMSO is also regarded as one of the most commonly employed organic solvents for fructose dehydration [53]. Previous computational studies of solvent-water mixtures reported the favorable arrangement of DMSO molecules near the hydroxyl group of glucose and fructose, which generated an improvement in desirable reactions [26]. The preferable coordination between DMSO and the carbonyl group of HMF, where the off-path rehydration polymerization was triggered, was also reported [25]. The HMF yield increased and fructose steadily decreased because the fructose dehydration proceeds over time, as shown in Fig. 4.7. The HMF concentration continued to increase in response to the consumption of fructose and attained the plateau of 49.2% at 20 min in the presence of Y_{pho} (Fig. 4.7d). A lower

plateau was also indicated for BEA of 35.0% at 20 min (Fig. 4.7b). No plateau was observed for the catalyzed fructose conversion of Z5 and Y_{phi}, and the HMF yield over Z5 and Y_{pho} was only 24.9% and 16.5%, respectively, even at 40 min. These results suggested that the positive relation between the HMF yield and strong acidity of zeolites as Y_{pho} > BEA > Z5 (type 3 acidity in Table 4.3), with the exception that Y_{phi} has the largest amount of strong acidity (type 3 acidity in Table 4.3) but showed the lowest HMF yield over 40 min. These results confirmed that hydrophilicity was one of the key factors that impeded the HMF formation over Y_{phi}. In addition, the HMF selectivity showed the same trend as the HMF yield, as shown in Fig. 4.8, i.e., Y_{pho} > BEA > Z5 > Y_{phi}, which can be attributed to same factors, i.e., water affinity and strong acidity. In addition, note that HMF selectivity over Y_{pho} was 50% within 1 min, while no HMF was detected for Z5, BEA, and Y_{phi} in the same time period, which suggests the higher activity, HMF selectivity and stability of Y_{pho}. The kinetic study confirmed that the high selectivity toward desirable reactions can be attributed to the favorable coordination among the substrates, the catalysts and the solvent-product interactions.
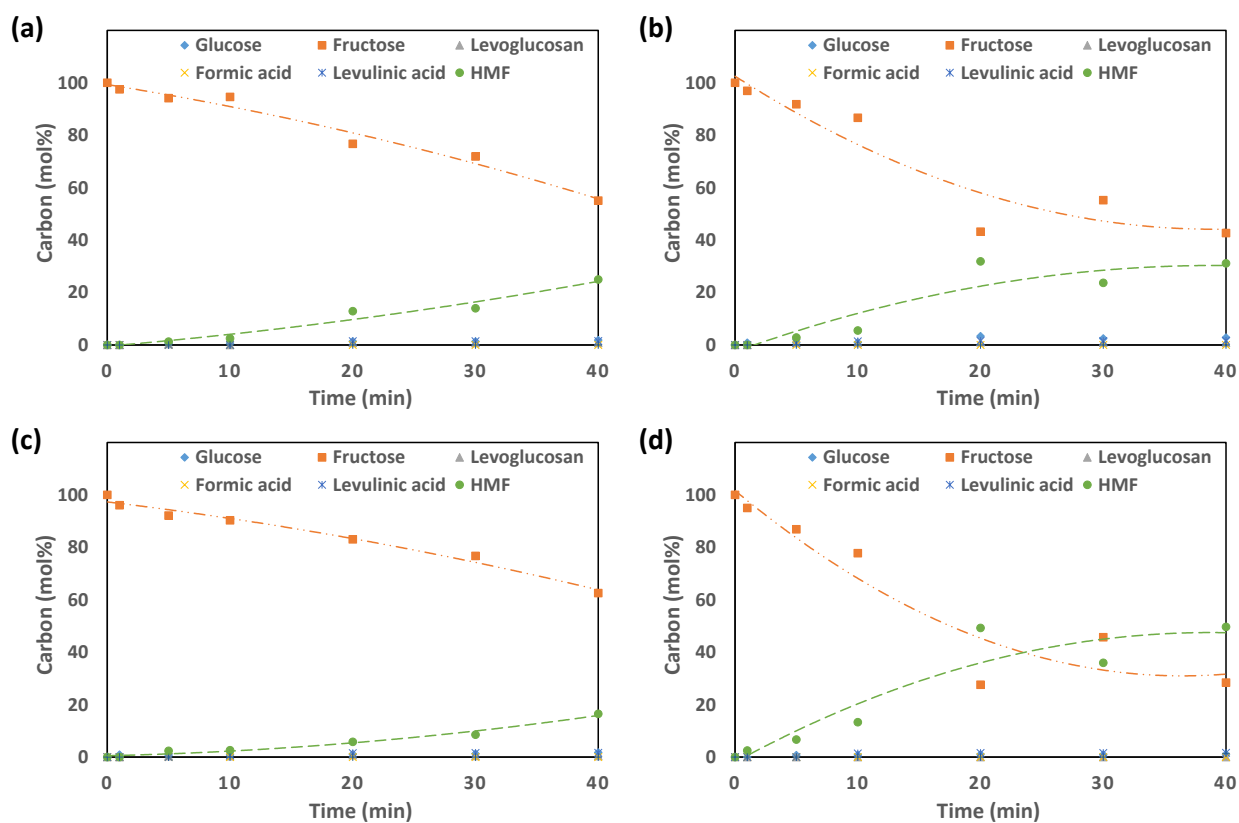
Fig. 4.7 Carbon distribution during the fructose conversion in the medium of DMSO/H$_2$O over zeolites of (a) Z5, (b) BEA, (c) Y$_{phi}$, and (d) Y$_{pho}$. (Conditions: 5 wt/v% fructose and 0.2 g zeolite catalyst in solvent mixture (1:1 v/v) at 160 ^{o}C for 1 to 40 min)
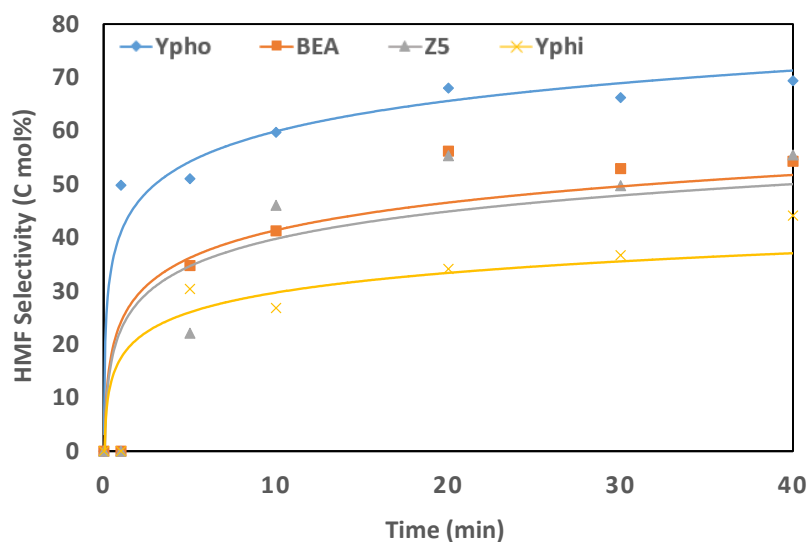
Fig. 4.8 HMF Selectivity during the fructose conversion in the medium of DMSO/H$_2$O over zeolites of (a) Z5, (b) BEA, (c) Y$_{phi}$, and (d) Y$_{pho}$. (Conditions: 5 wt/v% fructose and 0.2 g zeolite catalyst in solvent mixture (1:1 v/v) at 160 ºC for 1 to 40 min)

4.4 Conclusions

This study elucidates the relationship and the effects of different organic solvents and zeolites with different characteristics (i.e., structure, acidity and water affinity) on fructose dehydration to HMF. The synthesized MFI zeolites and commercial zeolites were employed as acid catalysts for the glucose/fructose conversion, in the medium of water and water-organic mixtures, i.e., DMSO/H$_2$O, acetone/H$_2$O, GVL/H$_2$O and PC/H$_2$O. Specifically, the relative role of heterogeneous chemistry (both solvent and zeolite-induced) was delineated during fructose dehydration. The HMF yield is independent of particle size for the same type of zeolite. The secondary porosity that was introduced by carbon templates, however, significantly influenced the glucose/fructose conversion due to enlarged channels that enabled the formation of large undesired byproducts (via dehydration and polymerization). The addition of different zeolite

117

types and organic/water mixtures promoted fructose conversion differently. The total catalyst activity and stability increase on the order Z5 < BEA < Y_{phi} < Y_{pho}. The total solvent performance on the HMF yield and selectivity increase on the order acetone < PC < GVL < DMSO. Particularly, the highest fructose conversion (72.4%) and HMF yield (49.2%) were achieved in the DMSO/H_2O mixture in the presence of Y_{pho} as the catalyst. The superior activity and stability of Y_{pho} were attributed to the strong acidity and the hydrophobic nature of the catalyst. The DMSO/H_2O mixture was also determined to efficiently suppress the formation of byproducts. The kinetic study further confirmed that the high HMF selectivity can be attributed to the synergistic effect of the substrates, catalysts and solvent-product interactions.

4.5 References

[1] M. Dashtban, A. Gilbert, P. Fatehi, Recent advancements in the production of hydroxymethylfurfural, RSC Adv., 4 (2014) 2037-2050.

[2] A. Mukherjee, M.-J. Dumont, V. Raghavan, Sustainable production of hydroxymethylfurfural and levulinic acid: Challenges and opportunities, Biomass Bioenergy, 72 (2015) 143-183.

[3] P.K. Rout, A.D. Nannaware, O. Prakash, A. Kalra, R. Rajasekharan, Synthesis of hydroxymethylfurfural from cellulose using green processes: A promising biochemical and biofuel feedstock, Chem. Eng. Sci., 142 (2016) 318-346.

[4] I.K.M. Yu, D.C.W. Tsang, Conversion of biomass to hydroxymethylfurfural: A review of catalytic systems and underlying mechanisms, Bioresour. Technol., 238 (2017) 716-732.

[5] G. Festel, Market Structure and Growth Rates of Industrial Biorenewables, Industrial Biorenewables: A Practical Viewpoint, (2016) 245-254.

[6] P. Wrigstedt, J. Keskiväli, M. Leskelä, T. Repo, The Role of Salts and Brønsted Acids in Lewis Acid-Catalyzed Aqueous-Phase Glucose Dehydration to 5-Hydroxymethylfurfural, ChemCatChem, 7 (2015) 501-507.

[7] X. Li, K. Peng, X. Liu, Q. Xia, Y. Wang, Comprehensive Understanding of the Role of Brønsted and Lewis Acid Sites in Glucose Conversion into 5-Hydromethylfurfural, ChemCatChem, 9 (2017) 2739-2746.

[8] G. Tsilomelekis, M.J. Orella, Z. Lin, Z. Cheng, W. Zheng, V. Nikolakis, D.G. Vlachos, Molecular structure, morphology and growth mechanisms and rates of 5-hydroxymethyl furfural (HMF) derived humins, Green Chem., 18 (2016) 1983-1993.

[9] J. Tang, L. Zhu, X. Fu, J. Dai, X. Guo, C. Hu, Insights into the Kinetics and Reaction Network of Aluminum Chloride-Catalyzed Conversion of Glucose in NaCl–H2O/THF Biphasic System, ACS Catalysis, 7 (2016) 256-266.

[10] I.K.M. Yu, D.C.W. Tsang, A.C.K. Yip, S.S. Chen, L. Wang, Y.S. Ok, C.S. Poon, Catalytic valorization of starch-rich food waste into hydroxymethylfurfural (HMF): Controlling relative kinetics for high productivity, Bioresour. Technol., 237 (2017) 222-230.

[11] B. Kuster, 5-Hydroxymethylfurfural (HMF). A review focussing on its manufacture, Starch-Stärke, 42 (1990) 314-321.

[12] I.K.M. Yu, D.C.W. Tsang, A.C.K. Yip, S.S. Chen, Y.S. Ok, C.S. Poon, Valorization of food waste into hydroxymethylfurfural: Dual role of metal ions in successive conversion steps, Bioresour. Technol., 219 (2016) 338-347.

[13] P. Carniti, A. Gervasini, S. Biella, A. Auroux, Niobic acid and niobium phosphate as highly acidic viable catalysts in aqueous medium: fructose dehydration reaction, Catal. Today, 118 (2006) 373-378.

[14] A. Takagaki, M. Ohara, S. Nishimura, K. Ebitani, A one-pot reaction for biorefinery: combination of solid acid and base catalysts for direct production of 5-hydroxymethylfurfural from saccharides, Chem. Commun., (2009) 6276-6278.

[15] X. Xiong, I.K.M. Yu, S.S. Chen, D.C.W. Tsang, L. Cao, H. Song, E.E. Kwon, Y.S. Ok, S. Zhang, C.S. Poon, Sulfonated biochar as acid catalyst for sugar hydrolysis and dehydration, Catal. Today, 314 (2018) 52-61.

[16] H. Wang, Q. Kong, Y. Wang, T. Deng, C. Chen, X. Hou, Y. Zhu, Graphene oxide catalyzed dehydration of fructose into 5-hydroxymethylfurfural with isopropanol as cosolvent, ChemCatChem, 6 (2014) 728-732.

[17] M. Moreno-Recio, J. Santamaría-González, P. Maireles-Torres, Brönsted and Lewis acid ZSM-5 zeolites for the catalytic dehydration of glucose into 5-hydroxymethylfurfural, Chem. Eng. J., 303 (2016) 22-30.

[18] Z. Ma, H. Hu, Z. Sun, W. Fang, J. Zhang, L. Yang, Y. Zhang, L. Wang, Acidic Zeolite L as a Highly Efficient Catalyst for Dehydration of Fructose to 5-Hydroxymethylfurfural in Ionic Liquid, Chemsuschem, 10 (2017) 1669-1674.

[19] R. Otomo, T. Yokoi, T. Tatsumi, OSDA-Free Zeolite Beta with High Aluminum Content Efficiently Catalyzes a Tandem Reaction for Conversion of Glucose to 5-Hydroxymethylfurfural, ChemCatChem, 7 (2015) 4180-4187.

[20] S. Chin, M. Ahmad, M. Kamaruzaman, C. Cheng, Kinetic studies of the esterification of pure and dilute acrylic acid with 2-ethyl hexanol catalysed by Amberlyst 15, Chem. Eng. Sci., 129 (2015) 116-125.

[21] C. Moreau, Agro-Food-Industry Hi-Tech, 2002, January/February, 17-26.

[22] Y. Yang, C. Hu, M.M. Abu-Omar, Conversion of glucose into furans in the presence of AlCl3 in an ethanol–water solvent system, Bioresour. Technol., 116 (2012) 190-194.

[23] S. Jia, Z. Xu, Z.C. Zhang, Catalytic conversion of glucose in dimethylsulfoxide/water binary mix with chromium trichloride: Role of water on the product distribution, Chem. Eng. J., 254 (2014) 333-339.

[24] Y. Yang, C.-w. Hu, M.M. Abu-Omar, Conversion of carbohydrates and lignocellulosic biomass into 5-hydroxymethylfurfural using $AlCl_3 \cdot 6H_2O$ catalyst in a biphasic solvent system, Green Chem., 14 (2012) 509-513.

[25] S.H. Mushrif, S. Caratzoulas, D.G. Vlachos, Understanding solvent effects in the selective conversion of fructose to 5-hydroxymethyl-furfural: a molecular dynamics investigation, PCCP, 14 (2012) 2637-2644.

[26] V. Vasudevan, S.H. Mushrif, Insights into the solvation of glucose in water, dimethyl sulfoxide (DMSO), tetrahydrofuran (THF) and N, N-dimethylformamide (DMF) and its possible implications on the conversion of glucose to platform chemicals, RSC Adv., 5 (2015) 20756-20763.

[27] I.K.M. Yu, D.C.W. Tsang, S.S. Chen, L. Wang, A.J. Hunt, J. Sherwood, K. De Oliveira Vigier, F. Jerome, Y.S. Ok, C.S. Poon, Polar aprotic solvent-water mixture as the medium for catalytic production of hydroxymethylfurfural (HMF) from bread waste, Bioresour. Technol., 245 (2017) 456-462.

[28] I.K.M. Yu, D.C.W. Tsang, A.C.K. Yip, A.J. Hunt, J. Sherwood, J. Shang, H. Song, Y.S. Ok, C.S. Poon, Propylene carbonate and γ-valerolactone as green solvents enhance Sn(iv)-catalysed hydroxymethylfurfural (HMF) production from bread waste, Green Chem., 20 (2018) 2064-2074.

[29] V.V. Ordomsky, J. van der Schaaf, J.C. Schouten, T.A. Nijhuis, The effect of solvent addition on fructose dehydration to 5-hydroxymethylfurfural in biphasic system over zeolites, J. Catal., 287 (2012) 68-75.

[30] J.S. Kruger, V. Choudhary, V. Nikolakis, D.G. Vlachos, Elucidating the Roles of Zeolite H-BEA in Aqueous-Phase Fructose Dehydration and HMF Rehydration, ACS Catalysis, 3 (2013) 1279-1291.

[31] X. Jia, Y. Jeong, H. Baik, J. Choi, A.C. Yip, Increasing Resolution of Selectivity in Alkene Hydrogenation via Diffusion Length in Core-shell MFI zeolite, Catal. Today, (2018).

[32] H. Mochizuki, T. Yokoi, H. Imai, R. Watanabe, S. Namba, J.N. Kondo, T. Tatsumi, Facile control of crystallite size of ZSM-5 catalyst for cracking of hexane, Microporous Mesoporous Mater., 145 (2011) 165-171.

[33] C.J. Jacobsen, C. Madsen, J. Houzvicka, I. Schmidt, A. Carlsson, Mesoporous zeolite single crystals, J. Am. Chem. Soc., 122 (2000) 7116-7117.

[34] K. Zhu, K. Egeblad, C.H. Christensen, Mesoporous carbon prepared from carbohydrate as hard template for hierarchical zeolites, Eur. J. Inorg. Chem., 2007 (2007) 3955-3960.

[35] S. Han, Z. Wang, L. Meng, N. Jiang, Synthesis of uniform mesoporous ZSM-5 using hydrophilic carbon as a hard template, Mater. Chem. Phys., 177 (2016) 112-117.

[36] X. Jia, D. Jiang, D.C.W. Tsang, J. Choi, A.C.K. Yip, Stacking MFI zeolite structures for improved Sonogashira coupling reactions, Microporous Mesoporous Mater., (2018).

[37] I.K.M. Yu, D.C.W. Tsang, A.C.K. Yip, S.S. Chen, Y.S. Ok, C.S. Poon, Valorization of starchy, cellulosic, and sugary food waste into hydroxymethylfurfural by one-pot catalysis, Chemosphere, 184 (2017) 1099-1107.

[38] I.Z. Association, Database of Zeolite Structures, 2017.

[39] I. Halasz, S. Kim, B. Marcus, Hydrophilic and hydrophobic adsorption on Y zeolites, Mol. Phys., 100 (2002) 3123-3132.

[40] L. Xu, S. Wu, J. Guan, H. Wang, Y. Ma, K. Song, H. Xu, H. Xing, C. Xu, Z. Wang, Q. Kan, Synthesis, characterization of hierarchical ZSM-5 zeolite catalyst and its catalytic performance for phenol tert-butylation reaction, Catal. Commun., 9 (2008) 1272-1276.

[41] Q. Lei, T. Zhao, F. Li, L. Zhang, Y. Wang, Catalytic cracking of large molecules over hierarchical zeolites, Chem Commun (Camb), (2006) 1769-1771.

[42] D. Verboekend, G. Vilé, J. Pérez-Ramírez, Hierarchical Y and USY Zeolites Designed by Post-Synthetic Strategies, Adv. Funct. Mater., 22 (2012) 916-928.

[43] K. Kubo, H. Iida, S. Namba, A. Igarashi, Effect of steaming on acidity and catalytic performance of H-ZSM-5 and P/H-ZSM-5 as naphtha to olefin catalysts, Microporous Mesoporous Mater., 188 (2014) 23-29.

[44] L. Yang, Z. Liu, Z. Liu, W. Peng, Y. Liu, C. Liu, Correlation between H-ZSM-5 crystal size and catalytic performance in the methanol-to-aromatics reaction, Chin. J. Catal., 38 (2017) 683-690.

[45] I.K.M. Yu, D.C.W. Tsang, Z. Su, A.C.K. Yip, J. Shang, Y.S. Ok, K.-H. Kim, C.S. Poon, Contrasting Roles of Maleic Acid in Controlling Kinetics and Selectivity of Sn(IV)- and Cr(III)-catalyzed Hydroxymethylfurfural (HMF) Synthesis, ACS Sustain. Chem., (2018).

[46] F. Zhou, X. Sun, D. Wu, Y. Zhang, H. Su, Role of Water in Catalyzing Proton Transfer in Glucose Dehydration to 5-Hydroxymethylfurfural, ChemCatChem, 9 (2017) 2784-2789.

[47] R. Xiong, M. Leon, V. Nikolakis, S.I. Sandler, D.G. Vlachos, Adsorption of HMF from water/DMSO solutions onto hydrophobic zeolites: experiment and simulation, Chemsuschem, 7 (2014) 236-244.

[48] I. Graça, M.C. Bacariza, A. Fernandes, D. Chadwick, Desilicated NaY zeolites impregnated with magnesium as catalysts for glucose isomerisation into fructose, Appl. Catal. B Environ., 224 (2018) 660-670.

[49] H. Lin, Q. Xiong, Y. Zhao, J. Chen, S. Wang, Conversion of carbohydrates into 5-hydroxymethylfurfural in a green reaction system of CO2-water-isopropanol, AlChE J., 63 (2017) 257-265.

[50] S. Wang, Y. Zhao, H. Lin, J. Chen, L. Zhu, Z. Luo, Conversion of C5 carbohydrates into furfural catalyzed by a Lewis acidic ionic liquid in renewable γ-valerolactone, Green Chem., 19 (2017) 3869-3879.

[51] S. Gajula, K. Inthumathi, S.R. Arumugam, K. Srinivasan, Strategic Designing on Selection of Solvent Systems for Conversion of Biomass Sugars to Furan Derivatives and Their Separation, ACS Sustain. Chem., 5 (2017) 5373-5381.

[52] P.G. Jessop, D.A. Jessop, D. Fu, L. Phan, Solvatochromic parameters for solvents of interest in green chemistry, Green Chem., 14 (2012) 1245-1259.

[53] Y. Román-Leshkov, J.N. Chheda, J.A. Dumesic, Phase modifiers promote efficient production of hydroxymethylfurfural from fructose, Science, 312 (2006) 1933-1937.

Chapter 5

Increasing Resolution of Selectivity in Alkene Hydrogenation via Diffusion Length in Core-shell MFI zeolite

The work in this chapter was published as

5.1 Introduction

Zeolites are crystalline aluminosilicates with periodic arrangements of pores or channels in the microporous range (typically less than 1.5 nm). Their unique structures/topologies, thermal/mechanical stabilities, high specific surface area, ion-exchange capacities, superior catalytic activity and shape-selectivity have been widely used in refinery and petrochemical industries [1]. In particular, ZSM-5 (a MFI type zeolite which is the easiest to be synthesized in industrial scale) has attracted considerable research interest in recent years since it has been used as a catalyst for the first methanol-to-gasoline (MTG) process by Exxon Mobil [2, 3]. The thermally stable, interconnected 10-membered ring channels allow ZSM-5 and its supported catalysts to be highly selective in hydrocarbon conversions [4-8], nitrogen oxides (NOx) reduction [9-11], as well as other important industrial applications such as methanol-to-propene (MTP), N_2O decomposition, Fenton's reaction and photocatalytic reactions [12-20]. In addition, the para-selectivity of ZSM-5 has been demonstrated in selective formation of *p*-xylene over its isomers (*o*-xylene and *m*-xylene) in which the pore size of ZSM-5 only allows product molecules with specific pore size and shape to leave the framework [21-23]. Nevertheless, high reactant and product selectivities of zeolite based on pore size only prevail when the molecules are very distinct in terms of size and structure, for example, linear olefins and aromatics. Selectivity to reactants with similar molecular size and shape, such as 1-hexene and 1-heptene, however, usually are not distinguishable.

In zeolite-catalyzed reactions, reactant molecules diffuse into the pores and reach the active sites inside the channels, and the chemical reactions proceeds, followed by diffusion of product molecules into the bulk phase from zeolite pores. Therefore, the relation between reaction rate and diffusivity of reactant and product molecules within zeolite pores strongly affect activity and product selectivity of reactions [24]. To design porous catalysts using the chemical reaction engineering approach, the Thiele modulus (ø) and effectiveness factor, expressed as a function

of Thiele modulus, are used [25, 26]. The Thiele modulus for zeolite with a slab shape can be expressed as [27, 28]:

$$\o = L\sqrt{\rho k / D_{eff}} \tag{1}$$

where, L is the diffusion length of catalyst (half thickness of the slab), k is the reaction rate constant of catalytic reaction, ρ is the density and D_{eff} is the effective diffusivity of the molecules. Using the Thiele modulus, catalytic reactions with a porous catalyst have been classified into three types [25]: (1) reaction-control conditions ($\o<0.1$), (2) diffusion-control conditions ($\o>5$), and (3) transition conditions ($0.1<\o<5$; between reaction-control and diffusion-control conditions). Under the reaction-control conditions, active sites (acid sites) within the zeolite are fully utilized during reaction. In contrast, under diffusion-control conditions, less than 20% of active sites near the external surface of the zeolite are used. For the effective use of the selectivity caused by diffusion within the zeolite channels, the reaction should be conducted under diffusion control conditions. Since the Thiele modulus ($\o$) has a linear relation with the diffusion length of the catalyst (L), as shown in Eq. (1)., we herein propose a potential way to achieve high resolution of reactant/product selectivity using a core-shell ZSM-5 structure resulted from zeolite overgrowth [29-31].

Successful overgrowth of the zeolite shell layer and its thickness in the core-shell structure strongly depends on the Si/Al ratio and the crystal size and shape of the composite core [32-34]. Specifically, due to the layer-by-layer mechanism of zeolite crystal growth [35], the outer layer growth can only occur after the completion of the inner layer, suggesting a theoretical foundation that the core-shell structure is indeed possible and the core-shell zeolite crystal will grow uniformly as the shell layers build on. In this work, we successfully synthesized silicalite-1/Pd/ZSM-5 core-shell catalyst with different thickness of silicalite-1 layer formed from secondary crystallization on the Pd/ZSM-5 core. The catalytic performance of the core-shell

silicate-1/Pd/ZSM-5 catalysts in hydrogenation of 1-hexene, 1-heptene and cyclohexene was examined. We demonstrated herein a strong correlation between the diffusion length and the preferential selectivity among alkenes with similar molecular size.

5.2 Experimental

5.2.1 Materials

Tetraethyl orthosilicate (TEOS, 98%), aluminum isopropoxide (>98%), tetrapropylammonium hydroxide (TPAOH, 1.0 M in H_2O), palladium nitrate dihydrate (approximately 40% Pd basis), sodium borohydride (99%), 1-hexene (>99%), 1-heptene (97%) and cyclohexene (99%) were purchased from Sigma-Aldrich Chemical Co. Sodium hydroxide and ethanol (EtOH, 99.5%) were purchased from Thermo Fisher Scientific. Ethyl acetate (99%) was purchased from J.T. Baker. Instrument grade hydrogen and argon were purchased from BOC. Deionized (DI) water was prepared by a lab-based water-purification apparatus and was used to prepare all required samples and solutions. All chemicals were used as received without any further treatment.

5.2.2 Sample preparation

In a typical synthesis, 7.5 ml of TPAOH, 28 ml of DI water and 27.9 ml of TEOS were added sequentially to a polypropylene (PP) bottle. The resulting mixture was put into an incubator shaker (INFORS HT Multitron) at 298 K for 24 h. Thereafter, the solution containing 0.26 g of NaOH, 1.02 g of aluminum isopropoxide, 28 ml of DI water and 7.5 ml of TPAOH was added to the mixture. The prepared mother gel was stirred at 298 K for 3 h, followed by crystallization at 453 K for 42 h. The molar composition of the final gel was TPAOH:NaOH:Al(O-i-Pr)$_3$:SiO$_2$:H$_2$O = 3:1:1:25:750. The solid products were subsequently washed 3 times with DI water and collected by centrifugation. Finally, the Na-ZSM-5 samples

were obtained by calcination of the as-synthesized sample in a tube furnace at 823 K (ramping rate of 1 K/min from ambient temperature) for 10 h to remove the organic template.

The Pd/ZSM-5 core containing approximately 2.0 wt% palladium was obtained by adding a 5-ml $Pd(NO_3)_2$ aqueous solution to the ZSM-5 suspension (0.5 g of ZSM-5 immersed in 5 ml DI H_2O) and the mixture was stirred for 24 h at ambient temperature. Subsequently, a 0.1-mmol/ml sodium borohydride aqueous solution was added to the Pd^{2+}/ZSM-5 mixture under vigorous stirring for 1 h at ambient temperature. The resulting products were washed and collected by centrifugation, and then dried overnight in a vacuum oven at 353 K.

The core-shell S-1/Pd/ZSM-5 was synthesized following the method report by Miyake et al. [36]. The precursor solution was first prepared according to the molar ratio of SiO_2:TPAOH:EtOH:H_2O = 1:0.06:16:180. This solution was stirred at 298 K for 18 h and was divided equally into 5 portions. Equal amount of Pd/ZSM-5 was then added to each portion of silica precursor solution. After 20-minute of mixing in an incubator shaker, all these 5 solutions were transferred to 5 Teflon-lined autoclaves and hydrothermally treated at 403 k for 1 day to 5 days (one autoclave was taken out each day). The S-1/Pd/ZSM-5 core-shell products were washed by DI water and collected by centrifugation, followed by calcination in a tube furnace at 823 K (ramping rate of 1 K/min from ambient temperature) for 5 h. The samples were donated as SZ-X, where X is from 1 to 5 representing samples produced from hydrothermally treated Pd/ZSM-5 in S-1 precursor solution from 1 day to 5 days (i.e. SZ-1, SZ-2, SZ-3, SZ-4, and SZ-5).

5.2.3 Characterization

The X-ray diffraction (XRD) patterns of the samples were recorded using a Philips PW1700 XRD instrument equipped with a Co-Kα radiation source. The specific surface area was measured by N_2 adsorption/desorption measurements at 77 K using a Gemini VI surface area and pore size analyzer. The metal dispersion on catalysts was measured by CO chemisorption technique using BELCAT II. Scanning electron microscopy (SEM) images were obtained using a JEOL 700F scanning electron microscope. Transmission electron microscopy (TEM) images were obtained using Tecnai G^2 F30ST field emission TEM. In addition, scanning transmission electron microscopy (STEM) images and the corresponding energy dispersive X-ray spectroscopy (EDX) elemental mapping images of Si, Al, and Pd were obtained by using FEI XFEG-Titan themis[3] Double Cs & Mono. TEM. For TEM analysis, the Pd/ ZSM-5 particles were dispersed in a solvent (water) and then 3–4 drops of the suspension were dropped onto a copper TEM support grid. Chemical compositions of Al, Si and Pd were measured by a Varian 720 Inductively Coupled Plasma Optical Emission Spectrometry (ICP-OES) using an acid digestion method.

5.2.4 Catalytic alkene hydrogenation

Catalytic alkene hydrogenation was conducted in a temperature-controlled batch reactor [37-39]. In a typical process, given amount of catalyst (Pd/ZSM-5, SZ-1, SZ-2, SZ-3, SZ-4, or SZ-5) was dispersed in 4 ml of ethyl acetate solvent under stirring. Then, 2 mmol of 1-hexene and 2 mmol of cyclohexene were added to the catalyst/solvent mixture under vigorous stirring. After the reactor was flushed several times with hydrogen (H_2) to remove the residual air, the reactor was filled with H_2 to 137.9 kPa. The reaction was then conducted at 308 K for 24 h under stirring (350 rpm). After the reaction, the catalyst was separated by centrifugation and the filtrate was analyzed using a gas chromatograph (GC) equipped with a capillary column

(Rxi-5Sil, 30 m × 0.25 mm × 0.25 um) and a flame ionization detector. Same experimental procedures were followed for hydrogenation of 1-hexene and 1-heptene. Kinetic data was collected by terminating the reaction at 4 h, 8 h, 12 h, 16 h and 20 h. Adsorption tests were done by replacing H_2 with Argon (Ar) under the same experimental conditions as alkene hydrogenation. In this report, the conversion (X) and selectivity (S) are defined as follows:

$$X = \frac{alkane\ produced}{alkane\ produced + unreacted\ alkane} \tag{2}$$

$$S = \frac{targeted\ alkane\ in\ product}{all\ alkanes\ produced} \tag{3}$$

5.3 Results and discussion

5.3.1 Characterization of the synthesized samples

The Si/Al ratio of as-prepared ZSM-5 substrate is 31, and the Pd/ZSM-5 contained 1.9 wt% Pd based on the ICP measurement. Fig. 5.1 shows the XRD patterns of the synthesized uncoated Pd/ZSM-5 sample, along with coated SZ-1, SZ-2, SZ-3, SZ-4 and SZ-5 samples. The results show no amorphous silica and impurities present in the samples other than an MFI structure (refer to the S-1 and ZSM-5 simulated patterns), indicating that the secondary growth of the S-1 shell was successfully performed on the Pd/ZSM-5 core between 1 and 5 days of crystallization. The XRD pattern also confirmed that Pd contents in all the samples were very small and bulky Pd species were not present. It is noted that the intensity of the first two peaks (approximately $2\theta = 9.2°$ and $10.3°$) of Pd/ZSM-5 is slightly lower compared with ZSM-5 due to the presence of Pd as the charge balancing cations [40]. Furthermore, the results of ICP measurement (Table 5.1) shows that the Pd/Si ratio decreased as the silicalite-1 shell layer built up.
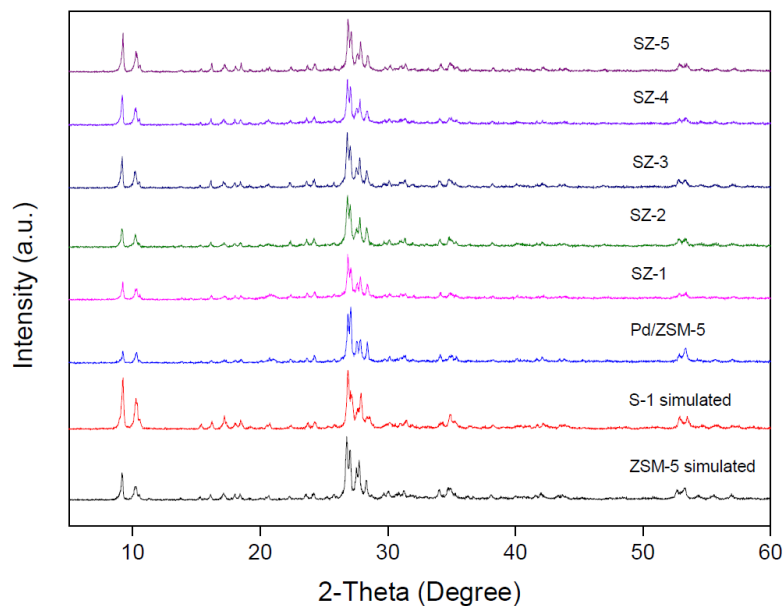
Fig. 5.1 XRD patterns of the synthesized Pd/ZSM-5, SZ-1, SZ-2, SZ-3, SZ-4 and SZ-5 samples.

The BET surface area and pore volume (Table 5.1) were generally comparable on all samples even after the S-1 coating was processed for 5 days. The slightly lower BET surface area of the SZ-1 (290 m^2/g) could be attributed to some minor defects in the interface between ZSM-5 core and S-1 shell formed during the first coating. The BET surface area, however, started to increase slightly after the first coating, which is consistent with the results reported by Li et al. [41]. Fig. 5.2 shows the relationship between the product yields as a function of crystallization time (from 1 to 5 days) of Pd/ZSM-5 in the presence of S-1 precursor. The trend of increasing zeolite product yield over time is consistent with the result reported by Cundy et al. where a positive linear relationship was observed between zeolite growth yield and crystallization time [42], indicating the size of MFI zeolite crystal increased as the S-1 shell thickens from 1 to 5 days secondary crystallization.

Table 5.1 The BET surface areas and Pd/Si ratios of the core-shell MFI zeolite.

Catalysts	$S_{BET}(m^2/g)^a$	$V_p(cm^3/g)^b$	Pd/Si(-)^c
Pd/ZSM-5	301	0.12	0.020
SZ-1	290	0.11	0.015
SZ-3	305	0.12	0.010
SZ-5	308	0.12	0.009

^{a} BET surface area, ^{b} pore volume calculated by t-Plot, ^{c} measured by ICP.
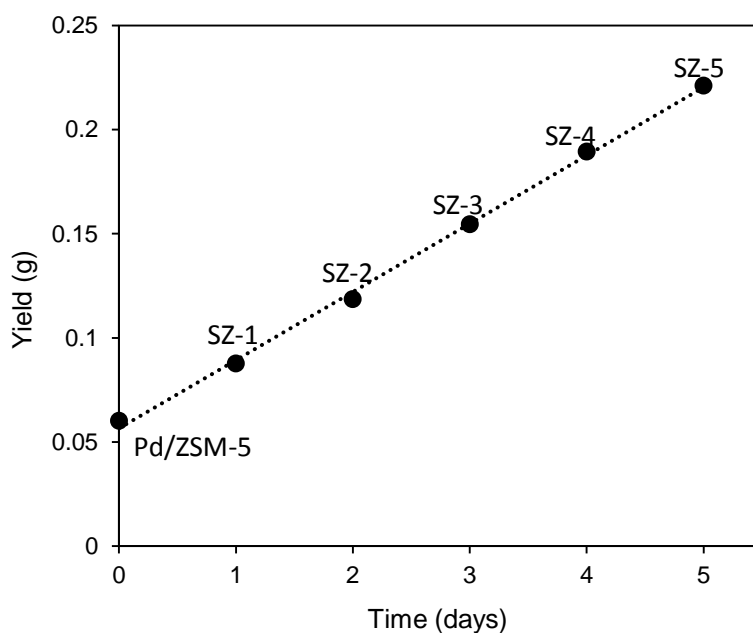
Fig. 5.2 Yield of MFI zeolite as a function of secondary crystallization time.

Fig. 5.3 shows the SEM images of Pd/ZSM-5 particle and core-shell S-1/Pd/ZSM-5 particles with different shell thickness made from different crystallization time (SZ-1 to SZ-5). Overgrowth of silicalite-1 was observed with gradual increase of crystallite size and morphological change as S-1 layers built up. The dimension of the crystal increased from 3.5×2.5 um to 10.5×4.7 um (c and a direction) resulting in a hexagonal shape along c-axis (Fig.

5.3d), which is in good agreement with the report of Miyamoto et al. [21] that the S-1 layer is extremely thin along the a and b directions and had grown rapidly in the c direction. After the initial S-1 coating, a uniform crystal growth was observed in all SZ samples. S-1 was also found to grow epitaxially on the Pd/ZSM-5 core in the same way as the S-1-coated ZSM-5 reported in literature [43]. Interestingly, the first coating layer of silicalite-1 appeared to be well-oriented on the ZSM-5 surface. This is consistent with the results reported by Vu et al. [23] that oriented growth of silicalite-1 crystals was found along the surface of ZSM-5 core specifically at the early stage of hydrothermal synthesis. Under this condition, the silicalite-1 channels are likely to be connected continuously to the ZSM-5 pores. On the other hand, Figs. 5.3c to 3f show that the top S-1 crystal layers formed after the second coating tend to be randomly oriented. Furthermore, the ICP results (Table 5.1) confirm that the proportion of Si content increased as the outer layers built up, suggesting that the surface of Pd/ZSM-5 crystals are fully covered by S-1 layers with MFI zeolitic structure. Besides, Fig. 5.3 (e) and (f) shows that the size dimension of SZ-4 and SZ-5 was very close (both of them are around 10.5×4.7 um), also indicating that the crystallization reached equilibrium at this source gel atmosphere in 5 days' time period resulted in S-1 shell stopped growing on Pd/ZSM-5 core. The reason of SZ-5 still gained weight that showed in Fig. 5.2 was because of few S-1 crystals started forming independently from the time period of SZ-4 to SZ-5, even though the number of S-1 particles was reasonably small.
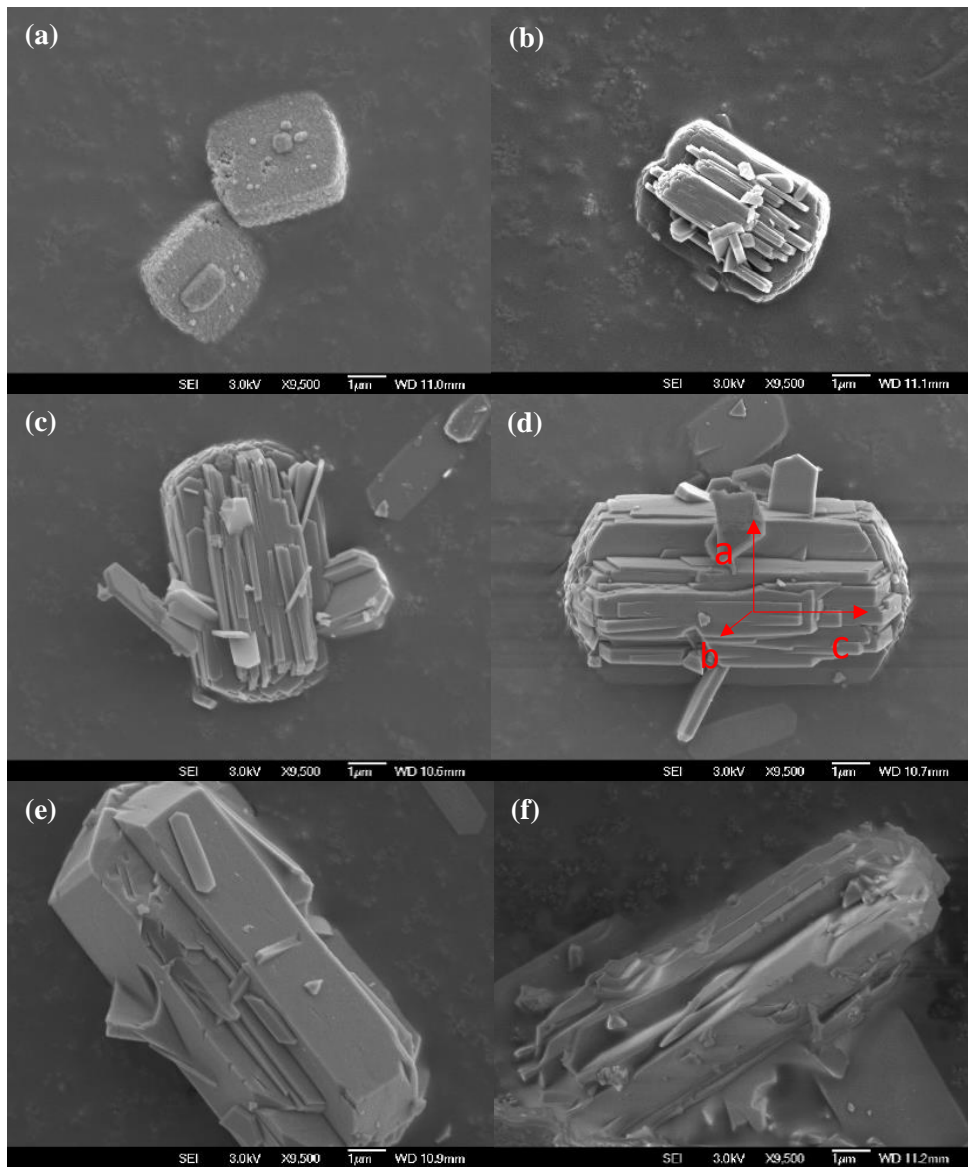
Fig. 5.3 SEM images of (a) Pd/ZSM-5 and (b to f) core-shell S-1/Pd/ZSM-5 (SZ-1 to SZ-5) synthesized from different from secondary crystallization time (1 to 5 days).

An examination on potential dissolution and recrystallization of the ZSM-5 core during the synthesis process of S-1 layers was conducted by hydrothermally treating the ZSM-5 core with an alkaline precursor solution (a mixture of TPAOH, EtOH and water) in the absence of silica source (TEOS). The SEM images in Fig. 5.4 show that there was neither apparent change in ZSM-5 morphology nor crystal size after the hydrothermal test. Therefore, it is confirmed that the ZSM-5 core is stable in structure and did not dissolve and/or recrystallize during the

secondary crystallization in which the S-1 layers emerge. The same results were reported by Miyamoto et al. [21].
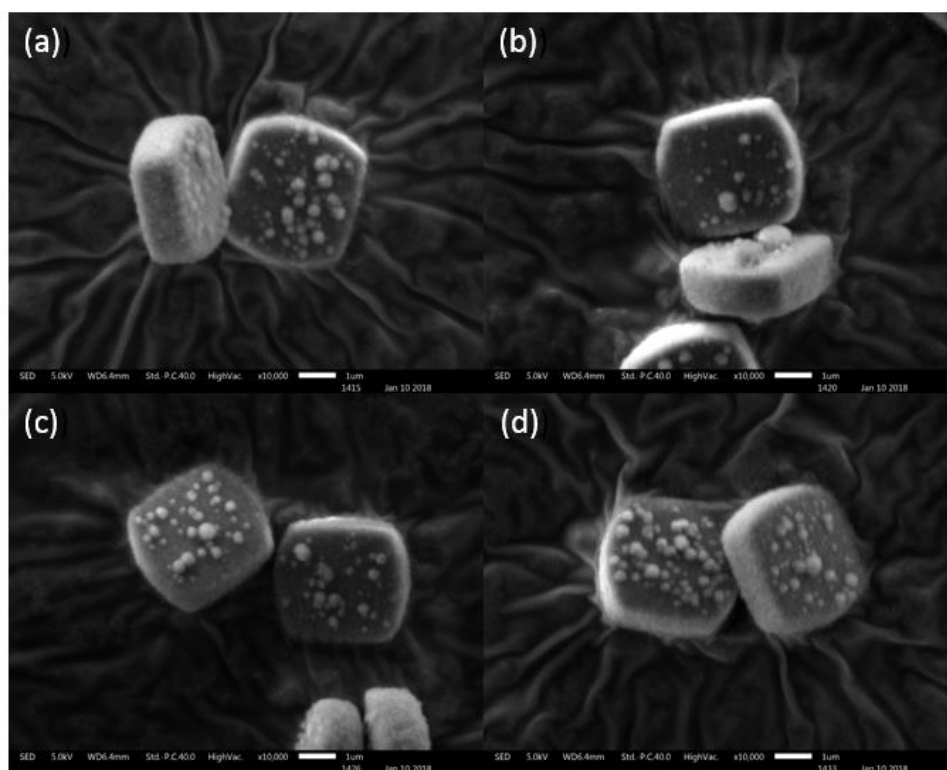
Fig. 5.4 SEM images of (a) Pd/ZSM-5 and it's hydrothermally threated without Si source for (b) 1 day (c) 3 days and 5 days.

The metal dispersions (measured by chemisorption of CO) in ZSM-5, Pd/ZSM-5, SZ-3 and SZ-5 samples were presented in Table 5.2. While Pd/ZSM-5 gives the highest dispersion (> 50%) of metal, SZ-3 and SZ-5 with increasing thickness of S-1 shell exhibit a significant decrease in metal dispersion to 22.5% and 20.7%, respectively. This is so because more inert (Si) surface is contributed by the S-1 shell (compared with Pd/ZSM-5), which results in the decrease of the Pd/Si ratio over single SZ particles and, thus, the lower metal dispersion. This is also consistent with the ICP results that the Pd/Si ratio decreased as the S-1 layers built up.

Table 5.2 The Metal dispersion and CO adsorption amount of the core-shell MFI zeolite

Catalysts	Metal dispersion (%)	Adsorption amount (cm^3/g)
ZSM-5	-	0.03
Pd/ZSM-5	52.4	0.31
SZ-3	22.5	0.15
SZ-5	20.7	0.07

Analysis of SZ particles using TEM is not possible because of the thickness of the shell (in micron size). Nevertheless, TEM images of the Pd/ZSM-5 core (Fig. 5.5) reveal that the size of Pd particles in the ZSM-5 core are approximately 3–4 nm. Large agglomerates of Pd with a size of 30–40 nm are also observed (STEM images in Fig. 5.6). Since the typical free aperture of ZSM-5 is approximately 0.45–0.60 nm, active Pd are most probably existed as nanoparticles and are located on the external surface of the ZSM-5 core. We intend to use Focused Ion Beam-Scanning Transmission Electron Microscopy (FIB-STEM) to further characterize the core-shell interface in our future study on nano-sized SZ particles.
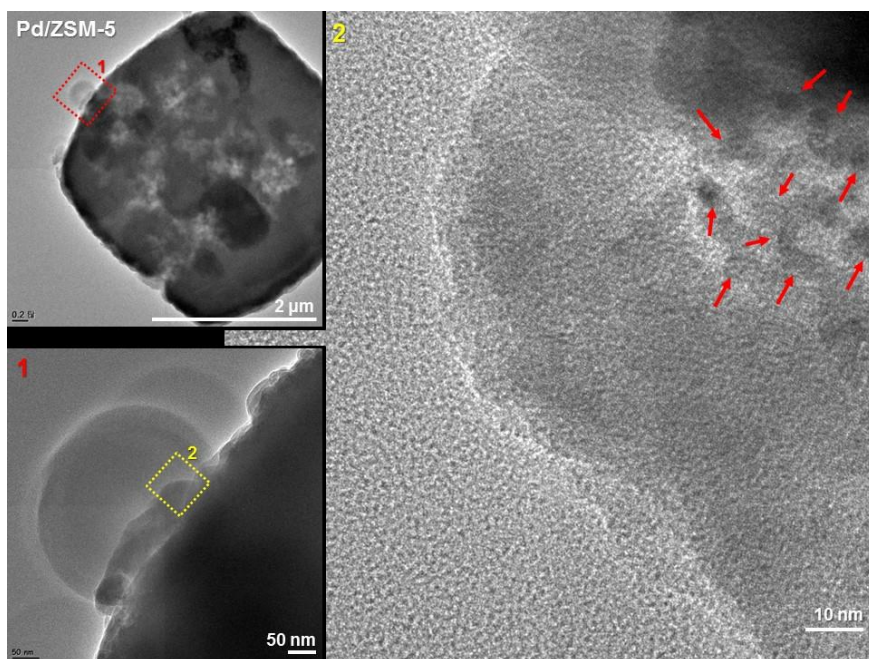
Fig. 5.5 TEM images of Pd/ZSM-5.
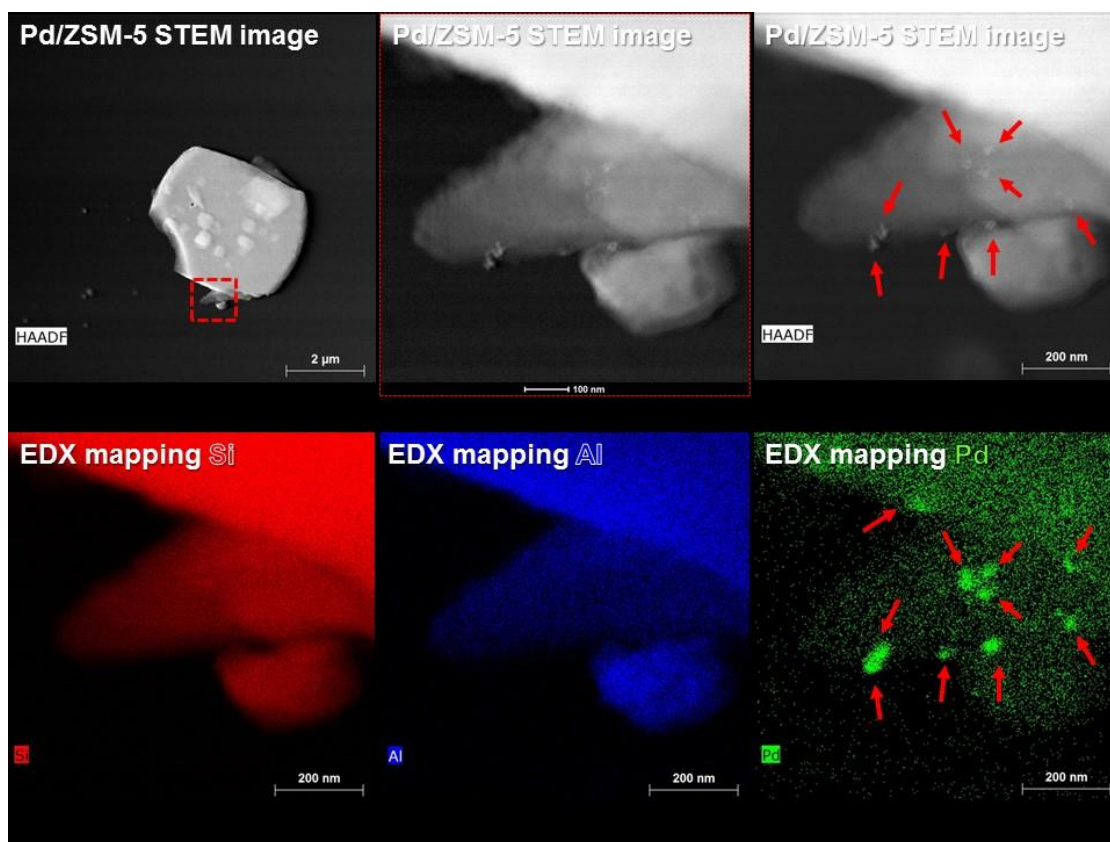
Fig. 5.6 STEM and EDX mapping of Pd/ZSM-5.

5.3.2 Selective catalytic alkene hydrogenation

Given the average pore size of MFI zeolites was approximately 5.6 Å [39], liquid-phase hydrogenation of 1-hexene (1.7 Å), 1-heptene, and cyclohexene (4.2 Å) [44] were used as probe reactions to evaluate the core-shell effect of S-1/Pd/ZSM-5 on reactant/product selectivties because these molecules are small enough to diffuse through the pores of the S-1 shell without serious impediment. The kinetic diameter of 1-hexene and 1-heptene are considered comparable but much smaller than that of cyclohexene. Pd/ZSM-5 without the S-1 layer (or the core of S-1/Pd/ZSM-5) was also tested for alkene hydrogenation under the same conditions as a reference. Table 5.3 shows the catalytic activities of ZSM-5 and Pd/ZSM-5 in hydrogenation of 1-hexene, 1-heptene and cyclohexene. It is apparent that the pure ZSM-5 gives zero conversion in hydrogenation, while the Pd/ZSM-5 catalyst without S-1 shell gives 100% conversion of -hexene, 1-heptene and cyclohexene their respective alkanes in 24 h, confirming that Pd is the only active specie within the zeolite that is responsible for hydrogenation. Moreover, Pd/ZSM-5 also gives approximately 99% conversion of 1-hexene and cyclohexene when an equimolar mixture of 1-hexene and cyclohexene was added as a reactant. This result suggests that the probed alkene hydrogenation catalyzed by Pd/ZSM-5 is non-selective and that both surface Pd and the Pd located inside the ZSM-5 substrate are accessible by 1-hexene and cyclohexene. Nearly complete alkene conversion (> 99%) were also achieved for equimolar mixture reactants of 1-hexene/1-heptene and 1-heptene/cyclohexene. It is worth noting that the three sets of hydrogenation experiment for equimolar mixtures of 1-hexene/cyclohexene, 1-hexene/1-heptene and 1-heptene/cyclohexene (Table 5.3) were conducted under 206.8 kPa of hydrogen, which is in excess of what is stoichiometrically requiredfor complete hydrogenation of the co-fed alkenes.

Table 5.3 Hydrogenation of different reactants over ZSM-5 and Pd/ZSM-5 catalysts[a].

Reactant (s)	Catalysts	Conversion (%)		
		1-hexene	1-heptene	cyclohexene
1-hexene[a]	ZSM-5	0	-	-
1-heptene[a]	ZSM-5	-	0	-
cyclohexene[a]	ZSM-5	-	-	0
1-hexene[a]	Pd/ZSM-5	100	-	-
1-heptene[a]	Pd/ZSM-5	-	100	-
cyclohexene[a]	Pd/ZSM-5	-	-	100
1-hexene/cyclohexene[b]	Pd/ZSM-5	>99	-	>99
1-hexene/1-heptene[b]	Pd/ZSM-5	>99	>99	-
1-heptene/cyclohexene[b]	Pd/ZSM-5	-	>99	>99

[a]Reaction performed at 308 K for 24 h under 137.9 kPa of H_2 in 4.0 ml ethyl acetate.

[b]Reaction performed at 308 K for 24 h under 206.8 kPa of H_2 in 4.0 ml ethyl acetate.

The effect of the core-shell MFI design on alkene selectivity was investigated by hydrogenation of equimolar mixtures of 1-hexene/cyclohexene and 1-hexene/1-heptene liquid phase. Fig. 5.7a and b show that the conversion and selectivity of 1-hexene and cyclohexene over Pd/ZSM-5, SZ-1, SZ-2, SZ-3, SZ-4 and SZ-5 catalysts, respectively. In the absence of the S-1 shell (i.e. 0 day of secondary crystallization), the conversion of both 1-hexene and cyclohexene by Pd/ZSM-5 are the same at 94%. As the thickness of the S-1 layers increased, the conversion of cyclohexene decreased notably to 12% while the conversion of 1-hexene remain as high as 79% with SZ-5 catalyst. Since the kinetic diameter of both 1-hexene (1.7Å) and cyclohexene (4.2 Å) are smaller than the pore size of the S-1 shell (5.6 Å), molecular sieving or size exclusion properties of zeolite are not deemed to be responsible for the high selectivity of 1-hexene over cyclohexene achieved. The S-1 shell layer offers a diffusional path through which the reactants

are restricted by mass transfer limitations. The diffusion rate of cyclohexene from the outermost surface of the S-1 shell layer to the Pd active sites inside the Pd/ZSM-5 core is significantly slower than the diffusion rate of 1-hexene due to the its large molecular size and weight. Fig. 5.7b shows the selectivity of 1-hexene over cyclohexene increased from 50% in the absence of S-1 shell to 87% (SZ-5) as the diffusion length increased due to increasing thickness of the S-1 layer. The results confirm that the competition between the two reacting alkenes for the Pd active sites becomes much more favorable to 1-hexene by the controllable core-shell zeolite design.
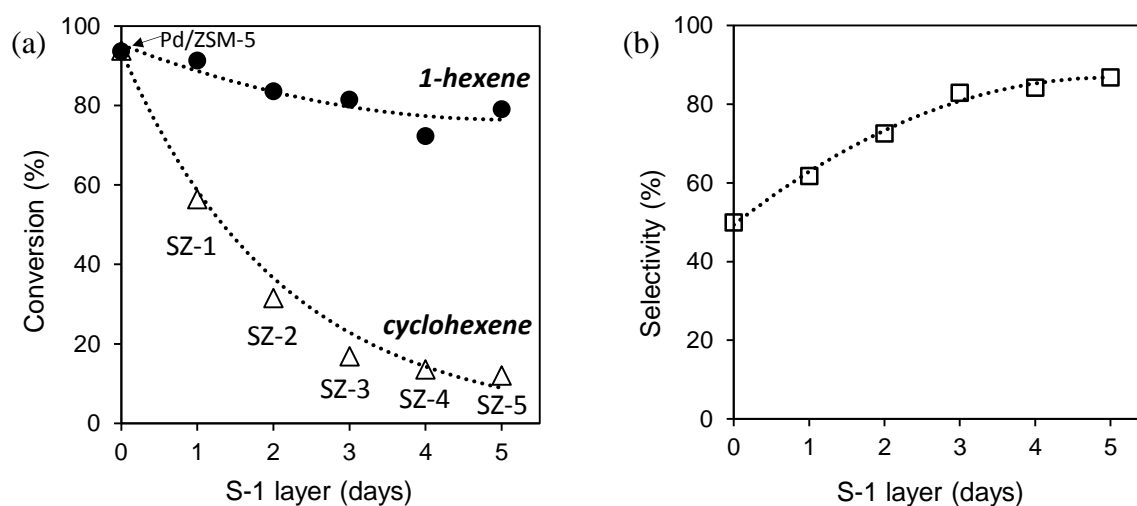
Fig. 5.7 Hydrogenation of 1-hexene and cyclohexene catalyzed by Pd/ZSM-5, SZ-1, SZ-2, SZ-3, SZ-4 and SZ-5: (a) conversion of 1-hexene and cyclohexene (b) selectivity of 1-hexene over cyclohexene.

To further confirm the important role of diffusive length within the core-shell zeolite on the selectivity of reactants with similar size and shape. A reactant mixture consists of equimolar of 1-hexene and 1-heptene was examined under the same experimental procedure as 1-hexene/cyclohexene. 1-hexene and 1-heptene possess linear structure and similar molecular

size except 1-heptene has one more alkyl at the far end. Both of their molecular size are much smaller than the pore size of MFI zeolites.

Fig. 5.8a shows that 1-hexene and 1-heptene reached almost the same conversion (82-85%) over Pd/ZSM-5 in the absence of S-1 shell layer. The conversion of 1-heptene decreased notably to 51% over the SZ-5 catalyst, while the conversion of 1-hexene still kept at approximately 83%. Fig. 5.8b further shows the selectivity of 1-hexene over 1-heptene gradually increased from 49% to 63% as the S-1 shell layer emerges from Pd/ZSM-5 to SZ-4. This is so because 1-heptene (98.2 g/mol) has a slightly larger molecular weight than 1-hexene (84.2 g/mol), which leads to a slower diffusion rate along the S-1 shell channel. The difference between the diffusion rate of 1-hexene and 1-heptene can be seen from the adsorption kinetic obtained in argon for the mixture of 1-hexene and 1-heptene over SZ-3 catalyst (Fig. 5.9). The fact that adsorption of 1-hexene (32.9%) is significant higher than that of 1-heptene (9.7%) after 24 h on SZ-3 reflects a faster diffusion rate with 1-hexene over 1-heptene through the S-1 shell layer. Moreover, it is worth noting that the enhancement of selectivity towards 1-hexene over 1-heptene requires a longer diffusion length to prevail in the S-1 shell (i.e. a larger thickness in the shell is required) compared with the previous experiment with 1-hexene/cyclohexene as reactants (Fig. 5.7). These results suggest that the cut-size or the distinguishability of similar molecules are strong dependent on the shell thickness which is controllable in the catalyst synthesis. Moreover, given the conversions of 1hexene (Figs. 5.7 and 5.8a) in the hydrogenation tests were remained at above 80% overall from SZ-0 to SZ-5, the particle size of Pd located in the ZSM-5 core is likely to be maintained without significant change during or after secondary crystallization. Otherwise, apparent decrease in conversions of all accessible reactants (including 1-hexene) would be expected due to attrition or reduction of active Pd surface. In addition, small amount of randomly oriented crystals started to emerge from SZ-2 to SZ-5 (Fig. 5.3), indicating potential minor defects could be resulted during the

development of S-1 layers. These small defects, however, did not affect the S-1 shell selectivity towards light olefins, given the selectivity towards light olefins was increasing from SZ-2 and SZ-5 for both hydrogenations of 1-hexene/cyclohexene (Fig. 5.7b) and 1-hexene/ 1-heptene (Fig. 5.8b). It is worth to note that the slight decrease in conversions of both reactants from SZ-4 to SZ-5 were probably due to random blockage or coverage of pores by single S-1 particles, which obstructed the passage of reactants to the zeolite. This is in agreement with the images shown in Fig. 5.3e and f where the crystal growth reached equilibrium from SZ-4 and after which S-1 single particles started to develop. The hydrogenation of co-fed 1-hexene and 1-heptene confirms further that the compactness and thickness of the outer S-1 shell is able to increase the resolution in zeolite selectivity between molecules with similar size and shape.
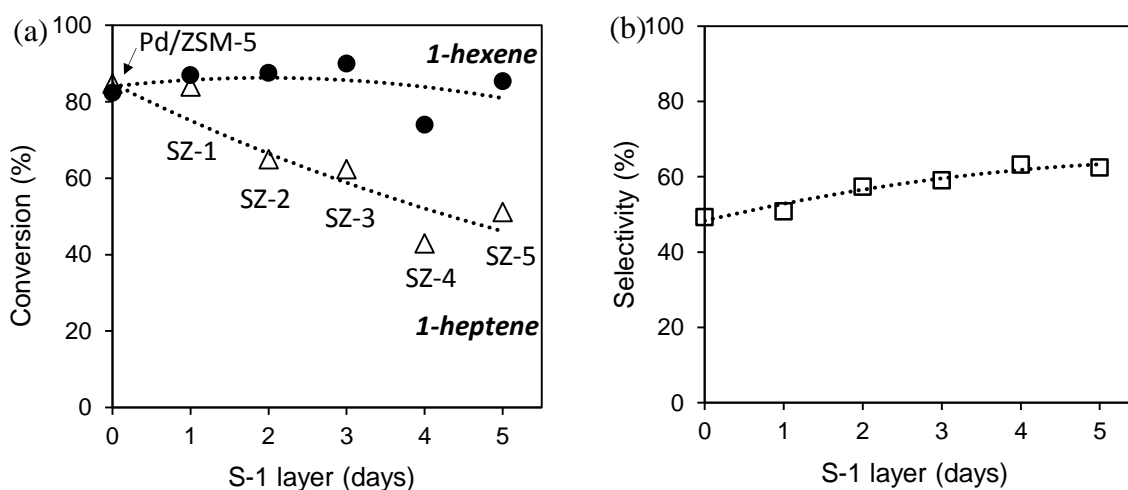
Fig. 5.8 Hydrogenation of 1-hexene and 1-heptene catalyzed by Pd/ZSM-5, SZ-1, SZ-2, SZ-3, SZ-4 and SZ-5: (a) conversion of 1-hexene and 1-heptene (b) selectivity of 1-hexene over 1-heptene.
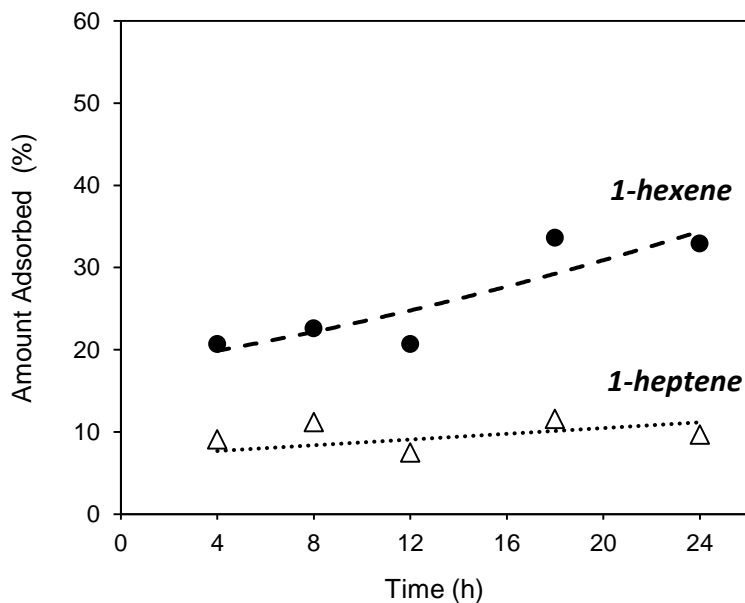
Fig. 5.9 Adsorption kinetic of 1-hexene and 1-heptene over SZ-3 over 24 h under argon with stirring at 350 rpm.

The reaction kinetic of 1-hexene/1-heptene hydrogenation over SZ-4 is shown in Fig. 5.10. It can be seen that the conversion of 1-hexene and 1-heptene was comparable in the first 12 h. The difference in conversions, however, gradually increased after 12 h and resulted in 74% and 43% conversions of 1-hexene and 1-heptene, respectively at 24 h. This result indicates that the contribution of diffusion length towards reactant selectivity given by the S-1 shell (and its thickness) is more significant at low reactant concentrations in which smaller molecules possess a faster mass transfer rate in the zeolite microporous channel relative to larger molecules.
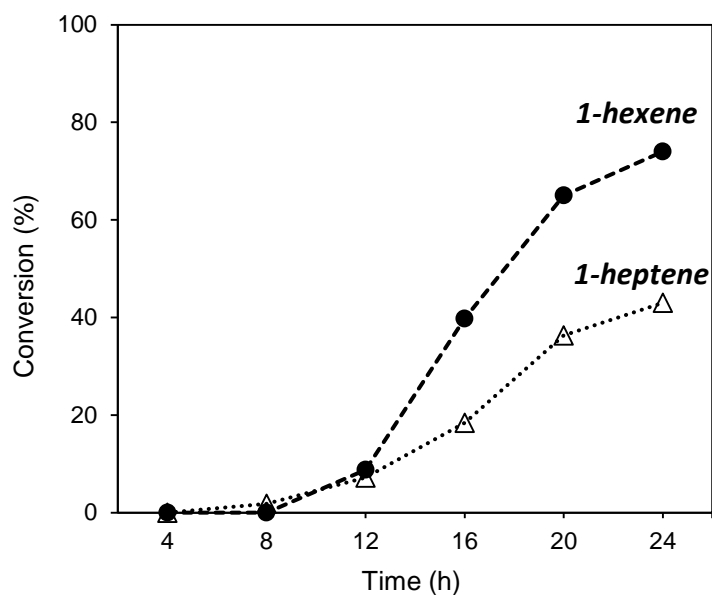
Fig. 5.10 Reaction kinetic of 1-hexene/1-heptene hydrogenation over SZ-4.

5.4 Conclusions

A new type of core-shell MFI catalyst consists of Pd/ZSM-5 as an active core and silicalite-1 (S-1) layer with variable thickness as the shell was successfully synthesized. The effectiveness of the core-shell design on increasing the resolution of selectivity in alkene hydrogenation, particularly to reactants with very similar size and shape, was investigated. The core-shell S-1/Pd/ZSM-5 exhibited preferential selectivity to 1-hexene over cyclohexene or 1-heptene in liquid phase hydrogenation as the S-1 layers built up. In this study, we conceptually demonstrated a strong correlation between the thickness of the S-1 shell layer and the selectivity towards light alkenes due to faster mass transfer rate. It is concluded that the core-shell structure in this work is a feasible design that allows ZSM-5 supported catalysts to be highly selective in reactions in which the molecular size of the reactants are smaller than the aperture of MFI zeolite. Mapping of the molecular cut-size of the core-shell MFI zeolite (e.g. C_2/C_3, C_3/C_4, C_5/C_6 alkene pairs) against the diffusion length (thickness) of the S-1 shell layer will be conducted in future studies.

5.5 References

[1] J. Weitkamp, Zeolites and catalysis, Solid State Ionics, 131 (2000) 175-188.

[2] C.D. Chang, A. Silvestri, MTG-origin, evolution, operation, Chem. Tech., 17 (1987) 624-631.

[3] I. Maxwell, W. Stork, Hydrocarbon processing with zeolites, Stud. Surf. Sci. Catal., 58 (1991) 571-630.

[4] C.D. Chang, S.S. Grover, Conversion of methanol to gasoline components, Google Patents, 1977.

[5] A. Corma, Inorganic solid acids and their use in acid-catalyzed hydrocarbon reactions, Chem. Rev., 95 (1995).

[6] H.S. Lacheen, E. Iglesia, Stability, structure, and oxidation state of Mo/H-ZSM-5 catalysts during reactions of CH_4 and CH_4–CO_2 mixtures, J. Catal., 230 (2005) 173-185.

[7] X. Li, D. Han, H. Wang, G. Liu, B. Wang, Z. Li, J. Wu, Propene oligomerization to high-quality liquid fuels over Ni/HZSM-5, Fuel, 144 (2015) 9-14.

[8] X. Li, B. Shen, C. Xu, Interaction of titanium and iron oxide with ZSM-5 to tune the catalytic cracking of hydrocarbons, Appl Catal a-Gen, 375 (2010) 222-229.

[9] F. Bin, C. Song, G. Lv, J. Song, S. Wu, X. Li, Selective catalytic reduction of nitric oxide with ammonia over zirconium-doped copper/ZSM-5 catalysts, Appl. Catal. B Environ., 150 (2014) 532-543.

[10] A. De Lucas, J. Valverde, F. Dorado, A. Romero, I. Asencio, Influence of the ion exchanged metal (Cu, Co, Ni and Mn) on the selective catalytic reduction of NOx over mordenite and ZSM-5, J. Mol. Catal. A: Chem., 225 (2005) 47-58.

[11] M. Salazar, R. Becker, W. Grünert, Hybrid catalysts—an innovative route to improve catalyst performance in the selective catalytic reduction of NO by NH_3, Appl. Catal. B Environ., 165 (2015) 316-327.

[12] G. Centi, S. Perathoner, T. Torre, M.G. Verduna, Catalytic wet oxidation with H_2O_2 of carboxylic acids on homogeneous and heterogeneous Fenton-type catalysts, Catal. Today, 55 (2000) 61-69.

[13] Z.M. El-Bahy, M.M. Mohamed, F.I. Zidan, M.S. Thabet, Photo-degradation of acid green dye over Co–ZSM-5 catalysts prepared by incipient wetness impregnation technique, J. Hazard. Mater., 153 (2008) 364-371.

[14] N. Hadi, A. Niaei, S. Nabavi, M.N. Shirazi, R. Alizadeh, Effect of second metal on the selectivity of Mn/H-ZSM-5 catalyst in methanol to propylene process, Journal of Industrial and Engineering Chemistry, 29 (2015) 52-62.

[15] M. Kögel, V. Sandoval, W. Schwieger, A. Tissler, T. Turek, Catalytic Activity and Hydrothermal Stability of Cu-ZSM-5 Used for the Decomposition of N_2O, Chemical engineering & technology, 21 (1998) 655-658.

[16] B. Palella, M. Cadoni, A. Frache, H. Pastore, R. Pirone, G. Russo, S. Coluccia, L. Marchese, On the hydrothermal stability of CuAPSO-34 microporous catalysts for N_2O decomposition: a comparison with CuZSM-5, J. Catal., 217 (2003) 100-106.

[17] R. Qi, T. Fu, W. Wan, Z. Li, Pore fabrication of nano-ZSM-5 zeolite by internal desilication and its influence on the methanol to hydrocarbon reaction, Fuel Process. Technol., 155 (2017) 191-199.

[18] M.-L. Tsai, R.G. Hadt, P. Vanelderen, B.F. Sels, R.A. Schoonheydt, E.I. Solomon, [Cu$_2$O] 2+ Active Site Formation in Cu–ZSM-5: Geometric and Electronic Structure Requirements for N2O Activation, J. Am. Chem. Soc., 136 (2014) 3522-3529.

[19] J. Wang, N. Mizuno, M. Misono, Comparison of catalytic decomposition of dinitrogen oxide and nitrogen monoxide over Cu/ZSM-5 and Cu/Y zeolites, Bull. Chem. Soc. Jpn., 71 (1998) 947-954.

[20] W. Zou, P. Xie, W. Hua, Y. Wang, D. Kong, Y. Yue, Z. Ma, W. Yang, Z. Gao, Catalytic decomposition of N_2O over Cu-ZSM-5 nanosheets, J. Mol. Catal. A: Chem., 394 (2014) 83-88.

[21] M. Miyamoto, T. Kamei, N. Nishiyama, Y. Egashira, K. Ueyama, Single Crystals of ZSM-5/Silicalite Composites, Adv. Mater., 17 (2005) 1985-1988.

[22] D. Van Vu, M. Miyamoto, N. Nishiyama, Y. Egashira, K. Ueyama, Selective formation of para-xylene over H-ZSM-5 coated with polycrystalline silicalite crystals, J. Catal., 243 (2006) 389-394.

[23] D. Van Vu, M. Miyamoto, N. Nishiyama, S. Ichikawa, Y. Egashira, K. Ueyama, Catalytic activities and structures of silicalite-1/H-ZSM-5 zeolite composites, Microporous Mesoporous Mater., 115 (2008) 106-112.

[24] Y. Nakasaka, T. Okamura, H. Konno, T. Tago, T. Masuda, Crystal size of MFI-type zeolites for catalytic cracking of n-hexane under reaction-control conditions, Microporous Mesoporous Mater., 182 (2013) 244-249.

[25] O. Levenspiel, C. Levenspiel, Chemical reaction engineering, Wiley New York etc.1972.

[26] E.W. Thiele, Relation between catalytic activity and size of particle, Industrial & Engineering Chemistry, 31 (1939) 916-920.

[27] J. Cejka, A. Corma, S. Zones, Zeolites and catalysis: synthesis, reactions and applications, John Wiley & Sons2010.

[28] T. Masuda, Journal of the Japan Petroleum Institute, 46 (2003) 281-294.

[29] E. de Vos Burchart, J. Jansen, H. Van Bekkum, Ordered overgrowth of zeolite X onto crystals of zeolite A, Zeolites, 9 (1989) 432-435.

[30] K. Kloetstra, H. Zandbergen, J. Jansen, H. Van Bekkum, Overgrowth of mesoporous MCM-41 on faujasite, Microporous Mater., 6 (1996) 287-293.

[31] A. Yonkeu, V. Buschmann, G. Miehe, H. Fuess, A. Goossens, J. Martens, Structural characterization of a new "core-shell" zeolite overgrowth system: faujasite on micro sized EMT-crystals, Cryst. Eng., 4 (2001) 253-267.

[32] C.-Y. Lee, D. Liu, Nonlinear analysis of composite plates using interlaminar shear stress continuity theory, Compos. Eng., 3 (1993) 151-168.

[33] Q. Li, J. Hedlund, J. Sterte, D. Creaser, A.-J. Bons, Synthesis and characterization of zoned MFI films by seeded growth, Microporous Mesoporous Mater., 56 (2002) 291-302.

[34] Q. Li, Z. Wang, J. Hedlund, D. Creaser, H. Zhang, X. Zou, A.-J. Bons, Synthesis and characterization of colloidal zoned MFI crystals, Microporous Mesoporous Mater., 78 (2005) 1-10.

[35] J.W. Mullin, Crystallization, Butterworth-Heinemann2001.

[36] K. Miyake, Y. Hirota, K. Ono, Y. Uchida, S. Tanaka, N. Nishiyama, Direct and selective conversion of methanol to para-xylene over Zn ion doped ZSM-5/silicalite-1 core-shell zeolite catalyst, J. Catal., 342 (2016) 63-66.

[37] G. Lu, S. Li, Z. Guo, O.K. Farha, B.G. Hauser, X. Qi, Y. Wang, X. Wang, S. Han, X. Liu, Imparting functionality to a metal–organic framework material by controlled nanoparticle encapsulation, Nature chemistry, 4 (2012) 310-316.

[38] T. Zhang, X. Zhang, X. Yan, L. Lin, H. Liu, J. Qiu, K.L. Yeung, Core–shell Pd/ZSM-5@ ZIF-8 membrane micro-reactors with size selectivity properties for alkene hydrogenation, Catal. Today, 236 (2014) 41-48.

[39] H. Yin, J. Choi, A.C. Yip, Anti-poisoning core–shell metal/ZIF-8 catalyst for selective alkene hydrogenation, Catal. Today, 265 (2016) 203-209.

[40] A. Kumbhar, S. Kamble, A. Mane, R. Jha, R. Salunkhe, Modified zeolite immobilized palladium for ligand-free Suzuki–Miyaura cross-coupling reaction, J. Organomet. Chem., 738 (2013) 29-34.

[41] N. Li, Y.-Y. Zhang, L. Chen, C.-T. Au, S.-F. Yin, Synthesis and application of HZSM-5@ silicalite-1 core–shell composites for the generation of light olefins from CH_3Br, Microporous Mesoporous Mater., 227 (2016) 76-80.

[42] C.S. Cundy, B.M. Lowe, D.M. Sinclair, Direct measurements of the crystal growth rate and nucleation behaviour of silicalite, a zeolitic silica polymorph, J. Cryst. Growth, 100 (1990) 189-202.

[43] M. Miyamoto, K. Mabuchi, J. Kamada, Y. Hirota, Y. Oumi, N. Nishiyama, S. Uemiya, Para-selectivity of silicalite-1 coated MFI type galloaluminosilicate in aromatization of light alkanes, J. Porous Mater., 22 (2015) 769-778.

[44] L. Lin, T. Zhang, X. Zhang, H. Liu, K.L. Yeung, J. Qiu, New Pd/SiO_2@ ZIF-8 Core–Shell Catalyst with Selective, Antipoisoning, and Antileaching Properties for the Hydrogenation of Alkenes, Industrial & Engineering Chemistry Research, 53 (2014) 10906-10913.

Chapter 6

Development of new Anti-humidity Palladium-based core-shell MFI zeolite as ethylene scavenger

6.1 Introduction

Ethylene is known as one of several plant growth regulators, and it plays a very important role in many physiological process in plants [1]. The influence of ethylene on plants includes seed germination and growth, abscission, fruit ripening and senescence etc. [2-4]. Ethylene can diffuse into and out of plant tissues from both endogenous and exogenous sources. Endogenous ethylene is an essential part of climacteric fruits, while the application of exogenous ethylene is commonly employed for trigging some fruits such as banana with uniformed ripening [5]. However, in order to decrease the loss caused by over-ripening in transit or storage, most commercial strategies for fresh products are commonly focused on minimizing the ethylene production or avoiding exposure to ethylene [6]. The removal of ethylene and/or inhibition of the effect of ethylene in stored environments, hence is the key to maintaining postharvest quality of the climacteric products.

Various methods of ethylene control have been studied extensively. 1-methylcyclopropene (1-MCP) is one of the most commonly used commercial ethylene inhibitors in market, which can block ethylene binding sites, however, it only works on few type of horticultural products and may cause side-effects on products [5]. In addition, potassium permanganate ($KMnO_4$) as the oxidizing agents also can manipulate the ethylene concentration by oxidation of ethylene to CO_2 and water, but it has drawback of low resistance to high relative humidity (RH) that decreasing its long-term efficiency [7]. Ventilation is an economic and non-toxic method, however, it is not applicable in sealed environments, such as controlled atmosphere or some packaging formats [8]. In comparison, ethylene sorbents are alternative materials to control ethylene concentration with high efficiency and recyclability, including activated carbon, clay and zeolites, which have been reported as ethylene scavenger, due to their high surface area. Among all these sorbents available, zeolites has additional merits such as uniformed porous structure, thermal/mechanical stability, ion-exchange capacities, and tunable water affinity (i.e.

hydrophobicity and hydrophilicity) [9]. It has been reported the noble metals promoted zeolites showed improved ethylene removal efficiency than plain zeolites [7, 8], yet the introduced metal particles may block some the zeolite channels, resulted in the potential loss of the ethylene scrubbing ability of the complex. On the other hand, it has been reported that palladium (Pd) promoted ethylene adsorbent had an approximately 10-fold ethylene uptake increasing under dry conditions (low %RH) compare to 100% RH environment, indicating the negative influence of water molecule on palladium [7]. In a real life application, the high RH environment is unavoidable for fresh products storage, thus the utilization of pd promoted sorbent with high water tolerance still remain unsolved.

Silicalite-1 is a MFI type zeolite with great hydrophobicity and has been extensively studied over last decades [10-12]. In this work, we designed a new palladium based core-shell zeolite structure with nano-sized ZSM-5 core and silicalite-1 (S-1) shell. The Pd particles were introduced in the nano-sized ZSM-5 core with ion-exchange method before the S-1 shell was built up. The S-1 shell was synthesized with different layer thickness by prolonged secondary crystallization time. We herein demonstrated a new type of ethylene scavenger with MFI core-shell structure, which can improve the ethylene uptake and have improved humidity tolerance.

6.2 Experimental

6.2.1 Materials

Tetraethyl orthosilicate (TEOS, 98%), aluminum isopropoxide (>98%), tetrapropylammonium hydroxide (TPAOH, 1.0 M in H_2O), palladium nitrate dihydrate (approximately 40% Pd basis), sodium borohydride (99%), and aluminum nitrate nonahydrate were purchased from Sigma-Aldrich Chemical Co. Sodium hydroxide and ethanol (EtOH, 99.5%) were purchased from Thermo Fisher Scientific. Instrument grade Ethylene was purchased from BOC. Deionized (DI)

water was prepared by a lab-based water-purification apparatus and was used to prepare all required samples and solutions. All chemicals were used as received without any further treatment. Commercial zeolites ZSM-5 (CBV2314), BEA (CP814E), and Y (CBV300) were supplied by Zeolyst International.

6.2.2 Sample preparation

The nano-sized ZSM-5 core was synthesized following the method reported by Mochizuki et al. [13]. In a typical synthesis, 15 ml of TPAOH, 16 ml of DI water and 13.68 ml TEOS were added sequentially to a PP bottle. The resulting mixture was kept in an oil bath at 80 $^{\circ}$C for 24 h. Thereafter, a solution containing 4 ml of DI water, 0.46 g of $Al(NO_3)_3 \cdot 9H_2O$ and 0.24 g of NaOH was added to the mixture. The prepared mother gel was stirred at room temperature for 30 min, followed by crystallization at 170 $^{\circ}$C for 24 h. The molar composition of the final gel was SiO_2:Al_2O_3:TPAOH:NaOH:H_2O=1:0.01:0.25:0.1:30. The solid product was subsequently washed 3 times with DI water and was collected by centrifugation. Finally, the Na-ZSM-5 samples were obtained by calcination of the as-synthesized sample in a tube furnace at 550 $^{\circ}$C (ramping rate of 1 $^{\circ}$C/min from ambient temperature) for 10 h to remove the organic template.

The Pd/ZSM-5 core containing approximately 5.27 wt% palladium was obtained by adding 10 ml $Pd(NO_3)_2$ aqueous solution to the ZSM-5 suspension (1.0 g of ZSM-5 immersed in 10ml DI H_2O), and the mixture was stirred at 80 $^{\circ}$C for 24 h. Subsequently, a 0.1-mmol/ml sodium borohydride aqueous solution was added to the Pd^{2+}/ZSM-5 mixture under vigorous stirring for 1 h at ambient temperature. The resulting products were washed and collected by centrifugation, and then dried overnight in a vacuum oven at 80 $^{\circ}$C. The similar procedures, except of the Pd loading, were applied for synthesizing Pd/BEA (commercial BEA) for preliminary test.

The core-shell S-1/Pd/ZSM-5 was synthesized following the method report by Miyake et al. [14]. The precursor solution was first prepared according to the molar ratio of SiO_2:TPAOH:EtOH:H_2O =1:0.06:16:180. This solution was stirred at 25 °C for 18 h and was divided equally into 5 portions. Equal amount of Pd/ZSM-5 was then added to each portion of silica precursor solution. After 5 h of mixing in an incubator shaker, all these 5 solutions were transferred to 5 Teflon-lined autoclaves and hydrothermally treated at 130 °C for 1 day to 5 days (one autoclave was taken out each day). The S-1/Pd/ZSM-5 core-shell products were washed by DI water and collected by centrifugation, followed by calcination in a tube furnace at 550 °C (ramping rate of 1 °C/min from room temperature) for 5 h. The samples were donated as SZ-X, where X is from 1 to 5 representing samples produced from hydrothermally treated Pd/ZSM-5 in S-1 precursor solution from 1 day to 5 days (i.e. SZ-1, SZ-2, SZ-3, SZ-4, and SZ-5).

6.2.3 Characterization

The X-ray diffraction (XRD) patterns of the samples were recorded using a Philips PW1700 XRD instrument equipped with a Co-Kα radiation source. The specific surface area was measured by N_2 adsorption/desorption measurements at -196 °C using a Gemini VI surface area and pore size analyzer. The metal dispersion on catalysts was measured by CO chemisorption technique using BELCAT II. Scanning electron microscopy (SEM) images were obtained using a JEOL 700F scanning electron microscope. Transmission electron microscopy (TEM) images were recorded using a Philips CM-200. Chemical compositions of Al, Si and Pd were measured by a Varian 720 Inductively Coupled Plasma Optical Emission Spectrometry (ICP-OES) using an acid digestion method. Thermogravimetric analysis (TGA; SDT Q600) was conducted to check the humidity tolerance ability as the temperature increased from room temperature to 300 °C at a ramping rate of 2 °C·min^{-1} under N_2 atmosphere.

6.2.4 Ethylene adsorption measurement

Ethylene adsorption test was conducted by using the system [15] as shown in Fig. 6.1. The samples were pretreated under vacuumed environment at 200 °C for 12 h. A known weight of the samples was placed into the sample chamber. To remove any residual gases from the samples during the transfer, valves V-01, V-04, and V-05 were opened to dynamic vacuum (<0.1 torr) for 2 h. Immediately after degassing, valves V-01 and V-04 were closed, and the feed volume filled with approximately 1 bar (14.5 psi) of the ethylene to be measured (by opening V-02 or V-03). Valve V-04 was then opened for 1 s, filling the sample chamber with the ethylene. Valve V-04 was then closed, the pressure decrease in the sample chamber was measured over time until a constant pressure (P_f) was observed. The pressure difference, corrected for the empty cell, (Equation 1) was used to calculate the amount of ethylene adsorbed by the sample in units of mol_{gas} (Equation 2). The amount of gas adsorbed was then normalized by the amount of sample. Each measurement was repeated 3 times for each sample (i.e. cycled), and the average values and standard deviations were reported. Between measurements, degassing was achieved by opening valves V-01, V-04 and V-05 to dynamic vacuum (<0.1 torr) for 2 h.

$$\Delta P = P_i - P_f - \Delta P_{Blank}$$

$$\Delta P_{Blank} = P_{i(empty)} - P_{f(empty)}$$

Equation 1: P_i = the initial pressure (time zero); P_f = the final pressure (time final).

$$n_{gas} = \frac{\Delta P \cdot V}{R \cdot T}$$

Equation 2: n_{gas} = moles of gas adsorbed; V = volume of the sample chamber and pipelines till valve V-04 (i.e. volume d and e in Fig. 1); R = the ideal gas constant; T = temperature of sample chamber.

Fig. 6.1 The experimental set up for measurement of gas adsorption using the pressure drop method. Where V, PT, and T are valve, pressure sensor, and gas tank, respectively.

6.2.5 Humidity pre-treatment

Humidity pre-treatment was processed through a well-sealed beaker with certain amount of DI water. Open-mouthed vials with Pd/ZSM-5 and SZ samples were put inside the beaker before it was sealed. The samples were pretreated under vacuumed environment at 200 °C for 12 h. The ratio of sample/DI water inside the beaker is from 2 mg/ml to 7.5 mg/ml regarding different test. The well-sealed beaker was placed on a hotplate and kept for 2 to 5 h at 50 °C. Thereafter the samples were tested by TGA to check the amount the water been absorbed, and the samples were also tested for the ethylene loading with same procedures as dry condition.

6.3 Results and discussion

6.3.1 Characterization of the synthesized samples

The Si/Al ratio of as-prepared ZSM-5 substrate is 28, and the Pd/ZSM-5 contained 5.27 wt% Pd based on ICP measurement. Fig. 6.2 shows the XRD patterns of the synthesized uncoated Pd/ZSM-5 sample, along with coated SZ-1, SZ-2, SZ-3, SZ-4 and SZ-5 samples. The results show no amorphous silica and impurities present in the samples other than an MFI structure (refer to the ZSM-5 simulated patterns), indicating that the secondary growth of the S-1 shell was successfully performed on the Pd/ZSM-5 core between 1 and 5 days of crystallization. The XRD patterns also confirmed that Pd contents in all the samples were very small and bulky Pd species were not present. It is worth noting that the decreased intensity of the ZSM-5 after loading of Pd, including Pd/ZSM-5 and SZ-X samples, could be attributed to the presence of Pd as the charge balancing cations [16]. Furthermore, the results of ICP measurement (Table 6.1) shows that the Pd/Si ratio decreased as the silicalite-1 shell layer built up.
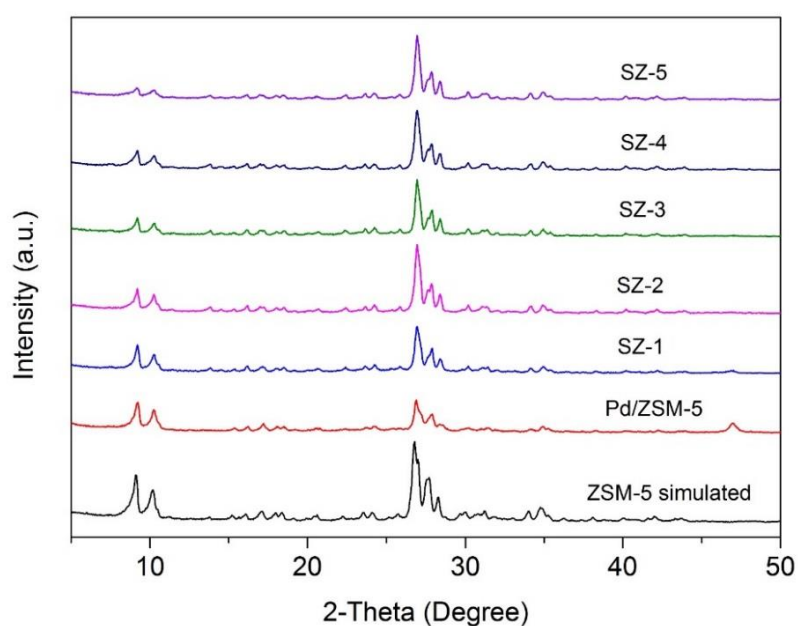
Fig. 6.2 XRD patterns of the synthesized Pd/ZSM-5, SZ-1, SZ-2, SZ-3, SZ-4 and SZ-5 samples.

The BET surface area and pore volume (Table 6.1) were greatly increased on the S-1 coated samples (SZ-1, SZ-3 and SZ-5) compare to uncoated ones (ZSM-5 and Pd/ZSM-5), which could be attributed to the newly generated channels by the S-1 shell. The slightly lower BET surface area of Pd/ZSM-5 (318 m^2/g) than plain ZSM-5 (326 m^2/g) likely due to the Pd nano particles that generated inside the ZSM-5 channels. It is worth noting that the surface area gradually increased over SZ-1 to SZ-3 samples, while the surface area started to decrease on SZ-4 and SZ-5 samples, which could be due to the growth of S-1 layers reached equilibrium at this source gel atmosphere in 3 days' time period coating, resulted in the S-1 shell slowed down the growing speed on Pd/ZSM-5 core, and S-1 particles started to generated independently, which may randomly covered on the SZ-4 and SZ-5 particles and blocked the channels.

Table 6.1 The BET surface areas and Pd/Si ratios of the core-shell MFI zeolite.

Catalysts	$S_{BET}(m^2/g)^a$	$V_p(cm^3/g)^b$	Pd/Si(-)^c
ZSM-5	326	0.22	-
Pd/ZSM-5	318	0.20	0.212
SZ-1	415	0.24	0.050
SZ-3	473	0.27	0.023
SZ-5	410	0.23	0.019

^{a} BET surface area

^{b} pore volume calculated by t-Plot

^{c} measured by ICP.

Fig. 6.3 shows the SEM images of Pd/ZSM-5 nano particles and core-shell S-1/Pd/ZSM-5 particles with different shell thickness made from different crystallization time (SZ-1 to SZ-5).

Overgrowth of S-1 was observed with gradual increase of crystallite size and morphological change as the S-1 layers built up. The dimension of the crystal increased from $0.1 \times 0.1 \times 0.1$ µm to $1.8 \times 0.8 \times 0.3$ µm, resulting in a hexagonal shape, which is agreed with our previous work [9] and the study reported by Miyamoto et al. [17]. After the initial S-1 coating, a uniform crystal growth was observed in all SZ samples. S-1 was also found to grow expitaxially on the Pd/ZSM-5 core in the same way as the S-1 coated ZSM-5 reported in literature [18]. In addition, the layer-by-layer growth mechanism was clearly showed in Fig. 6.3c that a smooth layer overgrown above inner layers. It is worth noting that the coating layers of S-1 appeared to be well-oriented on the ZSM-5 core, due to all the coated samples showed relative smooth morphology and no rough appearance has been observed. Under this condition, the S-1 channels are likely to be connected continuously to the pores of ZSM-5 core. Furthermore, the ICP results (Table 6.1) confirmed that proportion of Si content increased as the outer layers built up, suggesting that the surface of Pd/ZSM-5 crystals are fully covered by S-1 layers with MFI zeolitic structure. Besides, Fig. 6.3 also shows that the growth rate of SZ particles' dimension is faster in SZ-1 to SZ-3 than that in SZ-3 to ZS-5, suggesting S-1 layers likely reached equilibrium at this gel condition, agreed with BET surface area of SZ-4 and SZ-5 started decreasing as shown in Table 6.1.
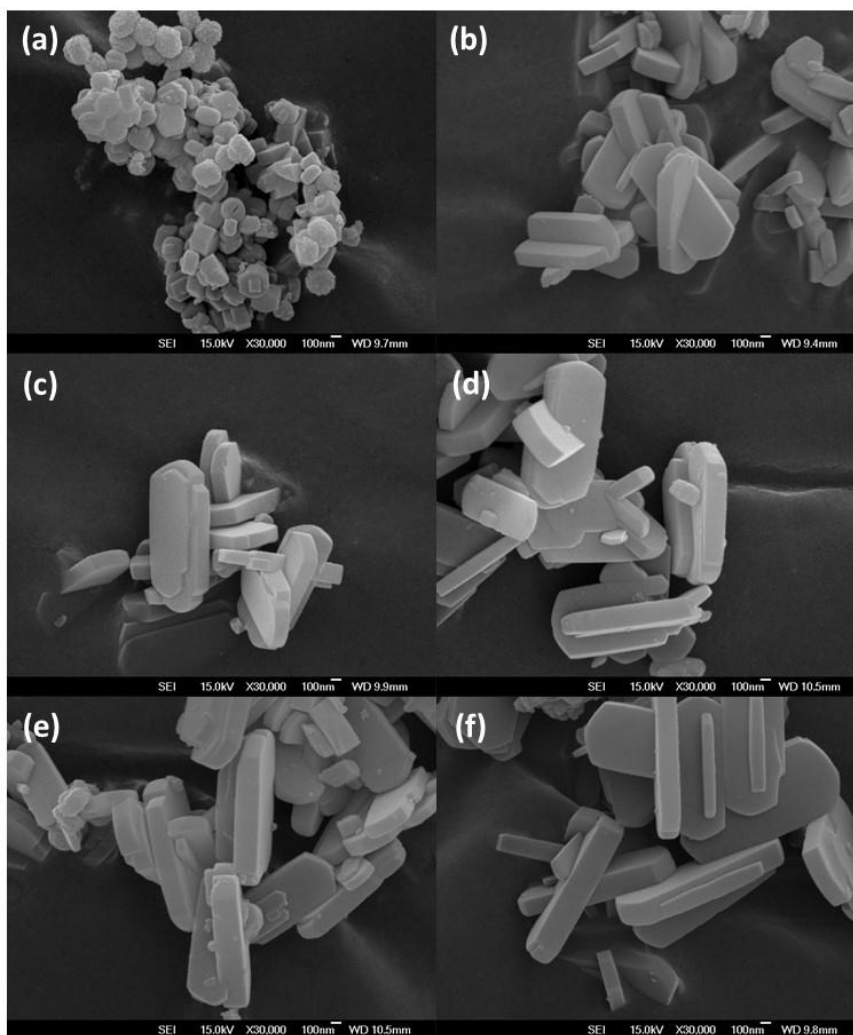
Fig. 6.3 SEM images of (a) Pd/ZSM-5 nano particles and (b to f) core-shell S-1/Pd/ZSM-5 (SZ-1 to SZ-5) synthesized from different secondary crystallization time (1−5 days).

Analysis of SZ particles using TEM is not possible because of the thickness of the shell (in micron size). Nevertheless, TEM images of the nana-sized core (Fig. 6.4) reveal that the Pd particles are generally uniformly dispersed over all over the ZSM-5 core (Fig. 6.4b) compare to plain ZSM-5 particle (Fig. 6.4a). CO-chemisorption results show that average size particle of Pd/ZMS-5 is approximately 4.0 nm, yet large agglomerates of Pd with a size of 20−30 nm are also observed in Fig. 6.4b. Since the typical free aperture of ZSM-5 is approximately 0.45−0.60 nm, active Pd are most probably existed as nanoparticles and are located on the external

surface of the ZSM-5 core. In addition, the metal dispersions (measured by chemisorption of CO) in ZSM-5, Pd/ZSM-5, SZ-1, SZ-3 and SZ-5 samples were present in Table 6.2. While Pd/ZSM-5 gives the highest dispersion (28.26%) of Pd, SZ-1, SZ-3 and SZ-5 with increased thickness of S-1 shell exhibit a significant decrease in Pd dispersion to 12.23%, 6.79% and 3.88%, respectively. This is so because more inert (Si) surface is contributed by S-1 shell (compared with Pd/ZSM-5), which results in the decrease of the Pd/Si over single SZ particles, thus, the lower metal dispersion. This is also consistent with the ICP results that the Pd/Si ratio decreased as the S-1 layers built up.
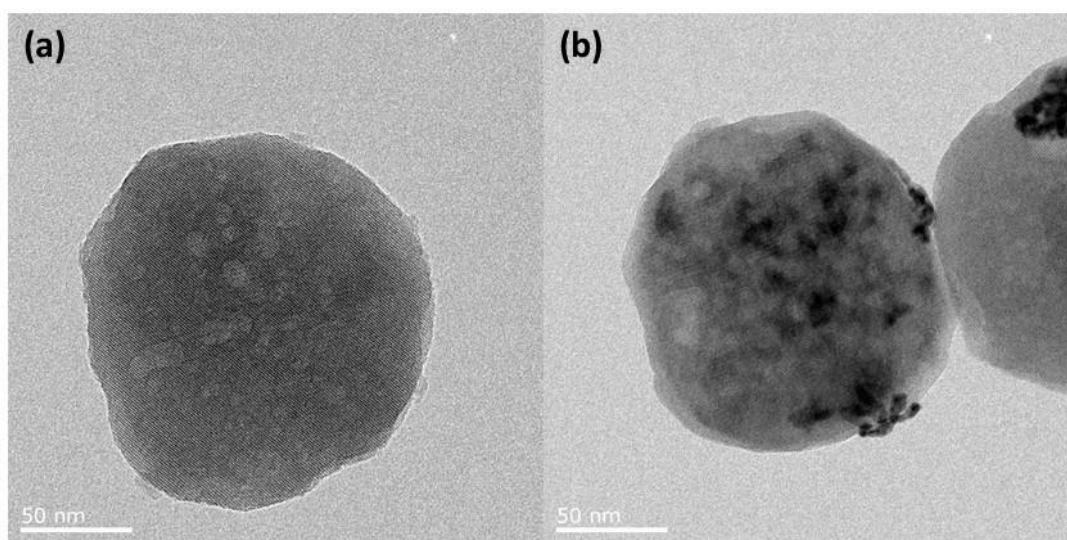
Fig. 6.4 TEM images of (a) ZSM-5 and (b) Pd/ZSM-5 nano particles.

Table 6.2 Metal dispersion and amount of CO adsorption on the core-shell MFI zeolite.

Catalysts	Metal dispersion (%)	Adsorption amount (cm^3/g)
ZSM-5	-	0.03
Pd/ZSM-5	28.26	0.31
SZ-1	12.23	0.23
SZ-3	6.79	0.14
SZ-5	3.88	0.08

The water affinity of the Pd/ZSM-5 and SZ samples were tested by immersing these samples in DI water as show in Fig. 6.5. Most of the Pd/ZSM-5 powders still showed well dispersed after 3 hours sediment, while slight deposition was found on the bottom. In contrast, SZ-3 and SZ-5 were found hard to disperse in the water, a clear phase was observed after 3 hours sediment test, which could be attributed to the hydrophobic nature of the S-1 shell, resulted in the high water resistance of the SZ samples. The results agreed with the literature that hydrophobic samples are difficult to disperse in water [19]. In addition, Fig. 6.6 shows the TGA results of the pretreated SZ samples in humid environment. As the S-1 shell thickness increased, the less water was adsorbed by the SZ samples. It is worth noting that the increasing rate of humidity tolerance from SZ-3 to SZ-5 is slower than that from SZ-1 to SZ-3, which is likely due to the growth of S-1 shell was almost approaching to the equilibrium for SZ-3 sample under the tested source gel conditions, resulted in less S-1 was generated during the period of SZ-3 to SZ-5 than S-1 to S-3. The observations are consistent with BET (Table 6.1) and SEM (Fig. 6.3) results.
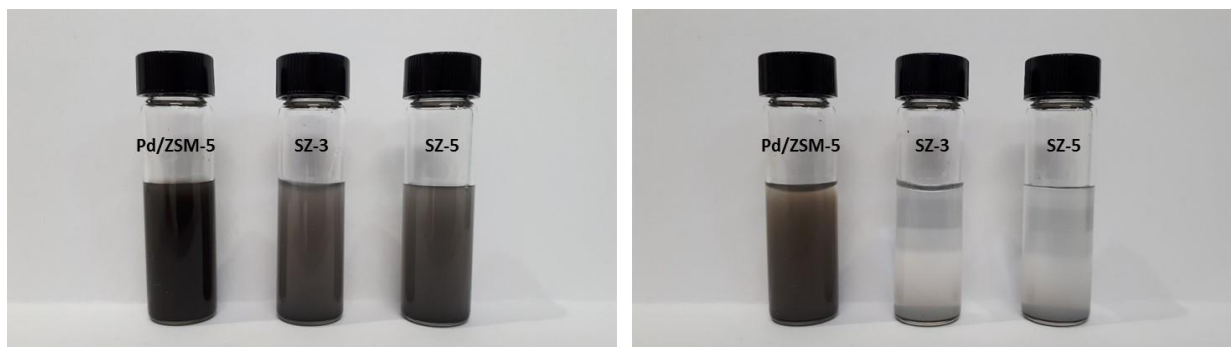
Fig. 6.5 Images of Pd/ZSM-5, SZ-3 and SZ-5 sample in water before (Left) and after 3 hours sediment test (Right). (Condition: 50 mg sample in 5 ml DI H_2O, ultrasound for 10 mins before the sediment)
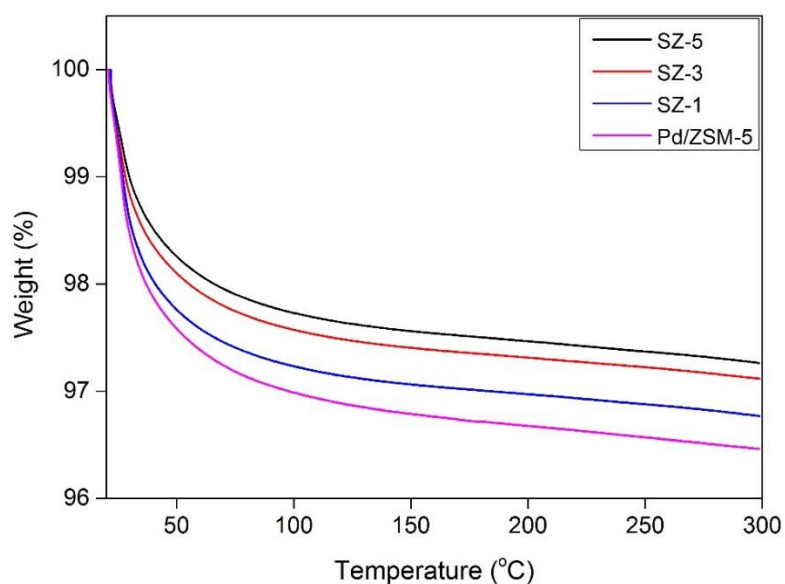
Fig. 6.6 TGA spectra of the Pd/ZSM-5, SZ-1, SZ-3, and SZ-5 after the humidity treatment. (Condition: sample/DI water = 2 mg/ml, 50 ^{o}C sealed environment for 2 h)

6.3.2 Ethylene adsorption with pressure drop method

Preliminary test on commercial zeolites

The adsorption test was preliminarily processed for two standard commercial zeolites (MFI and BEA) with similar Si/Al ratio (Table 6.3). BEA zeolite (5.95Å) has a larger pore size than MFI (4.7Å), resulted in a higher BET surface area of BEA (680 m^2/g) than that of MFI (425 m^2/g). Since the molecular diameter of ethylene is 4.16 Å [20], suggesting it can pass through both MFI and BEA porous structure without impediment. The ethylene uptake over BEA is around 1.3 times higher than that of MFI zeolites, which is close to the BET surface area ratio of BEA/MIF (i.e. 1.6) as in Table 6.3, indicating that the surface area is the key parameter that affect ethylene adsorption over these two types of zeolites. Pd/BEA sample with a Pd loading of 1.0 wt% was tested later on to check the influence of Pd on ethylene adsorption. Even though the surface area decreased 10% (from 680 to 611 m^2/g), the ethylene uptake was greatly increased by 37% (from 0.317 to 0.434 mmol/g), indicating Pd doped zeolite can promote ethylene adsorption, which is consistent with previous study that Pd is one of best promoter metals for ethylene scrubbing [7, 8].

Table 6.3 Ethylene adsorption amount on commercial zeolites and Pd-doped commercial BEA.

Sorbents	Ring size (# T-atoms)[a]	Large pore size (Å)[b]	Si/Al ratio (-)[c]	$S_{BET}(m^2/g)$[d]	$mmol_{ethylene}/g_{sorbent}$
MFI	10	4.7	11.5	425	0.237
BEA	12	5.95	12.5	680	0.317
Pd/BEA (1.0 wt% Pd)[e]	-	-	-	611	0.434

[a,b] According to the International Zeolite Association database.

[c,d] Data are referred to SDS provided by Zeolyst International Co., except that Pd/BEA was measured by BET afterwards.

[e] measured by ICP.

Ethylene adsorption on SZ samples

The ethylene adsorption was tested over SZ samples as shown in Fig. 6.7, plain nano-sized ZSM-5 core (i.e., no Pd loading) was also compared as control. Synthesized ZSM-5 has a 0.155 mmol/g ethylene uptake, which is 1.5 times more than commercial MFI (Table 6.3; 0.237 mmol/g), given the higher surface area of commercial MFI (Table 6.3; 425 m^2/g) than synthesized nano ZSM-5 (Table 6.1; 326 m^2/g), which is approximately 1.3 times higher, agreed with previous results that ethylene is positively related with surface area of the sorbents. In addition, the loading of Pd increased the ethylene uptake by 57 %, even though the surface is lightly decreased (Table 6.1, from 326 to 318 m^2/g), which is consistent with the results observed on commercial BEA and Pd/BEA samples, confirming that Pd could significantly promoted ethylene uptake. Moreover, it can be clearly seen that ethylene uptake generally increased after the S-1 layers built up, which could be attributed to the increased surface area

that introduced by S-1 shell. The highest ethylene was found by SZ-3 sample, which increased the ethylene uptake by 2.9 times more than plain ZSM-5 zeolites, indicating the synergistic effect of the Pd and S-1 shell. The decreased ethylene uptake over SZ-4 and SZ-5 samples likely due to randomly generated S-1partilces partially blocked the porous structure of SZ samples, which is consistent with their decreased surface area (Table 6.1) and observation from SEM images (Fig. 6.3).
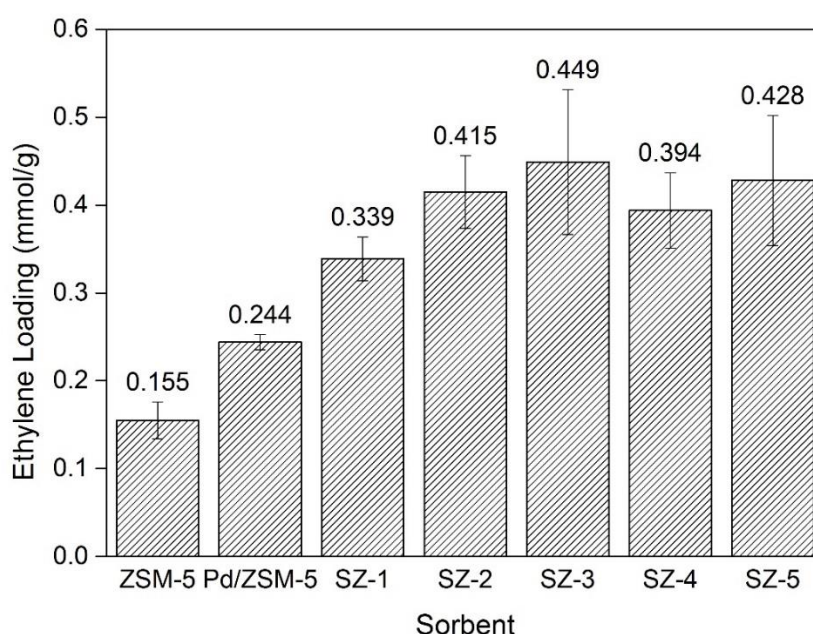
Fig. 6.7 Ethylene adsorption of ZSM-5, Pd/ZSM-5, and SZ-X (X= 1 to 5) samples at 21 °C.

Ethylene adsorption on humidity treated SZ-3 sample

In order to further investigate the core-shell samples in a humid condition. The SZ-3 sample was treated in a humidity environment before transferred to the test chamber, Pd/ZSM-5 sample without S-1 was also tested as comparison. Both of the tested samples showed decreased ethylene loading as shown in Fig. 6.8 The ethylene adsorption amount on Pd/ZSM-5 showed approximately 20% decrease (from 0.244 to 0.195 mmol/g), which agreed with

previous study that Pd promoted ZSM-5 has less humidity tolerance than that in dry environment [7]. In comparison, the SZ-3 only showed a 7.6% decrease of ethylene uptake (from 0.449 to 0.415 mmol/g), and still showed a high ethylene adsorption ability after 5 h humidity treatment, suggesting the S-1 shell effectively protect the Pd and inner porous channels from blocking by water. The 7.6% loss of the ethylene loading on SZ-3 sample could be attributed to the slight defects over S-1 shell, which has also been observed by our previous work [9].
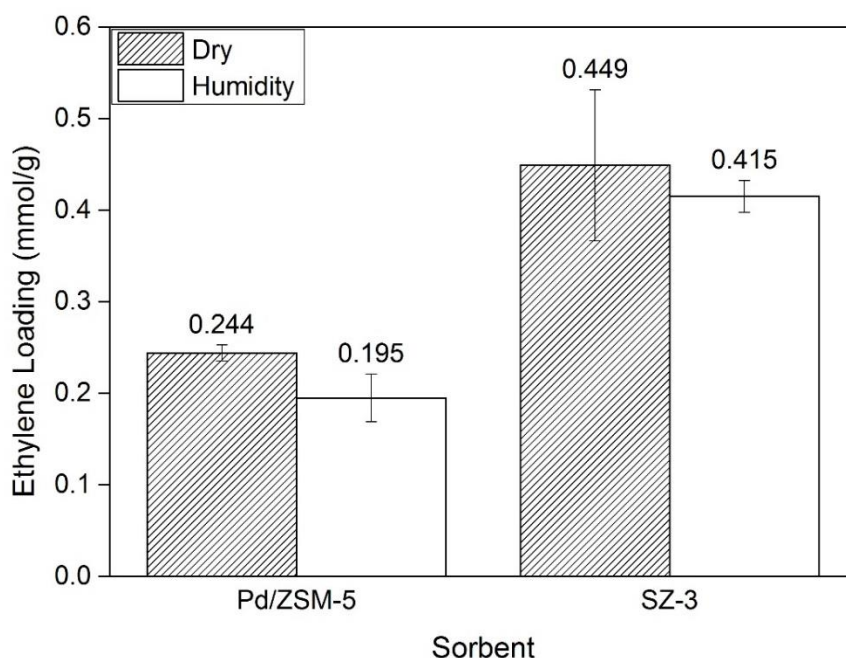
Fig. 6.8 Ethylene adsorption of pre-treated Pd/ZSM-5 and SZ-3 samples in humid environment. (Pretreatment condition: sample/DI water = 7.5 mg/ml, 50 °C sealed environment for 5 h)

6.4 Conclusions

A new type of core-shell MFI ethylene scavenger consists of a nano-sized Pd/ZSM-5 core and Silicalite-1 (S-1) layers with variable thickness as the shell was successfully synthesized. The effectiveness of the core-shell design on increasing the ethylene adsorption, particular when the sorbent was pre-treated under humid environment, was investigated. The core-shell S-1/Pd/ZSM-5 with different S-1 shell thickness showed improved ethylene uptake by 219 to 290% compared to plain ZSM-5, among which SZ-3 sample showed the highest ethylene loading likely due to the increased the surface area by S-1 and less generated S-1 single particles. Moreover, all the S-1 coated samples showed increased humidity tolerance than Pd/ZSM-5. SZ-3 samples still persevered 92.4% ethylene uptake after the sample was pretreated under humid environment for 5 h, in comparison, Pd/ZSM-5 lost 20% of the ethylene after the humidity treatment for 5 h time period. The improved ethylene uptake of SZ samples could be attributed to synergistic effect between Pd and S-1 shell. That is, Pd has a stronger affinity to ethylene, S-1 offers a larger surface area to the core-shell composite for adsorption to take place. The improved resistance to humidity of the SZ samples most likely due to the hydrophobic nature of the S-1 shell.

6.5 References

[1] M.E. Saltveit, Effect of ethylene on quality of fresh fruits and vegetables, Postharvest Biol. Technol., 15 (1999) 279-292.

[2] A. El Blidi, L. Rigal, G. Malmary, J. Molinier, L. Torres, Ethylene removal for long term conservation of fruits and vegetables, Food quality and preference, 4 (1993) 119-126.

[3] N.A. Khan, Ethylene action in plants, Springer2006.

[4] F.B. Abeles, P.W. Morgan, M.E. Saltveit Jr, Ethylene in plant biology, Academic press2012.

[5] C.B. Watkins, The use of 1-methylcyclopropene (1-MCP) on fruits and vegetables, Biotechnol. Adv., 24 (2006) 389-409.

[6] C.B. Watkins, Ethylene synthesis, mode of action, consequences and control, Fruit quality and its biological basis, (2002) 180-224.

[7] L.A. Terry, T. Ilkenhans, S. Poulston, L. Rowsell, A.W.J. Smith, Development of new palladium-promoted ethylene scavenger, Postharvest Biol. Technol., 45 (2007) 214-220.

[8] A.W.J. Smith, S. Poulston, L. Rowsell, L.A. Terry, J.A. Anderson, A New Palladium-Based Ethylene Scavenger to Control Ethylene-Induced Ripening of Climacteric Fruit, Platinum Met. Rev., 53 (2009) 112-122.

[9] X. Jia, Y. Jeong, H. Baik, J. Choi, A.C. Yip, Increasing Resolution of Selectivity in Alkene Hydrogenation via Diffusion Length in Core-shell MFI zeolite, Catal. Today, (2018).

[10] N. Desbiens, A. Boutin, I. Demachy, Water condensation in hydrophobic silicalite-1 zeolite: a molecular simulation study, The Journal of Physical Chemistry B, 109 (2005) 24071-24076.

[11] K. Ueno, H. Negishi, M. Miyamoto, S. Uemiya, Y. Oumi, Effect of deposition seed crystal amount on the α-Al$_2$O$_3$ support and separation performance of silicalite-1 membranes for acetic acid/water mixtures, Sep. Purif. Technol., 174 (2017) 57-65.

[12] M. Miyamoto, S. Ono, K. Kusukami, Y. Oumi, S. Uemiya, High Water Tolerance of a Core–Shell-Structured Zeolite for CO_2 Adsorptive Separation under Wet Conditions, Chemsuschem, 11 (2018) 1756-1760.

[13] H. Mochizuki, T. Yokoi, H. Imai, R. Watanabe, S. Namba, J.N. Kondo, T. Tatsumi, Facile control of crystallite size of ZSM-5 catalyst for cracking of hexane, Microporous Mesoporous Mater., 145 (2011) 165-171.

[14] K. Miyake, Y. Hirota, K. Ono, Y. Uchida, S. Tanaka, N. Nishiyama, Direct and selective conversion of methanol to para-xylene over Zn ion doped ZSM-5/silicalite-1 core-shell zeolite catalyst, J. Catal., 342 (2016) 63-66.

[15] M.G. Cowan, W.M. McDanel, H.H. Funke, Y. Kohno, D.L. Gin, R.D. Noble, High ethene/ethane selectivity in 2,2'-bipyridine-based silver(i) complexes by removal of coordinated solvent, Angew. Chem. Int. Ed. Engl., 54 (2015) 5740-5743.

[16] A. Kumbhar, S. Kamble, A. Mane, R. Jha, R. Salunkhe, Modified zeolite immobilized palladium for ligand-free Suzuki–Miyaura cross-coupling reaction, J. Organomet. Chem., 738 (2013) 29-34.

[17] M. Miyamoto, T. Kamei, N. Nishiyama, Y. Egashira, K. Ueyama, Single Crystals of ZSM-5/Silicalite Composites, Adv. Mater., 17 (2005) 1985-1988.

[18] M. Miyamoto, K. Mabuchi, J. Kamada, Y. Hirota, Y. Oumi, N. Nishiyama, S. Uemiya, Para-selectivity of silicalite-1 coated MFI type galloaluminosilicate in aromatization of light alkanes, J. Porous Mater., 22 (2015) 769-778.

[19] S. Han, Z. Wang, L. Meng, N. Jiang, Synthesis of uniform mesoporous ZSM-5 using hydrophilic carbon as a hard template, Mater. Chem. Phys., 177 (2016) 112-117.

[20] S. Aguado, G. Bergeret, C. Daniel, D. Farrusseng, Absolute molecular sieve separation of ethylene/ethane mixtures with silver zeolite A, J. Am. Chem. Soc., 134 (2012) 14635-14637.

Chapter 7

Conclusions and Recommendations

7.1 Conclusions

In this thesis, a systematic study has been given on zeolite modification and functionalization. The hierarchical and core-shell structures have been synthesized with novel features, such as improved catalytic activity, molecular size excluded selectivity, tunable hydrophobicity and hydrophilicity. The synthesized zeolites have been tested on Sonogashira coupling reaction, fructose dehydration to 5-hydroxymethylfurfural, alkene hydrogenation, and ethylene adsorption. The main findings of this study have been delineated as following:

We successfully demonstrated an effective synthesis method for stacking ZSM-5 by using hydraulic pressing and programmed temperature calcination; this method differs from a traditional industrial zeolite matrix made by using binders. ZSM-5 zeolites with different particle sizes were modified to stacking type for comparison. The as-prepared stacking ZSM-5 was used as a support for depositing palladium. The Pd/stacking ZSM-5 composites showed great improvement on Sonogashira coupling reactions that outcompete their unit counterparts, and they also exhibited good durability by recycling 4 runs without losing significant catalytic activity. This result is important to the research community of zeolite modification because it provides new information for increasing the activity, stability and durability of zeolite supported metal catalysts. Our study also optimized the preparation conditions of the Pd/stacking ZSM-5 catalyzed Sonogashira coupling reactions. Therefore, it gives insights into the design of other metal/stacking zeolites systems, especially those with potential in industrial liquid phase reactions.

We also elucidated the roles of zeolite-solvent combination in the conversion of biomass-derived fructose to 5-hydroxymethylfurfural (HMF), which is the primary building block of the new generation of bioplastics, namely polyethylene furanoate (PEF).

Functionalized MFI zeolite with different particle sizes and hierarchical structures, and different types of zeolites (MFI, BEA, and Y) were tested in water and water/organic solvent systems, under 160 °C with microwave-assisted heating. The results revealed that the HMF yield is independent of particle size for MFI zeolites in water medium. The introduced secondary porosities in zeolites improved the HMF yield due to the enlarged channels. All the tested zeolites showed higher activities (i.e., fructose conversion, HMF yield, and HMF selectivity) in organic-water mixtures than water. In particular, we found that hydrophobic Y zeolite in DMSO/H_2O medium gave the highest fructose conversion (72.4%) and HMF yield (49.2%). We also confirmed that strong acidity and water affinity were two important factors that make hydrophobic Y zeolite the most active and stable in performance. This paper is also supplemented by the kinetic study that shows the synergistic effect of the substrates, catalysts, and solvent-products interactions in the hydrophobic Y/DMSO system under microwave conditions. The effect of different properties of zeolite-solvent medium (e.g., micro-/mesoporosity, acidity, and water affinity) on simultaneous pathways of fructose dehydration in biorefinery were presented.

Furthermore, we reported a synthesis method for core-shell Silicalite-1/Pd/ZSM-5 composites. This core-shell structure consists of a ZSM-5 core loaded with Pd nanoparticles and a Silicalite-1 (S-1) layer which is formed from secondary crystallization. The core-shell S-1/Pd/ZSM-5 catalyst exhibits highly preferential selectivity to 1-hexene over cyclohexene and 1-heptene even though all of these three molecules are smaller than the pore size of MFI zeolite. The selectivity is a strong function of diffusion length given by the S-1 shell layer. This study provides a strategy for modifying and improving the existing hydrogenation catalysts to be used in industry, particularly by providing a feasible way to distinguish reactant molecules with

similar size and shape. More specifically, it sheds light on how selectivity in a zeolite-catalyzed reaction can be changed without relying on the molecular size exclusion process.

Lastly, we continued the development of core-shell structured zeolites with nano-sized ZSM-5 core and Silicalite-1 shell. The nano-sized ZSM-5 was deposited by Pd before the secondary crystallization of S-1 shell. The core-shell S-1/Pd/ZSM-5 showed higher ethylene adsorption ability than ZSM-5 due to the synergistic effect between Pd and S-1 shell, i.e., Pd has a higher ethylene affinity and S-1 provided extra surface. It was also found that the ethylene uptake is positively related to the surface area of the sorbent. Moreover, the hydrophobic nature of the S-1 shell gives core Pd/ZSM-5 a protective layer to humid environment, which may offer the advantage of long-term economic benefit and sustainability for fresh products market, due to most current ethylene scavengers on market are susceptible to water inhibition.

7.2 Recommendations

In this thesis, synthesis strategies for hierarchical and core-shell zeolites have been developed. Even though they have shown improved performance on Sonogashira reaction, fructose dehydration, selective hydrogenation and ethylene adsorption, the following recommendations can be considered for future study.

For the stacking synthesis method, the size of the stacking units have dimensions of approximately 30 µm to 40 µm in the present study, smaller unit sizes (i.e., ~ 10 to 20 µm) may achieve even better catalytic performance due to the decreased diffusion limitation. In addition, the present work elucidated the performance of hierarchical zeolites synthesized from hydrophilic carbon black templates, other hard template sources such as cellulose and biochar can be considered as the hard template to synthesize hierarchical zeolites.

In current work, the core-shell zeolites are mainly focused on MFI type zeolites, other types of zeolites with different porous structures may also offer improved performance, such as BEA and Y zeolites, which both have bigger pores and allow bigger molecules to pass through. In addition, the metal loading is limited to palladium in this study, other metals can also be tried as the deposited material on core zeolites, such as Cu, Sn and Ag, which have a relatively high affinity to alkenes according to their performance in alkene hydrogenation. In particular, for ethylene adsorption, silver is potentially a very good alternative since it has been reported as showing great ethylene removal performance. Moreover, the present work demonstrated a strong correlation between the diffusion length and the preferential selectivity among C_6/C_7 alkenes, smaller gas alkenes such as C_2/C_3, C_3/C_4 would be interesting to test in future studies.

Appendices

Appendix A

Characterization data of the products:
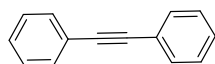
1,2-Diphenylethyne :

White solid, mp: 63-64 °C; ^{1}H NMR (400 MHz, CDCl$_3$) δ 7.56 – 7. 53 (m, 4H), 7.42 – 7.33 (m, 6H); ^{13}C NMR (101 MHz, CDCl$_3$) δ 132.51, 129.21, 128.45, 121.83, 81.56.
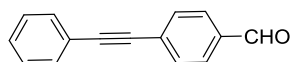
Phenylethynylbenzaldehyde:

White solid, mp: 93-95°C; ^{1}H NMR (400 MHz, CDCl$_3$) δ 10.04 (s, 1H), 7.88 (d, J = 8.2 Hz, 2H), 7.69 (d, J = 8.2 Hz, 2H), 7.60 – 7.55 (m, 2H), 7.42 – 7.36 (m, 3H); ^{13}C NMR (101 MHz, CDCl$_3$) δ 191.48, 135.39, 132.07, 131.80, 129.60, 129.58, 129.01, 128.48, 122.52, 93.48, 88.55.
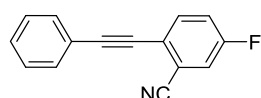
5-fluoro-2-(phenylethynyl)benzonitrile

Yellow solid, mp: 75-76 °C; ^{1}H NMR (400 MHz, CDCl$_3$) δ 7.67 (dd, J = 9.0, 4.9 Hz, 1H), 7.64 – 7.59 (m, 2H), 7.41 – 7.37 (m, 3H), 7.34 – 7.28 (m, 1H), 7.22 (ddd, J = 8.9, 7.9, 3.0 Hz, 1H); ^{13}C NMR (101 MHz, CDCl$_3$) δ134.90 (d, J = 8.1 Hz), 134.17 (d, J = 8.5 Hz), 131.96, 131.66, 129.35, 128.51, 121.89 (d, J = 22.4 Hz), 121.86, 121.31 (d, J = 25.6 Hz), 120.47 (d, J = 22.0 Hz), 119.69 (d, J = 25.3 Hz), 95.81, 84.58.
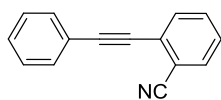
2-(phenylethynyl)benzonitrile

Yellow oil; ^{1}H NMR (400 MHz, CDCl$_3$) δ 7.74 – 7.53 (m, 5H), 7.51 – 7.34 (m, 4H); ^{13}C NMR

(101 MHz, CDCl$_3$) δ 134.34, 133.96, 133.22, 132.67, 132.46, 132.14, 132.02, 129.29, 128.49,

128.30, 127.69, 122.05, 117.60, 115.29, 96.01, 85.66.
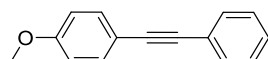
1-Methoxy-4-(phenylethynyl)benzene

Yellow solid, m.p. 56-57 °C; ^{1}H NMR (400 MHz, CDCl$_3$) δ 7.58 – 7.46 (m, 4H), 7.35 (dt, J =

3.5, 1.1 Hz, 3H), 6.90 (d, J = 8.9 Hz, 2H), 3.86 (s, 3H); ^{13}C NMR (101 MHz, CDCl$_3$) δ

159.62, 133.07, 131.46, 128.32, 127.95, 123.60, 115.39, 114.01, 89.37, 88.07, 55.32.

Appendix B
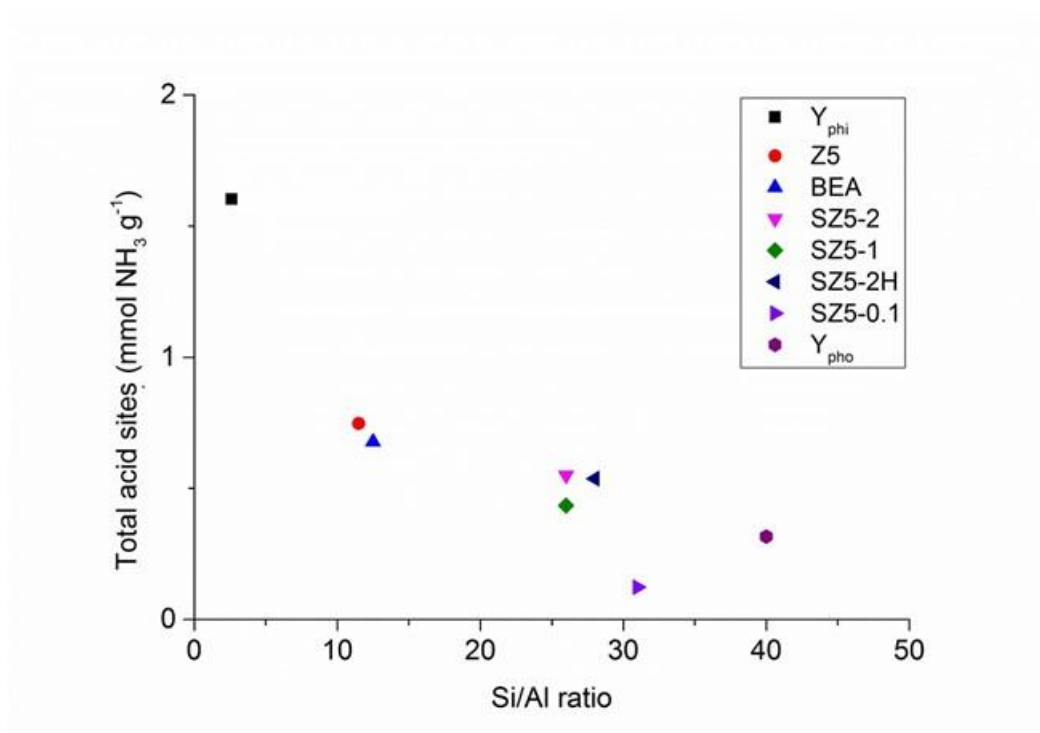
Fig. S1 Correlation of Si/Al ratio with total acid sites.